

**THE UNIVERSITY OF WESTERN ONTARIO  
DEPARTMENT OF CIVIL AND  
ENVIRONMENTAL ENGINEERING**

**Water Resources Research Report**

**Multi-hazard resilience model of an  
interdependent infrastructure system**

**By:  
Jingjing Kong  
and  
Slobodan P. Simonovic**

**Report No: 102  
Date: November 2017**

**ISSN: (print) 1913-3200; (online) 1913-3219  
ISBN: (print) 978-0-7714-3158-6; (online) 978-0-7714-3159-3**



**Multi hazard resilience model of interdependent  
infrastructure system**

**By**

**Jingjing Kong**

**Slobodan P. Simonovic**

**Department of Civil and Environmental Engineering  
Western University, Canada**

**November 2017**

**Abstract:** Multi hazard resilience is of significant practical value, as most of the world regions are subject to multiple natural and technological hazards. An analysis and assessment approach for multi hazard spatiotemporal resilience of interdependent infrastructure system is developed by integrating network theory, geographic information system and numerical analysis. First, we define multi hazard resilience and present a quantitative probabilistic metric based on the expansion of single hazard deterministic resilience model. Second, we define multi hazard relation analysis model with focus on hazards' impacts on infrastructure. The relation cube is constructed with two temporal and one spatial dimensions. Developed methodology is used for direct damage probability analysis of an infrastructure under twelve spatiotemporal combinations of two different hazards. A general method for evaluation of direct impacts on an infrastructure under multiple hazards is proposed. Third, we present an analysis of indirect multi hazard impacts on interdependent infrastructure. The methodology is implemented on the case study of Greater Toronto Area energy system (including electric, gas, and oil transmission networks). The results confirm that the effects of sequential hazards on resilience of infrastructure (network) are quite different than the simple sum of multiple single hazard effects. The resilience depends on the magnitude of the hazards, their spatiotemporal relationship and dynamic combined impacts, and infrastructure interdependencies. The paper presents a comparison between physical and functional resilience of electric transmission network, and finds functional resilience is always higher than physical resilience. The multiple hazard resilience evaluation approach is applicable to any type of infrastructure and hazard and it can contribute to the improvement of the infrastructure planning, design and maintenance decision making.

**Key words:** multiple hazards resilience, interdependent infrastructure system, restoration strategy, Greater Toronto Area

## **ACKNOWLEDGMENTS**

We are grateful to the Natural Sciences and Engineering Research Council (NSERC) of Canada, and the Institute of Catastrophic Loss Reduction (ICLR) supported by Chaucer PLC for funding of this research. Any opinions, findings, and conclusions or recommendations expressed in this report are those of the authors and do not necessarily reflect the views of the sponsors.

## TABLE OF CONTENTS

ACKNOWLEDGMENTS .....	3
TABLE OF CONTENTS .....	4
LIST OF TABLES .....	6
LIST OF FIGURES .....	7
1 INTRODUCTION .....	1
2 MULTI HAZARD RESILIENCE MODEL .....	3
2.1 Interdependent Infrastructure System Model.....	3
2.2 Deterministic Single Hazard Resilience Metric.....	4
2.3 Probabilistic Multi Hazard Resilience Metric.....	6
3 MULTI HAZARD RELATIONSHIPS AND DIRECT IMPACTS ON INFRASTRUCTURE .....	11
3.1 Relationships Between Multiple Hazards .....	11
3.1.1 Temporal relationships of multiple hazards .....	11
3.1.2 Spatial relationships of multiple hazards.....	14
3.1.3 Relationship cube of multiple hazards .....	15
3.2 Impacts of Multiple Hazards on Infrastructure Systems .....	16
3.2.1 Direct impacts of two hazards .....	17
3.2.2 Direct impacts of multiple hazards .....	21
3.2.3 Failures propagation mechanism and indirect impacts of multiple hazards on infrastructures	21
4 MULTI HAZARDS RESILIENCE ASSESSMENT APPROACH .....	22
5 MULTILAYER INTERDEPENDENT INFRASTRUCTURE NETWORK .....	24
5.1 GTA Energy Infrastructure Spatial Network .....	24
5.2 Infrastructure Interdependence Models .....	26
5.3 Physical and Functional Resilience Metric .....	28
6 SEQUENTIAL HAZARDS SCENARIO AND ITS IMPACTS .....	29
6.1 Sequential Hurricane and Flood Scenario.....	29
6.2 Single Hazard Impacts on Infrastructure.....	31
6.3 Sequential Hazard Impacts on Infrastructure.....	33
7 SEQUENTIAL HAZARD RESILIENCE SIMULATION .....	34
7.1 Joint Restoration Model of Interdependent Infrastructure System .....	34
7.2 Sequential Hazard Resilience Simulation Process.....	35
8 GTA ENERGY INFRASTRUCTURE SYSTEM PHYSICAL RESILIENCE.....	37
8.1 Infrastructure Physical Performance Spatial Analysis.....	37

8.2 Dynamic Infrastructure System Physical Resilience .....	41
9 GTA ENERGY INFRASTRUCTURE SYSTEM FUNCTIONAL RESILIENCE .....	42
9.1 Infrastructure Functional Performance Spatial Analysis .....	42
9.2 Dynamic Infrastructure System Functional Resilience .....	45
10 DISCUSSION .....	47
10.1 Single Hazard Marginal Impacts.....	47
10.2 Cascading Failure and Recovery Effects .....	49
10.3 Restoration Resource Limits.....	53
11 CONCLUSIONS.....	54
REFRENCES .....	55
APPENDIX A: Data Resources.....	63
APPENDIX B: Model Code for MATLAB.....	64
(1) Calculation of the performance of electric power system under hazard .....	64
(2) Calculation of the performance of gas supply system under hazard .....	66
(3) Calculation of the performance of oil supply system under hazard .....	67
(4) Generation of the flood scenario .....	68
(5) Generation of the hurricane scenario.....	69
(6) Calculation of the performance of three systems under combined hurricane and flood scenario .....	71
(7) Calculation of the performance of three systems under flood scenario .....	76
(8) Calculation of the performance of three systems under hurricane and flood scenario.....	80
APPENDIX C: List of Previous Reports in the Series .....	89

**LIST OF TABLES**

Table 1 GTA three-layer energy infrastructure spatial network information..... 26

## LIST OF FIGURES

Figure 1 Multi-layer infrastructure network .....	4
Figure 2 Typical interdependent infrastructure system performance under a single hazard/disturbance $A_i$ .....	5
Figure 3 Typical infrastructure system performance under two sequential hazards.....	7
Figure 4 Typical infrastructure system performance under two sequential hazards.....	8
Figure 5 Typical infrastructure system performance under two concurrent hazards.....	9
Figure 6 Temporal relationships between two hazards.....	13
Figure 7 Spatial relationships between two hazards.....	14
Figure 8 Relation cube of multiple hazards .....	16
Figure 9 Framework for the assessment of multiple hazards resilience of interdependent infrastructure system.....	23
Figure 10 GTA three-layer energy infrastructure spatial network .....	25
Figure 11 Population supported by electric transmission substations in GTA .....	29
Figure 12 Sequential hurricane and flood impacts on GTA .....	31
Figure 13 Simulation procedure of GTA infrastructure system resilience under sequential hurricane and flood .....	36
Figure 14 Spatial physical performance of GTA three-layer energy infrastructure network under different hazard scenarios .....	39
Figure 15 GTA three-layer infrastructure network dynamic physical resilience .....	41
Figure 16 Spatial functional impacts of GTA three-layer energy infrastructure network under different hazards scenarios.....	44
Figure 17 GTA electric transmission network dynamic functional and physical resilience.....	45
Figure 18 Resilience profiles for different magnitude of hazards .....	48
Figure 19 Resilience profiles for different time interval of hazards.....	50
Figure 20 Resilience profiles for different spatial overlap area of hazards .....	52
Figure 21 Resilience profiles for different resource constraints.....	53

# 1 INTRODUCTION

Infrastructure systems, including electric power, telecommunications, natural gas and oil, transportation, water supply, and others, are large scale, man-made systems that function interdependently to produce and distribute essential goods and services for society and economy <sup>(1)</sup>. Infrastructure system resilience has gained attention of practitioners and researchers during the past decades due to its role in better understanding of risks associated with the inevitable disruptions of system components <sup>(2-4)</sup>. Multi hazard resilience is of significant practical value, as most world regions are subject to multiple natural and technological hazards <sup>(5)</sup>. Some examples include Prince William Sound region of USA Alaska in 1964 attacked by earthquake and following landslides and tsunami <sup>(6)</sup>; Mount Pinatubo 1991 volcanic eruption which triggered earthquake in Philippines; New Orleans destruction by Hurricane Katrina and follow up flood in 2005; and 2011 Tohoku disaster in Japan caused by sequential impacts of earthquake, flood and tsunami. Multi hazard resilience is critical for enhancing infrastructure system resilience.

Resilience implies the ability of a system to return to normal condition after an internal or external disturbance. Its origins are in ecology and work of C. S. Holling <sup>(7)</sup>. Due to the wide interest and application in various disciplines there is neither universal definition nor widely accepted general quantitative approach for its assessment. Excellent reviews are available in a number of published papers <sup>(4,8-10)</sup>. Infrastructure system resilience is always seen as the ability of the interconnected infrastructure system: (i) to resist (prevent, absorb and withstand) any possible hazard <sup>(11)</sup>; (ii) reduce the magnitude of impact and/or duration of disruptive event <sup>(12)</sup>; and (iii) recover and reconstitute critical services to the public with minimum damage <sup>(13)</sup>. Accordingly, resilience is not only the capacity of an infrastructure system, but also relates to the type, magnitude and other characteristics of the hazardous event <sup>(14-15)</sup>. Though most of the research focuses on resilience definition and outcome-oriented metrics <sup>(9,16-18)</sup>, some include the analysis of specific event resilience of infrastructure systems. Ouyang and Dueñas-Osorio <sup>(13,19)</sup> quantify annual expected hurricane resilience of contemporary electric power systems. Oddsdóttir et al. <sup>(20)</sup> evaluate the transportation and power supply system resilience subject to Hurricane Sandy. Shinozuka et al. <sup>(2)</sup> evaluate seismic resilience of electric power and water supply systems. Simonovic <sup>(21)</sup> and Kong et al. <sup>(22)</sup> focused on flood resilience of interdependent infrastructure system.

Generally, multi hazard resilience or risk analysis methods used up to now, simply sum up specific impacts of single hazards using historical data <sup>(23-26)</sup>. There are three major platforms for the computation of multi-hazard risks on a national level: Hazus, RiskScape, and CAPRA <sup>(27,28)</sup>. Their methodologies consider hazards as independent events <sup>(29,30)</sup>. Potential interactions between hazards and mixed impacts are rarely considered. Only a few approaches and studies on this topic are available <sup>(31)</sup>. Recently, two distinct approaches focusing on cause-and-effect of multi hazards have been proposed to tackle the problem of hazard interactions <sup>(32)</sup>. One is spatially oriented and aims at including all relevant hazards <sup>(33)</sup>, and the other is primarily thematically defined <sup>(31)</sup>. But hazard relations and interactions may have unexpected effects and pose threats that are not captured by means of separate single-hazard analyses. Advanced understanding of hazard processes, elements at risk and their vulnerabilities, without analysing the interactions between these components and their spatial and temporal dynamics, might not provide adequate support for developing preparedness, mitigation and response strategies to increase resilience or reduce risk <sup>(34,35)</sup>.

The primary objectives of this report are to propose a methodology for (i) development of complex multi hazard relations; (ii) consideration of complex infrastructure interdependencies; and (iii) integration of spatiotemporal impacts on infrastructure. It is our expectation that the proposed methodology will be able to capture and quantify multi-layer infrastructure network resilience subject to disturbing events caused by multiple hazards. Formulated as a large-scale, nonlinear, and combinatorial system evolution problem, the resilience assessment is performed using simulation.

The remainder of the report is organized as follows. Section 2 presents the multi hazard resilience definition and probabilistic model based on single hazard resilience metric. In Section 3, multi hazard impacts analysis framework is introduced. Direct impacts of multiple hazards on infrastructure are modeled using fragility curves. Indirect multi hazard impacts on interdependent infrastructure is also analyzed. Section 4 integrates the multi hazard resilience model. In Section 5, the Greater Toronto Area (GTA) energy infrastructure system (including electric, gas and oil transmission networks) is used as a case study to present an application of the sequential hazard resilience assessment method. GTA energy infrastructure system is modeled as a multi-layer network, and intra- and inter-network interdependence models are developed. Section 6 introduces sequential hurricane and flood disaster scenario, analyzes their direct impacts on infrastructure and indirect failure probabilities as a consequence of various interdependences. Section 7

describes sequential hazard resilience simulation procedure. Sections 8 and 9 are presenting temporal and spatial infrastructure system performance and resilience, using both, physical and functional perspectives. The report ends in Section 10 with the discussion of single hazard marginal impacts, cascading recovery effects, and cumulative resilience results. Conclusions are listed in Section 11.

## 2 MULTI HAZARD RESILIENCE MODEL

This section introduces the multi hazard resilience definition and probabilistic model based on single hazard resilience metric.

### 2.1 Interdependent Infrastructure System Model

Individual infrastructure systems, such as power grids, water supply networks and telecommunication networks, function together as a “system of systems,” in which two or more infrastructure types interact with one another <sup>(36)</sup>. A system-of-systems can be described by a topology that accounts for the representation of its components and the way they interact. Infrastructure systems (defined here as the systems of public works of a country, state, or region), with diverse clearly defined components, can be modeled as a network of networks <sup>(37)</sup> or a multilayer networks <sup>(38)</sup>.

Here infrastructure system is modeled as a multilayer spatial network  $G^{IS}$  (Figure 1), in which single layer denotes one kind of infrastructure system <sup>(22)</sup>. Each layer (such as power grid, water supply network, transportation network, information infrastructure network) is modelled in the same fundamental way <sup>(39)</sup>. Nodes are used to represent function source and transmission facilities, such as power plants and substations of electric network  $G^E$ , water treatment plants and pumping stations of water supply network  $G^W$ , gas compressor stations and storage facilities of gas network  $G^G$ , and so on. Arcs/edges represent function transmission facilities, such as power lines of electric transmission network  $G^E$ , pipelines of gas transmission network  $G^G$ , oil transmission network  $G^O$ , and so on. Nodes and edges in the same layer belong to the same type of infrastructure (shown using the same color solid lines within a single layer network in Figure 1). Edges between different layers denote interdependences between different types of infrastructure (shown as dotted lines between different layers in Figure 1). The color of an edge identifies the direction of dependency.

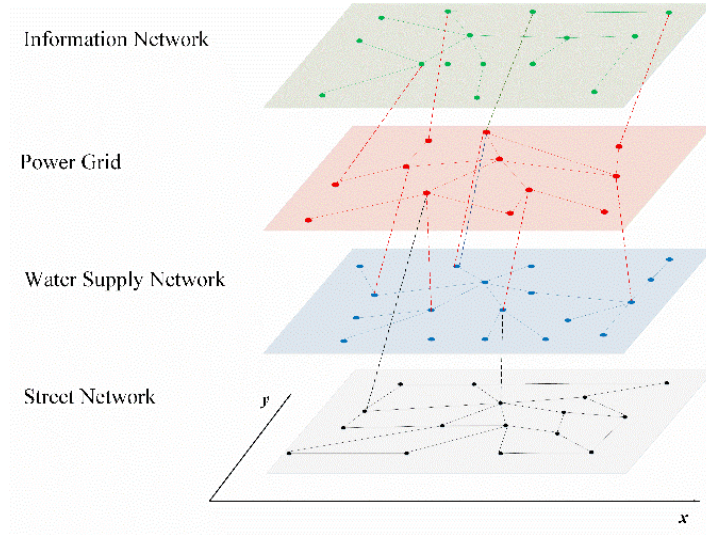


**Figure 1 Multi-layer infrastructure network**

Infrastructure components located in the same area may be subject to a specific disturbance/disaster, and the location of infrastructures and distance between them have important effects on topological properties, and consequently, on infrastructure functioning processes <sup>(37)</sup>. The spatial attributes of nodes and edges are included in a realistic infrastructure network model with geographical coordinates defined in a two-dimensional Euclidean coordinate system. Each node has three coordinates  $(\phi, x, y)$ , where  $\phi$  denotes the type of infrastructure, and  $(x, y)$  denote the geographical location of the node. Edges are denoted by the two adjacent nodes and can be divided into two types: (i) intra-infrastructure connection, same value of  $\phi$ ; and (ii) inter-infrastructure connection, different  $\phi$  value. The length of an arc can be represented as the weight of its importance.

## 2.2 Deterministic Single Hazard Resilience Metric

The infrastructure system resilience is defined as “*the ability to prepare for, and adapt to changing conditions, and withstand and recover rapidly from disruptions*”, including “*the ability to withstand and recover from deliberate attacks, accidents, or naturally occurring threats or incidents*” <sup>(40,41)</sup>. Original Space-Time Dynamic Resilience Measure developed by Simonovic <sup>(21,22,42)</sup> is adapted in this research to complex network infrastructure systems. It quantifies resilience as the difference between the area under expected system performance (dotted line in Figure 2)

and actual system performance (solid or dashed line in Figure 2). The mathematical representation of quantitative resilience is

$$r^{A_i}(t) = \frac{\int_{A_i^O}^t SP_{A_i}(t)dt}{\int_{A_i^O}^t SP_0(t)dt} = \frac{\int_{A_i^O}^t (SP_0(t) - SL_{A_i}(t))dt}{\int_{A_i^O}^t SP_0(t)dt} = 1 - \frac{\int_{A_i^O}^t SL_{A_i}(t)dt}{\int_{A_i^O}^t SP_0(t)dt} \quad (1)$$

where  $r^{A_i}(t)$  is resilience of infrastructure system to hazard/disturbance  $A_i$  at  $t$ ,  $SP_{A_i}(t)$  is actual performance of multilayer infrastructure network,  $SP_0(t)$  is the expected performance of multilayer infrastructure network,  $SL_{A_i}(t)$  is system performance loss of multilayer infrastructure network,  $t_{A_i}^O$  is the hazard/disturbance  $A_i$  occurrence time. Multi-layer infrastructure network performance always uses an uniform measure to capture the interdependent system service level, such as the proportion of surviving nodes <sup>(13,30)</sup>, operation rates of edges <sup>(43)</sup>, or size of the largest connected component <sup>(44)</sup>. The number of customers served by the infrastructure system can also be used as the performance measure <sup>(45,46)</sup>.

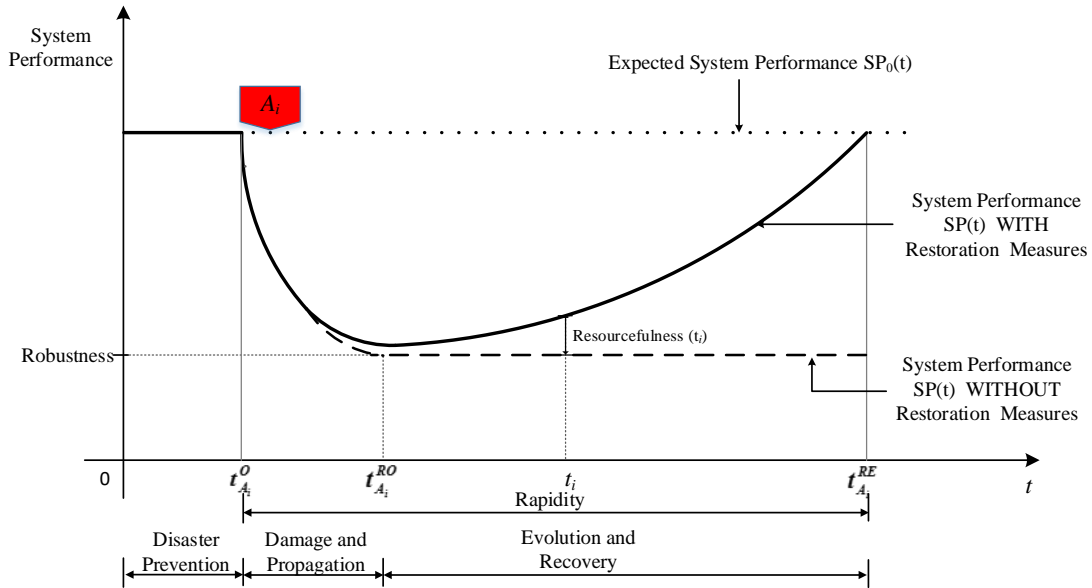


**Figure 2 Typical interdependent infrastructure system performance under a single hazard/disturbance  $A_i$**

In Figure 2, width of a red arrow displays the duration of the disturbance. Typical dynamic infrastructure performance can be divided into three phases: disaster prevention, damage and propagation, evolution and recovery <sup>(30,47,48)</sup>. Based

on the resilience model derived by MCEER (Multidisciplinary Center for Earthquake Engineering Research) <sup>(16)</sup>, the system resilience is a function of system performance and system adaptive capacity. System adaptive capacity can be described using four features of the diagram shown in Figure 2: Robustness, Redundancy, Resourcefulness and Rapidity. Robustness refers to the ability of a systems to withstand a given level of stress without suffering degradation or loss of function – minimum level of performance after the system disturbance. It is computed as the ratio of minimum number of operational elements after multiple disturbances to the total number. Redundancy describes the alternate functions and designs for the system mechanics to operate <sup>(49)</sup>. Redundancy is always seen as a function of robustness <sup>(50,51)</sup>. Resourcefulness is the capacity to develop and implement mitigation and response strategies for recovery from a specific disturbance. It is a function of restoration strategies, and can be calculated as the difference between system performance with and without restoration strategy. Rapidity is measured by the duration of all infrastructures recovery to normal operational levels. It is worth mentioning that performance metrics used should be based on the research focus and available data.

### **2.3 Probabilistic Multi Hazard Resilience Metric**

Multiple hazard/disturbance refers to a situation when hazards of different kinds or magnitudes occur at the same time, or more often, follow one another with damaging force. Examples include floods in the midst of drought, or hurricane followed by landslides and floods <sup>(52)</sup> and similar. With their diverse intensity, return periods, impacts, and uncertain relations, multiple hazards may have complex impacts and create unexpected threats very different from those caused by a single hazard/disturbance <sup>(5,24,31)</sup>. Multi hazard resilience is the dynamic nonlinear superposition of single hazard's spatiotemporal impacts on a complex infrastructure system. There are different relations between multiple hazards: cause-and-effect; temporal relation (such as co-occurrence, sequence); and spatial relation (such as scatter, block and overlap). They make their impacts much more complicated.

In the event of two or more hazards occurring at the same location the infrastructure may be placed under greater stress than if the hazards occurred at different locations. Sequence is a typical temporal relation of multiple hazards. Generally, infrastructure system resilience is analyzed individually with the assumption of later events occurring before full system recovery from the previous one, which is illustrated in Figure 3. Infrastructure system performance

and resilience can be calculated as single hazard resilience at different time periods, and evaluated individually. The infrastructure system performance can be expressed as

$$SP(t) = \begin{cases} SP_{A_i}(t) & t_{A_i}^O \leq t \leq t_{A_i}^{RE} \\ SP_{A_j}(t) & t_{A_j}^O \leq t \leq t_{A_j}^{RE} \end{cases} \quad (2)$$

where  $SP(t)$  is actual performance of multilayer infrastructure network.  $SP_{A_i}(t)$  and  $SP_{A_j}(t)$  are actual performances of multilayer infrastructure network under hazard  $A_i$  and  $A_j$ ;  $t_{A_i}^O$  and  $t_{A_j}^O$  are the occurrence times of hazard/disturbance  $A_i$  and  $A_j$ ; and  $t_{A_i}^{RE}$  and  $t_{A_j}^{RE}$  are the recovery times of hazard/disturbance  $A_i$  and  $A_j$ .

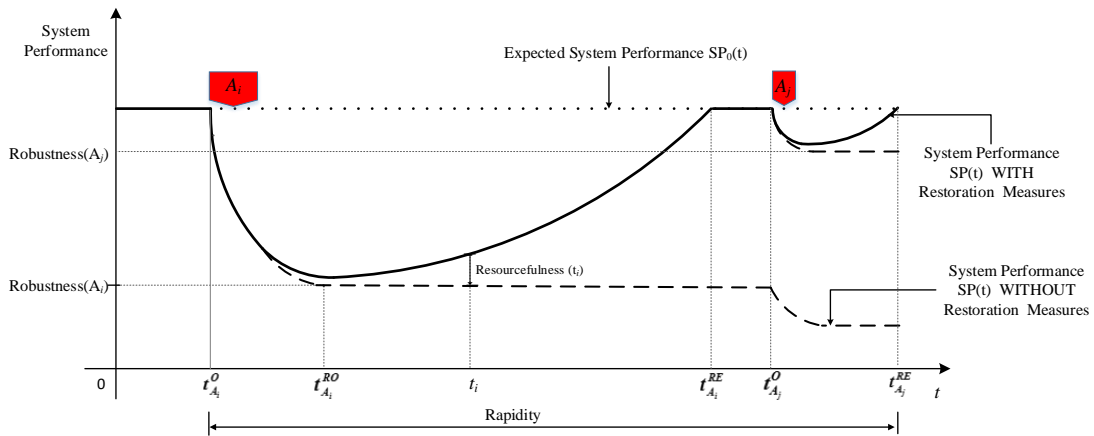


**Figure 3 Typical infrastructure system performance under two sequential hazards**

Actually, this illustration captures the situations when there are not enough time and resources for full infrastructure system recovery from the first disturbance before the second event occurs. The impact of one hazard on the physical infrastructure could increase the vulnerability to the secondary or future hazard events, therefore potentially amplifying the impacts of secondary or future hazards. For example, an earthquake may weaken buildings making them more susceptible to collapse in the event of the follow up earthquake, if the repairs are not completed. In this situation, infrastructures damaged by the initial hazard could not be repaired as planned, or they can be destroyed again by later hazards. In this case the operation or recovery of infrastructures would be impacted by later hazards.

The infrastructure resilience is not an integral of resilience of individual hazards at different time periods as illustrated in Figure 3. Contrary it is a result of interaction between impacts of multiple hazards on infrastructure system as shown in Figure 4.

Process of infrastructure adaptation can be divided into two phases. System performance evolution curve in each phase has the shape very different from the shape of the performance curve under a single hazard. Also, infrastructure system performance under the two sequential hazards would be expressed as

$$SP(t) = \begin{cases} SP_{A_i}(t) & A_i^o \leq t < A_j^o \\ SP_{A_j|A_i}(t) & t \geq A_j^o \end{cases} \quad (3)$$

where  $SP_{A_j|A_i}(t)$  is the actual system performance of multilayer infrastructure network under hazard/disturbance  $A_j$  followed by hazard/disturbance  $A_i$ .  $SP_{A_j|A_i}(t)$  usually does not equal to  $SP_{A_j}(t)$  as it is a function of hazard and infrastructure system. In this situation, the state of infrastructure system when  $A_j$  occurs is different from the state of the system before the hazard happens. The adaptive capacity of infrastructure system after occurrence of hazard  $A_j$  changes due to the impacts of hazard  $A_i$  and corresponding consumption of repair resources.

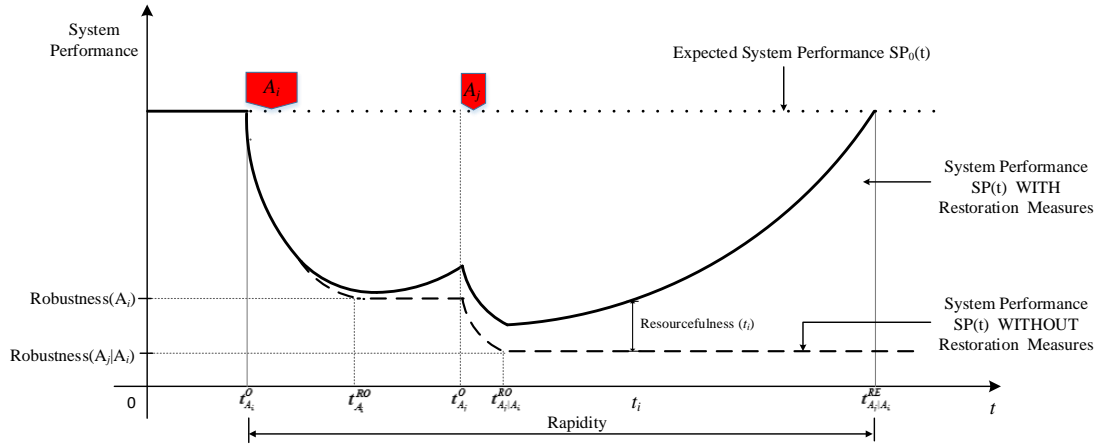


**Figure 4 Typical infrastructure system performance under two sequential hazards**

Another typical relationship of two hazards is concurrent occurrence of hazards. Infrastructure systems are exposed to two hazards simultaneously. State of the single infrastructure system under the interaction of the two hazards is usually much more complex due to various infrastructure interdependences. The two concurrent hazards can be considered as one sever hazard as the result of two joint forces to be addressed by infrastructures' adaptive capacity. The multilayer infrastructure network performance under two concurrent hazards is illustrated in Figure 5, which is similar to the system performance under the single hazard. However, robustness, resourcefulness and rapidity of multilayer infrastructure network under two concurrent hazards are lower than those exposed to a single hazard with the same available repair resources.

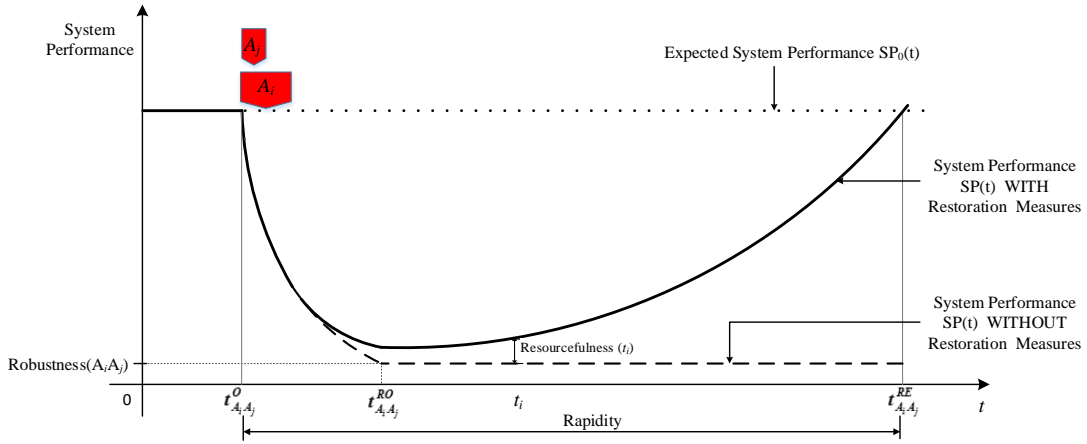


**Figure 5 Typical infrastructure system performance under two concurrent hazards**

Expanding on the deterministic resilience model in Equation (1) and system performance under multiple hazards relation, such as Figures 3-5 and Equations (2) and (3), multi hazard resilience could be expressed as

$$r^{A_1 \dots A_m}(t) = \frac{\int_{t_{A_1}^O}^t SP(t) dt}{\int_{t_{A_1}^O}^t SP_0(t) dt} = \frac{\sum_{i=1}^m \int_{t_{A_i}^O}^{t_{A_i}^*} SP(t) dt}{\int_{t_{A_1}^O}^t SP_0(t) dt} = 1 - \frac{\sum_{i=1}^m \int_{t_{A_i}^O}^{t_{A_i}^*} SL(t) dt}{\int_{t_{A_1}^O}^t SP_0(t) dt} \quad (4)$$

where  $r^{A_1, \dots, A_m}(t)$  is multi hazards  $A_1, \dots, A_m (m \geq 2)$  resilience of multilayer infrastructure network. Subscripts of hazard  $A_1, \dots, A_m$  are in order of precedence. The  $t_{A_i}^O$  is the occurrence of hazard  $A_i$ ,  $t_{A_i}^* = \min\{t_{A_i}^{RE}, t_{A_{i+1}}\}$ .

As vulnerability functions (fragility curves) of infrastructures obtained generalized agreement on multi-risk analysis <sup>(32,33)</sup>, state of infrastructures is random, and the actual system performance ( $SP(t)$ ) and system loss ( $SL(t)$ ) of multilayer infrastructure network are also of stochastic character. The multi hazards resilience can be seen as an expected value, and Equation (4) can be modified as

$$r^{A_1, \dots, A_m}(t) = \frac{\sum_{i=1}^m \int_{t_{A_i}^O}^{t_{A_i}^*} E(SP(t)) dt}{\int_{t_{A_1}^O}^t E(SP_0(t)) dt} = 1 - \frac{\sum_{i=1}^m \int_{t_{A_i}^O}^{t_{A_i}^*} E(SL(t)) dt}{\int_{t_{A_1}^O}^t E(SP_0(t)) dt} = 1 - \frac{\sum_{i=1}^m \int_{t_{A_i}^O}^{t_{A_i}^*} \frac{\sum_{u=1}^N P_u(t)}{N} dt}{\int_{t_{A_1}^O}^t \frac{\sum_{u=1}^N P_u^E(t)}{N} dt} \quad (5)$$

where  $E(SP(t))$  is the expected value of actual performance of multi-layer infrastructure network;  $E(SP_0(t))$  is the expected value of expected performance of multilayer infrastructure network;  $E(SL(t))$  is the expected value of expected loss of multilayer infrastructure network;  $N$  is the size of multilayer infrastructure network;  $P_u$  is the damage probability of  $u$ th infrastructure; and  $P_u^E$  is the expected damage probability of  $u$ th infrastructure, which always equals to 0. Accordingly, features (robustness, resourcefulness, rapidity) of multi hazards resilience are also the corresponding expected values.

Actually, infrastructure systems always have backup facilities, “slack” resources, redundancy or structure modularity <sup>(51)</sup>, so the functional loss would not be the same as the physical damages <sup>(53)</sup>. The normal way to analyze functional resilience of multi hazards is to measure importance of infrastructure ( $I_u$ ) with corresponding metrics. Examples may include operation facilities for system technical performance, population served, economic benefits of industry supported, or areas of society uninfluenced <sup>(53,54)</sup>, etc. Then the multi hazard functional resilience can be expressed as

$$r_F^{A_1, \dots, A_m}(t) = \frac{\sum_{i=1}^m \int_{t_{A_i}^o}^{t_{A_i}^*} E(SP(t)) dt}{\int_{t_{A_1}^o}^t E(SP_0(t)) dt} = 1 - \frac{\sum_{i=1}^m \int_{t_{A_i}^o}^{t_{A_i}^*} E(SL(t)) dt}{\int_{t_{A_1}^o}^t E(SP_0(t)) dt} = 1 - \frac{\sum_{i=1}^m \int_{t_{A_i}^o}^{t_{A_i}^*} \frac{\sum_{u=1}^N P_u(t) I_u}{N} dt}{\int_{t_{A_1}^o}^t \frac{\sum_{u=1}^N P_u^E(t) I_u}{N} dt} \quad (6)$$

The former resilience can be seen as the physical resilience of infrastructure system. The features (robustness, resourcefulness, rapidity) of multi hazard functional resilience would also change correspondingly.

### 3 MULTI HAZARD RELATIONSHIPS AND DIRECT IMPACTS ON INFRASTRUCTURE

This section provides framework for the analyses of multi hazard impacts.

#### 3.1 Relationships Between Multiple Hazards

A multitude of approaches is in use to describe relationships between multiple hazards<sup>(33)</sup>. Two basic ideas for the assessment of impacts of multiple hazards are: (i) to investigate the possible individual chains of hazardous events and to assess probability of impacts in order to develop risk maps or assess the risk of coincidences of multiple hazards; and (ii) to develop a matrix of possible hazard cascades and influences by proposing the respective processes<sup>(56)</sup>. Temporal and spatial relationships between multiple hazards are analyzed using the impacts of multiple hazards on infrastructure system, especially damage probability  $P_u$  (in Equation (2)) of each infrastructure. Therefore, diverse forms of impacts have to be considered: single hazard impact, impact of joint hazards, and conditional hazard impact.

##### 3.1.1 Temporal relationships of multiple hazards

The temporal relationships of multiple hazards are classified according to occurrence time of multiple hazards. Two main types of relationships are: (i) coincidence of multiple hazards in the event of more than one hazard occurring in the same general area and within a short time<sup>(5)</sup>; and (ii) sequence of multiple hazards when one hazard triggers other hazards with different occurrence probabilities<sup>(52)</sup>. Considering three sections of the dynamic system performance curve under a single hazard, both time and duration are relevant for multiple hazard resilience. Also, hazards can cause

fatigue damage in the case of a long duration. In this work, the time of hazard occurrence and end are considered as two dimensions of temporal relationships. It is worth noting that mutex hazards would never co-occur, so this kind of relationship is not being considered in this research.

Given disturbance event  $E$  including multiple hazards  $\{A_1, A_2, \dots, A_i, \dots, A_n\}$ , where  $A_i$  is  $i$ th hazard, and assuming that all hazards occur in the same area, there are three basic temporal relationships between multiple hazards: impacts of a single hazard; joint impacts; and conditional impacts. Single hazard impacts occur when only one hazard hits the area and no other hazards occur before or at the same time. Joint impacts occur when the area is impacted by two or more hazards at the same time. Conditional impacts describe the situation when the area is impacted by subsequent hazards before the end of initial hazardous event. Diverse temporal relationships between multiple hazards result in possibly large combinations of impacts.

Let us consider two hazards  $A_i$  and  $A_j$  ( $i \neq j$ ). There are four possible types of temporal relationships that could result in different impacts on the infrastructure. Here  $t_{A_i}^O$  and  $t_{A_i}^E$  denote the beginning and end times of hazard  $A_i$ , and  $D_i$  is the duration of hazard  $A_i$ .

*Type 1:* Joint impacts occur when  $A_i$  and  $A_j$  begin and end at the same time. Temporal relationship of the two hazards is shown in Figure 6 (a), and can be expressed as

$$t_{A_i}^O = t_{A_j}^O \text{ and } t_{A_i}^E = t_{A_j}^E \quad (7)$$

*Type 2:* Joint and conditional impacts occur when  $A_i$  and  $A_j$  begin at the same time and end at different times. Temporal relationship of the two hazards is shown in Figure 6 (b), and can be expressed as

$$t_{A_i}^O = t_{A_j}^O \text{ and } t_{A_i}^E \neq t_{A_j}^E \quad (8)$$

During  $\min\{D_i, D_j\}$ , the infrastructure is impacted by the two hazards jointly. During  $\max\{D_i, D_j\} - \min\{D_i, D_j\}$ , the infrastructure would be impacted by the hazard with longer duration but with the conditional impacts.

Type 3: Single and conditional impacts occur when  $A_i$  and  $A_j$  begin at different time and the end time of the  $A_i$  is not later then the beginning time of  $A_j$ . Temporal relationship of the two hazards is shown in Figure 6 (c), and can be expressed as

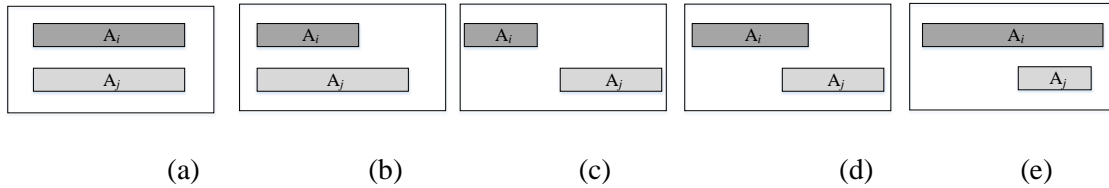
$$t_{A_i}^O \neq t_{A_j}^O \text{ and } t_{A_i}^E \leq t_{A_j}^O \quad (9)$$

Assuming  $A_i$  begins earlier than  $A_j$ , during  $D_i$ , the infrastructure is impacted only by  $A_i$ . After the  $A_j$  beginning, the infrastructure is impacted by  $A_j$  conditional on impacts of  $A_i$ .

Type 4: Single, joint and conditional impacts occur when  $A_i$  and  $A_j$  begin at different times and the end time of  $A_i$  is later then the beginning time of  $A_j$ . Temporal relationships of the two hazards are shown in Figures 6 (d) and (e), and can be expressed as

$$t_{A_i}^O \neq t_{A_j}^O \text{ and } t_{A_i}^E > t_{A_j}^O \quad (10)$$

Assuming  $A_i$  begins earlier than  $A_j$ , during  $A_j^{TO} - A_i^{TO}$  the infrastructure is only impacted by  $A_i$ . During  $\min\{t_{A_i}^E, t_{A_j}^E\} - t_{A_i}^O$ , it is impacted by the  $A_i$  and  $A_j$  jointly. During  $\max\{t_{A_j}^E - t_{A_i}^E, t_{A_i}^E - t_{A_j}^E\}$ , the infrastructure is only impacted by the hazard that ends later and is exposed to conditional impacts by the both hazards.



Light grey and dark gray rectangles denote two different hazards. Rectangle length denotes the duration.

**Figure 6 Temporal relationships between two hazards**

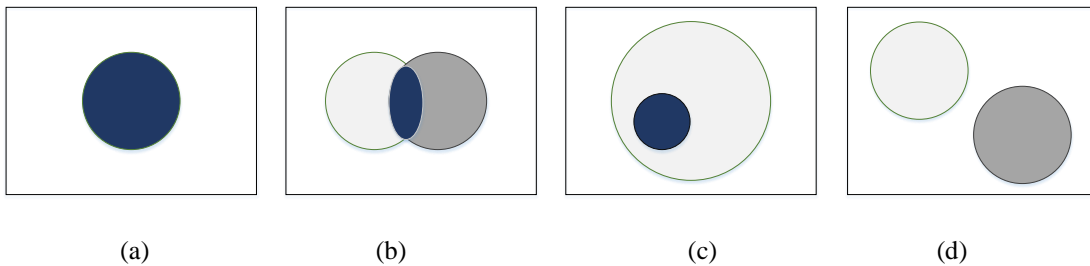
In the case of  $n$  hazards, there will be theoretically  $2n(n-1)$  types of temporal relationships among them. According to their cause-and-effect relationships, temporal relations among them might not occur in reality or may have a very small probability of co-occurrence. Most often the temporal relationships between multiple hazards might be the latter two conditions (different beginning and end times of multiple hazards). Multiple hazards result in diverse combinations of conditional and joint impacts on the area. Consideration of hazards durations using the event chain

and event tree methods could clearly show multiple hazards temporal relationships (and impacts) during the whole time an area is affected by hazards.

### 3.1.2 Spatial relationships of multiple hazards

Spatial relationships between multiple hazards describe their impacts within an area and their geographic interactions with more detailed evolution progress. Hazards usually affect limited areas with specific exposure. The damages from multiple hazards could be different, even if they have the same magnitude, due to their spatial evolution within the affected area.

Multiple hazards may have different spatial relationships with diverse magnitudes within a given area. The possible relationships may include: (i) overlap of areas impacted by multiple hazards as shown in Figure 7 (a); (ii) partial overlap of areas impacted by multiple hazards as illustrated in Figures 7 (b) and (c). Usually, the secondary hazards impact the smaller areas than the primary hazards - for example, the earthquake followed by fire, or hurricane followed by flood, and similar; and (iii) no overlap between areas impacted by multiple hazards as shown in Figure 7 (d). It is worth noting that the above three types of spatial relationships could occur in combination with any of the temporal relationships introduced earlier.



Light grey and dark grey circles denote two different hazards. Dark blue color is the overlap area impacted by two hazards.

**Figure 7 Spatial relationships between two hazards**

The three types of spatial relationships between multiple hazards will result in a single and joint impacts on the affected area. Let us consider an event  $E$  including multiple hazards  $\{A_1, A_2, \dots, A_i, \dots, A_n\}$  where  $S_{A_i}$  denotes the spatial area

impacted by the hazard  $A_i$ . Then, at a given time, the three spatial relations between multiple hazards can be expressed as follows.

*Type 1:* Joint impacts occur when all the hazards impact areas of overlap as shown in Figure 7 (a). Spatial relationship between the multiple hazards can be expressed as

$$S_{A_1} = S_{A_2} = \dots = S_{A_i} = \dots S_{A_n} \quad (\forall A_i, A_j \in E, i \neq j) \quad (11)$$

*Type 2:* Single and joint impacts occur when the impacted areas by multiple hazards partly overlap as in Figures 7 (b) and (c). Spatial relationship between the multiple hazards can be expressed as

$$S_{A_i} \cap S_{A_j} \neq \emptyset \quad (\exists A_i, A_j \in E, i \neq j) \quad \text{and} \quad S_{A_i} \neq S_{A_j} \cap \emptyset \quad (\exists A_i, A_j \in E, i \neq j) \quad (12)$$

*Type 3:* Single impact of multiple hazards occur when the impacted areas by multiple hazards do not overlap as in Figure 7(d). Spatial relationship between the multiple hazards can be expressed as

$$S_{A_i} \cap S_{A_j} = \emptyset \quad (\forall A_i, A_j \in E, i \neq j) \quad (13)$$

### 3.1.3 Relationship cube of multiple hazards

The multiple hazards impact analysis framework could be constructed as a cube (see Figure 8) by combining temporal and spatial relationships discussed previously. As infrastructure systems (like water storage facilities, pumping stations, electric substations, and so on) are sparsely located in space, their components could be impacted at different time by different hazards. The model presented in this study focuses on the impacts of multiple hazards on infrastructure system. Multiple hazards relationships within each sub-cube of the relationship cube (Figure 8) may result in different impacts on the infrastructure system.

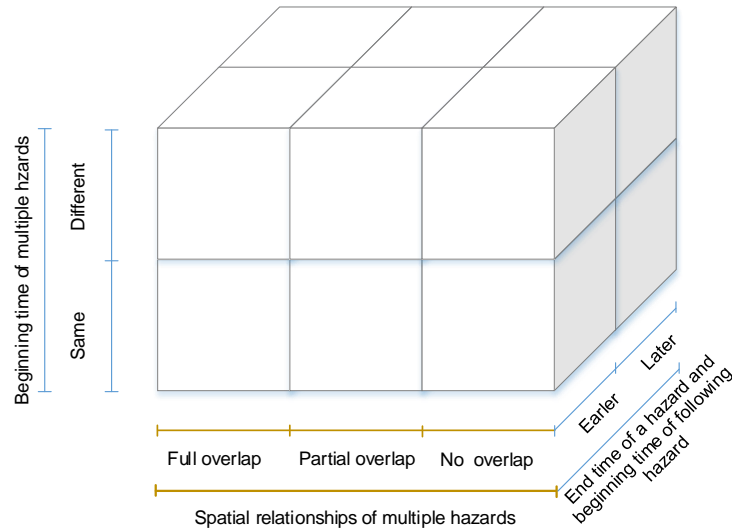


**Figure 8 Relation cube of multiple hazards**

Note, that both spatial and temporal scales can be very broad. Hazards can influence spatial areas, from fractions of a kilometer squared, such as a landslide, to hundreds of millions of kilometers squared, such as tsunamis. The durations of hazards can also range from seconds, such as an earthquake, to millennia, such as long-term climate change <sup>(52)</sup>. Temporal and spatial scales used for multiple hazards risk analyses should not focus on the characteristics of an individual hazard, but consider their impact and interaction ranges. Since the infrastructure systems are always sparsely located and operated within a governing structure, the spatial scale could be the same as the geographic boundaries of a community, a city, a province, or a country. Hourly temporal scale of multiple hazards impacts is appropriate in most cases, since the repair time of most infrastructure systems is measured in hours <sup>(19,57)</sup>.

### **3.2 Impacts of Multiple Hazards on Infrastructure Systems**

In current practice, there is almost a general agreement for using vulnerability functions (fragility curves) to facilitate risk analyses of multiple hazards <sup>(32,33)</sup>. Fragility stands for the probability of a system or a system component reaching or exceeding an established performance level under the impact of a perturbation of known intensity <sup>(58)</sup>. The failure probability of each element of infrastructure system depends on the type and intensity of hazards they are exposed to, while taking into account the local terrain and infrastructure structural characteristics. Mostly, fragility curves of diverse infrastructures can be obtained from the domain research. For example, the electric transmission station fragility curves under hurricane can be developed from the research in electrical engineering <sup>(13,19)</sup>, the hydropower

fragility curve under flood can be developed from the research in hydro technical engineering <sup>(59)</sup>, and so on. More recently, some statistic methods have been introduced to obtain the fragility curve/rule of single building/facility without experimental data <sup>(60)</sup>.

### 3.2.1 Direct impacts of two hazards

Let us consider two hazards  $A_i$  and  $A_j$  ( $i \neq j$ ).  $P_u(A_i)$ ,  $P_u(A_j)$  are corresponding damage probabilities of the  $u$ th infrastructure subject to single hazard  $A_i$  and  $A_j$  exceeding specific threshold (like flood inundation depth, gust wind speed of hurricane, or peak ground acceleration of an earthquake). Usually,  $P_u(A_i)$  and  $P_u(A_j)$  are kind of physical infrastructure characteristics corresponding to specific design criteria. They can be obtained from the statistical data, and are known as the fragility curves.

Based on the relationship cube, there are twelve types of relationships between two hazards. Their direct (physical) impacts on infrastructures are as follows:

(i) *Impacts of hazards  $A_i$  and  $A_j$  with temporal relationship shown by Equation (7) and spatial relationship shown by Equation (11)*

The two hazards  $A_i$  and  $A_j$  begin and end at the same time. Infrastructures located in the area are affected simultaneously. The state of the infrastructure would be determined by two hazards joint damage probability  $P_u(A_i A_j)$  during  $D_i$  (or  $D_j$ ), which is known as the fragility surface <sup>(61-63)</sup>, instead of sum of separate fragility curves.

(ii) *Impacts of hazards  $A_i$  and  $A_j$  with temporal relationship shown by Equation (7) and spatial relationship shown by Equation (12)*

The two hazards  $A_i$  and  $A_j$  begin and end in two areas with intersection. Infrastructures located in the intersected area are affected by the two hazards simultaneously, and their damage probability is determined by two hazards joint damage probability  $P_u(A_i A_j)$  during  $D_i$  (or  $D_j$ ). Infrastructure located in other areas is only affected by a single

hazard,  $A_i$  or  $A_j$ , and their damage probabilities could be obtained correspondingly as  $P_u(A_i)$  or  $P_u(A_j)$  during  $D_i$  (or  $D_j$ ).

(iii) *Impacts of hazards  $A_i$  and  $A_j$  with temporal relationship shown by Equation (7) and spatial relationship shown by Equation (13)*

The two hazards  $A_i$  and  $A_j$  begin and end in different areas. Infrastructures are only impacted by a single hazard,  $A_i$  or  $A_j$ . The damage probability of infrastructure located in specific area is determined by corresponding hazard, and equals to  $P_u(A_i)$  or  $P_u(A_j)$  during  $D_i$  (or  $D_j$ ).

(iv) *Impacts of hazards  $A_i$  and  $A_j$  with temporal relationship shown by Equation (8) and spatial relationship shown by Equation (11)*

The two hazards  $A_i$  and  $A_j$  begin in the same area at the same time, but end at different time. Assuming  $D_i$  shorter than  $D_j$ , infrastructures would be impacted by both hazards during  $D_i$ , and impacted by hazard  $A_j$  during  $D_j$ . So, the damage probability of infrastructures during  $D_i$  is two hazards joint damage probability  $P_u(A_i A_j)$ , and equals to  $P_u(A_j | A_i A_j)$  during  $D_j - D_i$ .

(v) *Impacts of hazards  $A_i$  and  $A_j$  with temporal relationship shown by Equation (8) and spatial relationship shown by Equation (12)*

The two hazards  $A_i$  and  $A_j$  begin at the same time, end at different time, and affect two areas with intersection. Assuming  $D_i$  shorter than  $D_j$ , there are two situations as the intersected area affected is different during  $D_i$  or  $D_j - D_i$ . If the intersected areas are affected during  $D_i$ , the state of infrastructures located in these areas would be determined by two hazards joint damage probability  $P_u(A_i A_j)$ , or else would be determined by conditional damage probability  $P_u(A_j | A_i)$ . The damage probabilities of infrastructures located in other impacted areas are determined by corresponding single hazards, equal to  $P_u(A_i)$  or  $P_u(A_j)$  during the  $D_i$  or  $D_j$ .

(vi) *Impacts of hazards  $A_i$  and  $A_j$  with temporal relationship shown by Equation (8) and spatial relationship shown by Equation (13)*

The two hazards  $A_i$  and  $A_j$  begin at the same time, end at different time, and affect two different areas. Infrastructures could only be affected by single hazard  $A_i$  or  $A_j$ . Damage probability of infrastructures located in specific area is determined by corresponding hazard, and equals to  $P_u(A_i)$  during  $D_i$  or  $P_u(A_j)$  during  $D_j$ .

(vii) *Impacts of hazards  $A_i$  and  $A_j$  with temporal relationship shown by Equation (9) and spatial relationship shown by Equation (11)*

The two hazards  $A_i$  and  $A_j$  begin at different time and affect the same area.  $A_j$  begins later than the end of  $A_i$ . During  $D_i$ , infrastructure can only be attacked by single hazard  $A_i$ , and the damage probability is equal to  $P_u(A_i)$ . During  $D_j$ , infrastructures are only affected by a single hazard  $A_j$ . Then the damage probability is equal to  $\eta P_u(A_j | A_i)$ , where  $\eta$  is a restoration parameter. It denotes the state of an infrastructure at the beginning time of  $A_j$ , and is a function of the restoration strategy.

(viii) *Impacts of hazards  $A_i$  and  $A_j$  with temporal relationship shown by Equation (9) and spatial relationship shown by Equation (12)*

The two hazards  $A_i$  and  $A_j$  begin at different time, don't have temporal overlap but overlap in space. During  $D_i$ , infrastructure can only be affected by a single hazard  $A_i$ , and its damage probability is equal to  $P_u(A_i)$ . During  $D_j$ , infrastructures located in the intersection area would have damage probabilities of  $\eta P_u(A_j | A_i)$ , or else as  $P_u(A_j)$ .

(ix) *Impacts of hazards  $A_i$  and  $A_j$  with temporal relationship shown by Equation (9) and spatial relationship shown by Equation (13)*

The two hazards  $A_i$  and  $A_j$  begin at different time and in different areas, and don't have temporal overlap. Then the infrastructures could only be affected by single hazard  $A_i$  or  $A_j$ . The damage probability of infrastructures located in specific area is determined by corresponding hazard, equals to  $P_u(A_i)$  during  $D_i$  and  $P_u(A_j)$  during  $D_j$ .

(x) *Impacts of hazards  $A_i$  and  $A_j$  with temporal relationship shown by Equation (10) and spatial relationship shown by Equation (11)*

The two hazards  $A_i$  and  $A_j$  begin at different time and in the same area, and have temporal overlap. Assuming  $t_{A_i}^o < t_{A_j}^o$ , the damage probability of infrastructures is equal to  $P_u(A_i)$  during  $t_{A_j}^o - t_{A_i}^o$ . During the temporal overlapping period, it is equal to  $\eta P_u(A_i A_j | A_i)$ . During the remaining time, it is equal to  $\eta P_u(A_i | A_i A_j)$  or  $\eta P_u(A_j | A_i A_j)$ .

(xi) *Impacts of hazards  $A_i$  and  $A_j$  with temporal relationship shown by Equation (10) and spatial relationship shown by Equation (12)*

The two hazards  $A_i$  and  $A_j$  begin at different time, and have both temporal and spatial overlap. Assuming  $t_{A_i}^o < t_{A_j}^o$ , the damage probability of infrastructures is equal to  $P_u(A_i)$  during  $t_{A_j}^o - t_{A_i}^o$ . During the temporal overlapping period, there are two situations. Damage probability of infrastructures located in the spatial overlapping area equals to  $\eta P_u(A_i A_j | A_i)$ , or else  $\eta P_u(A_i)$  or  $\eta P_u(A_j)$ . During the remaining time, the damage probability of infrastructures located in the spatial overlapping area is equal to  $\eta P_u(A_j | A_i A_j)$ , or else  $\eta P_u(A_i)$  or  $\eta P_u(A_j)$ .

(xii) *Impacts of hazards  $A_i$  and  $A_j$  with temporal relationship shown by Equation (10) and spatial relationship shown by Equation (13)*

The two hazards  $A_i$  and  $A_j$  begin at different time and in different areas, and have temporal overlap. Infrastructures could only be affected by single hazard  $A_i$  or  $A_j$ . The damage probability of infrastructure is determined by corresponding hazard and equals  $P_u(A_i)$  or  $P_u(A_j)$ .

The direct impact on infrastructures of two hazards with twelve temporal-spatial relationships analyzed above is the framework further developed in this study. The implementation takes into consideration: (i) that the damage probability of infrastructures characterized by different material and structural characteristics and acceptable loss threshold levels, affected by hazards of different magnitudes is different; (ii) the changing magnitude and force of hazards result in different damage probability of infrastructures that may be calculated with the same set of relationships; and (iii) different restoration strategies. Multiple hazard direct impact analysis framework includes two situations arising from combination of Equations (10) and (11), and combination of Equations (10) and (12). In these

scenarios, there are intervals between two hazards when the implementation of restoration strategies can be initiated. Besides, the implementation of response strategies can be initiated in the situations when the disaster lasts for more than several days and does not destroy the whole area.

### 3.2.2 Direct impacts of multiple hazards

Based on the analysis of two hazards above, it can be generalized that the infrastructure damage probability subject to events  $E$  with more than two hazards  $\{A_1, A_2, \dots, A_i, \dots, A_n\}$  can be expressed with combination of conditional and joint damage probabilities caused by individual hazards, as follows:

$$P_u(E) = \begin{cases} \eta P_u(\prod_m A_i | \prod A_{i-}^s) & \text{during } T_{overlap\_i} \\ \eta P_u(A_i) & \text{else} \end{cases} \quad (14)$$

where  $m$  denotes the number of spatially overlapping hazards during specific period;  $T_{overlap\_i}$  is the duration of overlapping multiple hazards before beginning time of hazard  $A_i$ ;  $A_{i-}^s$  denotes hazards affecting the infrastructure before  $A_i$ ; and  $\eta$  is the restoration parameter which is a function of restoration strategy.

### 3.2.3 Failures propagation mechanism and indirect impacts of multiple hazards on infrastructures

Individual infrastructure systems consist of numerous and distributed components. Several components' damage or localized impact of natural or manmade disasters would cause the whole system to fail <sup>(64)</sup>. In addition, the small failures of a few components could propagate to other infrastructure, and result into a huge disaster to the society and economy. Therefore, cascading failures need to be addressed in the analyses of infrastructure system resilience and risk. Two types of interdependences need to be considered: intra-network and inter-network failure propagation mechanisms.

As different kind of infrastructure systems have different operating rules, they may have different failure propagation mechanisms. Some examples include Motter-Lai (ML) model <sup>(65,66)</sup> and ORNL-Pserc-Alaska (OPA) model <sup>(67,68)</sup> of

power grid failure propagation <sup>(69)</sup>, router-based model of telecommunication system <sup>(70)</sup>, pipeline flow model of gas system <sup>(71)</sup>, and so on.

Infrastructures are interdependent in multiple ways. The interdependencies can be characterized as either physical, cyber, geographic and logical <sup>(72)</sup>, or physical, geospatial, policy and informational <sup>(40)</sup>. Based on these qualitative studies, network based approaches always use inter-links along with detailed descriptions of their topologies and flow patterns to describe inter-network interdependencies. Therefore, the network interdependences can be classified into topology- based methods and flow-based methods <sup>(73)</sup>. In many cases appropriate intra-network and inter-network interdependences can be modeled by the existing models or with some appropriate modifications to construct multi layer infrastructure network failure propagation mechanisms.

The intra-network and inter-network failure interdependence modes without indirect (or functional) link failures are determined by the failure of connecting nodes. Then indirect or actual damage probability of each node can be calculated as

$$P_u^{indirect}(t) = \prod_{u-p} \sum_{p-n} P_{u-pn}^i(t) \quad (15)$$

where  $P_u^{indirect}(t)$  is interdependent node damage probability at  $t$ ;  $u-p$  is the number of paths connecting the  $u$ th node to source nodes;  $p-n$  is the number of nodes on each path; and  $P_{u-pn}^i(t)$  is the node's damage probability.

#### **4 MULTI HAZARDS RESILIENCE ASSESSMENT APPROACH**

A multiple hazards resilience assessment methodology of interdependent infrastructure system is developed by integrating all the models presented above. The general approach contains three steps. The first step involves the interdependent infrastructure system modelling, which includes (i) single type of internally interdependent infrastructure; and (ii) multiple types of externally interdependent infrastructures <sup>(51)</sup>. The second step involves development of multiple hazards relationship model and assessment of indirect impacts on infrastructures. The third

step includes assessment of indirect failures as a consequence of infrastructure interdependencies, and spatial-temporal system resilience. The research framework and process are illustrated in Figure 9.

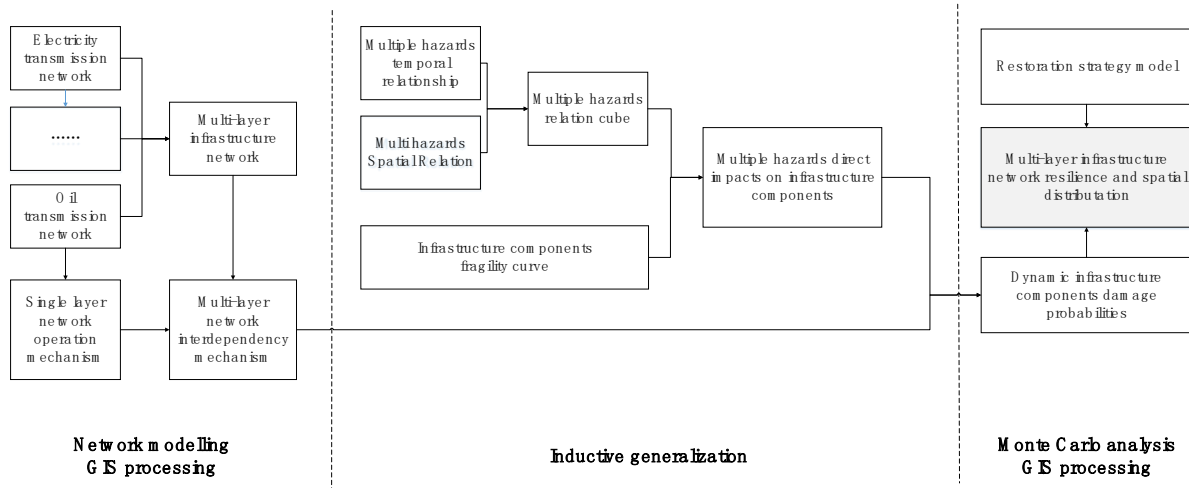


**Figure 9 Framework for the assessment of multiple hazards resilience of interdependent infrastructure system**

Network theory offers an important set of methods that can be used to model complex infrastructure system behavior under various disturbances. The spatial/geographic characteristics of the region under consideration play an essential role in the description of infrastructure system and characterization of hazards. Therefore, spatial network modelling is starting to get more serious attention. Many applications are being developed in disaster analysis and prevention using Geographical Information Systems (GIS) <sup>(45)</sup> as appropriate tools for processing spatial data. Network theory and GIS technology are combined in this study to model the response of large-scale interdependent infrastructure system under multiple disturbances/hazards.

Formulation of relationships between multiple hazards is the critical problem of risk and resilience analysis. With focus on their diverse combined impacts on the infrastructure system, temporal and spatial decompositions of relationships are done according to the relationship cube. Inductive generalization is used to construct the multiple hazards relationship analysis framework, which is not limited to a specific hazards chain. Statistical fragility of components and infrastructure network topology are combined to capture composite impacts of multiple hazards.

Infrastructure system resilience is not directly related to geographic distribution, topology and spatial interdependence of infrastructure components. However, the characteristics of resilience are directly related to the type, scale and

relationship of the disturbances. Some initial work on integrating temporal and spatial characteristics of complex system behaviour under disturbance in order to assess spatially dynamic resilience is available in the area of flood risk management <sup>(48)</sup> and multipurpose reservoir operations <sup>(74,75)</sup>. As the impacts of hazards always contain uncertainty and occur randomly, the infrastructure system resilience metric is defined in a probabilistic form and consists of a multiple hazards performance network analysis combined with Monte Carlo simulation. The results of the probabilistic infrastructure system resilience analyses are the multi-layer network temporal resilience curves and spatial distribution of damage probabilities.

## **5 MULTILAYER INTERDEPENDENT INFRASTRUCTURE NETWORK**

This section presents interdependent infrastructure system model of the Greater Toronto Area (GTA) energy infrastructure system. All the data used in this study are in public domain provided by the owners of the infrastructure. To validate the data, maps and reports available by the infrastructure owners including IESO (The Independent Electricity System Operator), Hydro One and CEPA (Canadian Energy Pipeline Association) are used together with the CanVec data. CanVec is a digital cartographic reference product of Natural Resources Canada (NRCan) combining the National Topographic Data Base (NTDB), the Mapping the North process conducted by the Canada Center for Mapping and Earth Observation (CCMEO), the Atlas of Canada data, the GeoBase initiative, and available satellite imagery.

### **5.1 GTA Energy Infrastructure Spatial Network**

The Greater Toronto Area (GTA) is the most populated metropolitan area in Canada, which is defined as the central City of Toronto and its four surrounding regional municipalities: Durham, Halton, Peel, and York. In this paper, electric, gas and oil transmission networks of the GTA are taken for the implementation of the proposed approach. GTA electric transmission network is built from the CanVec data <sup>(76)</sup>, IESO and Hydro One reports <sup>(77,78)</sup>. GTA gas and oil transmission networks are built from the CanVec data <sup>(76)</sup> and CEPA maps <sup>(79,80)</sup>. GTA three-layer energy infrastructure spatial network is illustrated in Figure 10.

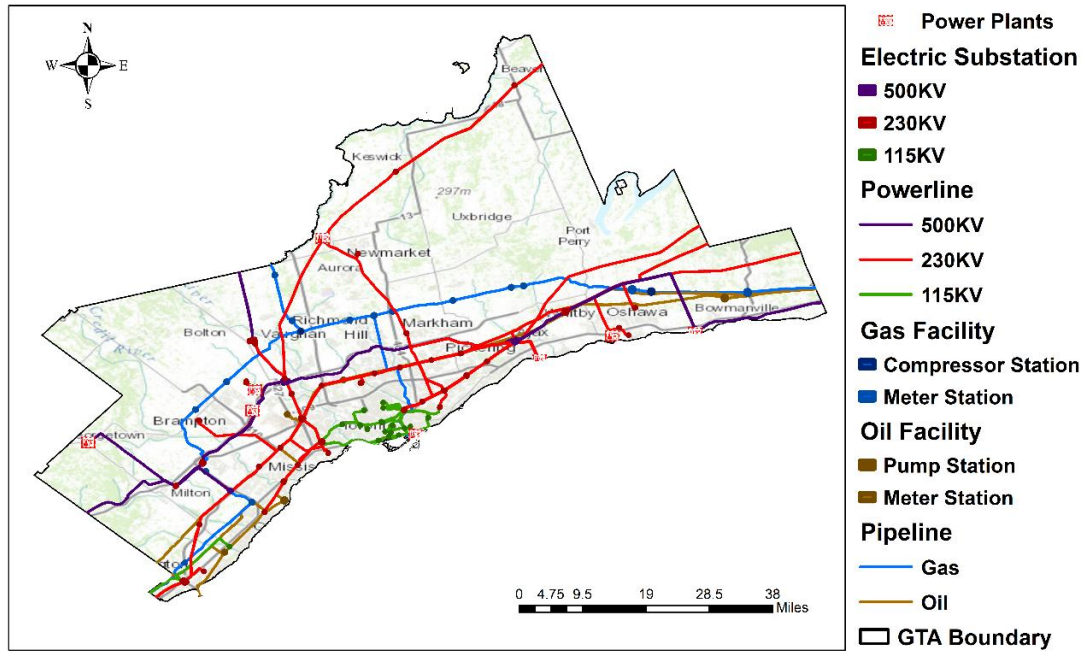


**Figure 10 GTA three-layer energy infrastructure spatial network**

GTA electric transmission network refers to the Bulk Power System (BPS) of GTA, including the generation and transmission stations and power lines. There are three types of power plants in GTA: nuclear, gas-fired and solar power stations; three types of transmission lines with different voltage- 500kv, 230kv and 115kv. GTAA Cogeneration Plant is not considered here as its capacity is only 90 MW and its primary role is to provide the power to the Toronto Pearson International Airport. There are no gas or oil production facilities in GTA. Therefore, the gas and oil transmission networks contain only transmission facilities: compressor stations, meter stations, pump stations and pipelines. Due to limited data availability, no information on the capacity of gas and oil facilities are provided here. GTA energy infrastructure system information is provided in Table 1.

**Table 1 GTA three-layer energy infrastructure spatial network information**

Infrastructure		Number
Electric Transmission Network		
Power Generation	Nuclear	2
	Gas -fired	6
Transmission Stations	500kv	4
	230kv	43
	115kv	26
Power line	500kv	13
	230kv	64
	115kv	30
Gas Transmission Network		
Compressor Stations		2
Meter Stations		15
Pipelines		22
Oil Transmission Network		
Pumping Stations		4
Meter Stations		1
Pipelines		6

## 5.2 Infrastructure Interdependence Models

Individual infrastructure systems consist of numerous and distributed components. Damage to several components or localized impact of natural or manmade disasters would cause the whole system to fail. In addition, the small failures of a few components could propagate to other infrastructure, and result into a large disaster to the society and economy. Therefore, cascading failures need to be addressed in the analyses of infrastructure system resilience and risk. Based on the three-layer GTA energy infrastructure network, two types of interdependences need to be considered: intra-network (within a layer) and inter-network (between the layers) failure propagation mechanisms. Intra-network interdependence is always modeled as operation mechanism for one type of infrastructure. Some examples include Motter-Lai (ML) model <sup>(80,81)</sup> of power grid failure propagation, pipeline flow model of gas system <sup>(82)</sup>, and so on. Inter-network interdependence focuses on the physical and functional interaction between different types of infrastructure, which includes topology-based or flow-based methods.

There are three types of infrastructure in the GTA energy infrastructure system: electric, gas and oil transmission networks. For electric transmission network, ML model is a prominent approach used to analyze cascading failures. In this model, nodes are differentiated as generators  $N_G$  (electricity generating plants) and loads  $N_L$ (substations). All nodes are interconnected by a set of edges representing power lines. The load of each substation node is defined as the number of most efficient paths from generations to substations that pass through that substation node <sup>(83)</sup>. Each substation node  $u$  is characterized by initial load  $L_u(0)$ , real load  $L_u(t)$ , and maximum load  $C_u = L_u(0) \times tp$ , where constant  $tp$  is a tolerance parameter. Each path connecting node  $u$  and  $v$  is characterized by the path efficiency  $e_{uv}(t)$ , representing relative link capacity. It is assumed that electricity is flowing between any pair of generator nodes and substation nodes through the most efficient path. An initial breakdown of edges surrounding a node causes power to be redistributed in the network, reflected by changes in the most efficient paths and, consequently, changes in the load at each node. Some nodes are then forced to operate above capacity (being overloaded), represented by decreases in efficiency of the edges of that node

$$e_{uv}(t+1) = \begin{cases} e_{uv}(0) & \text{else} \\ e_{uv}(0) \min\left(\frac{L_u(0)}{L_u(t)}, \frac{L_v(0)}{L_v(t)}\right) & \text{if } L_u(0) < L_u(t) \leq C_u \\ 0 & \text{if } L_u(t) > C_u \end{cases} \quad (16)$$

The substation fails when its path efficiency equals to 0. The failed substations would change the path efficiency of other substation nodes, and indeed change the electric transmission path in the network. Convergence in this iterative process occurs when the nodes states become stable. If we assume that the maximum load of every substation node in the network is the same, then the performance  $P(t)$  of electric power network can be computed as the fraction of available substation nodes. Here  $tp$  is set to 2 <sup>(84)</sup>. As the sizes of gas and oil transmission networks are small, their intra-network interdependence is also modeled using modified ML model without flow distribution or tolerance. The value of  $tp$  in each interdependence model is also set to 2.

The topology-based model is used for inter-network interdependence among the three types of infrastructure systems here. This report assumes that gas-fired power plants require gas to keep normal operation, and all types of gas and

oil nodes require electricity to keep their normal operation. As the networks considered are all limited to the major transmission systems, inter-network links are not shown in Figure 10 but are defined as follows: (i) gas-fired electric plants are supported by the nearest gas meter stations through gas transmission pipelines; (ii) gas and oil nodes are powered by the nearest electric transmission substations through power lines; and (iii) buffering is introduced as a popular emergency preparedness strategy that makes the infrastructure interdependence less tight. Each gas-fired electric plant has buffers in form of gas stock. The compressor stations, pumping stations and meter stations of gas and oil transmission networks have buffers in form of standby power generators. Buffers of the above infrastructure are measured in units of time and all assumed to be equal to one-time step (2 hours). Nodes would be non-operational in the case of malfunction of supporting nodes or destroyed connecting edges.

### 5.3 Physical and Functional Resilience Metric

Different aspects of infrastructure performance could be measured by using different units. To analyze details of the infrastructure dynamic evolution process, in this study the interdependent infrastructure system physical and functional resilience are evaluated respectively, which means different  $I_u$  in Equation (6). For physical resilience,  $I_u$  of each node in the multi-layer infrastructure network is calculated using its capacity. Then physical system performance is measured by the expected value of the proportion of weighted operational nodes. For example, the electric transmission substations weight is calculated proportional to their voltage.

The functional resilience,  $I_u$  of each node in the multi-layer infrastructure network is calculated using the number of customers being served. The functional system performance is measured by the expected value of the impacted population. As electric infrastructure is seen as the most important in the energy infrastructure system, population unaffected by electric loss is used as a measure of functional system performance here. Considering that the electric substations with larger than 500 kv capacity always function as the hub substations, population of GTA is allocated to a particular electric substation with 115 kv and 230 kv using the Thiessen Polygons (Figure 11). The Thiessen Polygons define areas of influence around each of a set of points whose boundaries define the area that is closest to given point relative to its neighbors. So, each single polygon can be considered as area served by one transmission

station. GTA population and the dissemination area boundaries data are obtained from the Canadian Census Analyser 2011<sup>(85)</sup>.

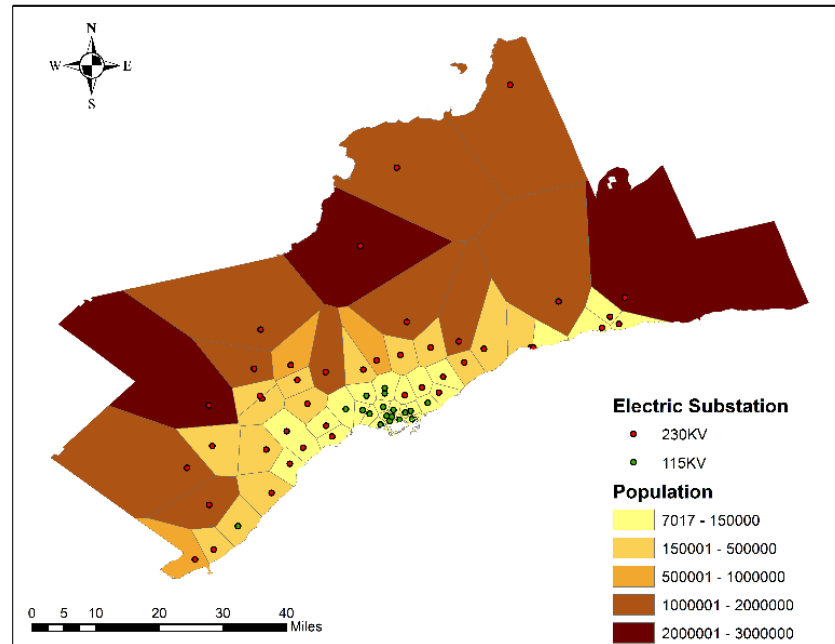


**Figure 11 Population supported by electric transmission substations in GTA**

## **6 SEQUENTIAL HAZARDS SCENARIO AND ITS IMPACTS**

This section describes a sequential hurricane-flood scenario used for GTA case study resilience analyses.

### **6.1 Sequential Hurricane and Flood Scenario**

Sequential hurricane and flood scenario is modelled based on the record of Hurricane Hazel, which was followed by a flood and struck Toronto on October 15, 1954. The path of Hurricane Hazel (Hurricane Hazel Storm Story Map) is downloaded from NOAA GeoPlatform. The information of the hurricane, storm surge and flood impacts are from government websites: Hurricane Hazel: 60th Anniversary and Environment and Climate Change Canada.

The records of Canadian Disaster Database<sup>(86)</sup> show that Hurricane Hazel, followed by flood, killed 81 people and left 1,896 families homeless. The record rainfall that the storm brought was unable to infiltrate the ground because the above-average rainfall in the preceding month had already saturated the soil. Most of the rain simply ran off the surface

into rivers and creeks, rapidly filling them to capacity and beyond. One estimate of runoff was that 90 percent of the precipitation ran off the land directly into rivers raising the water level by 6 to 8 meters <sup>(87)</sup>.

This disaster caused by combined impact of hurricane and flood is taken as the prototype disaster scenario for the implementation of the methodology developed in this study. Based on the historical records, the hurricane lasted for 24 hours with rainfall, then the flood occurred. It means the flood occurred during the damage and propagation phase, or evolution and recovery phase of the hurricane, dependent on the restoration starting time. Since the whole GTA area was affected by the hurricane, and only infrastructure located within the river basins was impacted by the flooding, there was a spatial overlap between the two hazards.

Based on the Saffir-Simpson Hurricane Wind Scale <sup>(88)</sup>, only hurricanes above category 3 (wind speed higher than 110 mph) cause flooding. The following assumptions are included in the GTA case study: (i) Hurricane Hazel was assumed to be a category 3 hurricane with gust wind speed of 120 mph and weakening to 40 mph after 24 hours; (ii) the hurricane path is the same as the path of Hurricane Hazel as retrieved from the ArcGIS web resources<sup>(89)</sup>; (iii) the area 50 kilometers from the hurricane path <sup>(90)</sup> was impacted by the hurricane with the same wind speed <sup>(91)</sup>; and (iv) impacted area of GTA is divided into four zones (with different hurricane occurrence time) perpendicular to hurricane path, and attacked successively from south to north. Figure 12 shows the spatial distribution of combined hurricane and flood impacts.

According to the flood classification of the National Weather Service Alaska-Pacific River Forecast Center, the flood following Hurricane Hazel is categorized as a major flooding event. As GTA is dissected by rivers and streams, infrastructure affected by the flood is also along rivers and streams. Based on the flood plain map of Toronto and Region <sup>(92)</sup> and Flood Vulnerable Area Clusters of GTA <sup>(93)</sup>, most impacted areas include Holland Marsh, Humber River basin, Woodbridge, Thistletown, Raymore Drive, Mount Dennis, Long Branch and Don River basin, and the flood depth in these areas exceeds 10 feet <sup>(94)</sup>. Combining the records of Hurricane Hazel impacts, hurricane occurrence time and the distance from the hurricane path, the flooded areas are identified and shown in Figure 12. There are only a limited number of infrastructure elements impacted directly (two power generating stations, six transmission substations, one submarine powerline, and one submarine gas transmission pipeline).

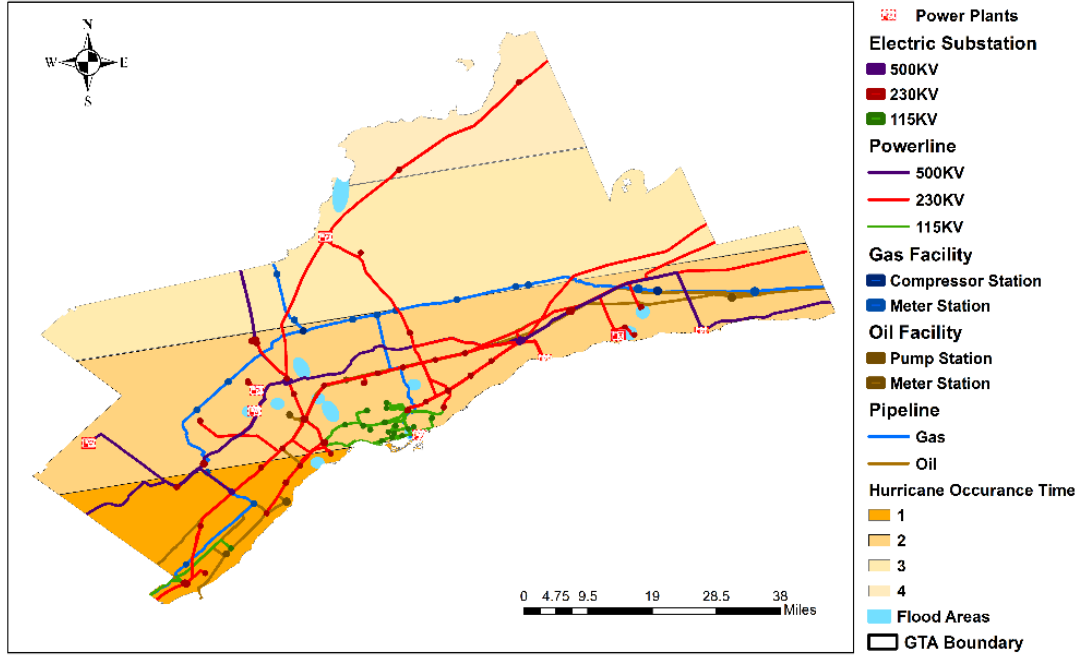


Figure 12 Sequential hurricane and flood impacts on GTA

## 6.2 Single Hazard Impacts on Infrastructure

Infrastructure component direct failure probabilities under single hazard can be computed by their fragility models under different hazards. All the infrastructure components vulnerability data under hurricane and flood are all from published papers, reports and HAZUS-MH platform.

In the case of a hurricane and power grid, power plants are mostly insensitive to structural hurricane damage and therefore their fragilities are not considered. The fragilities of transmission substations and transmission lines are estimated based on the work of Ouyang and Dueñas-Ororio<sup>(18)</sup>. The damage probability of substations is represented via log-normal fragility curves. These curves generate the probability of damage for a given wind gust speed ( $W_s$ ) while taking into account the local terrain and structural characteristics of the substation under consideration. The general form of the fragility curve is given as follows <sup>(95,96)</sup>.

$$P_{trans\_sub,u,l}(D \geq d_{ul} | W_s = x_u) = \int_0^{x_u} \frac{1}{\sqrt{2\pi}\sigma_{ul}w} \exp\left(\frac{-(\ln w - \mu_{ul})^2}{2\sigma^2}\right) dw \quad (17)$$

These curves generate four probabilities of the  $u$ th transmission station with different damage level ( $d_{ul}$ ): low, moderate, severe, and complete. Moderate level is used in this work.  $P_{trans\_sub,u,l}$  is the  $u$ th electric transmission substation moderate damage probability of exceedance given wind speed  $x_u$  at the substation site, calculated using the fragility curve corresponding to the terrain near the substation. The parameters  $\mu_{ul}$  and  $\sigma$  represent the logarithmic mean and standard deviation of the pertinent fragility curve. Fragility curves for each type of modeled terrain and building type are taken from HAZUS-MH technical report <sup>(96)</sup>.

Transmission lines consist of transmission support structures, conductors and various pieces of hardware. Due to design requirements <sup>(97)</sup>, the fragility of a transmission line under wind load (without considering debris impacts) is mainly determined by the failures of towers. The number of towers along a line is computed as the line length divided by the average span between two adjacent towers, which is set as 0.30 km based on the regional utility data. Based on the investigations by Quanta Technology <sup>(96)</sup>, the failure probability of the  $u$ th transmission support structure can be approximated by an exponential function under a given wind speed  $x_u$  <sup>(97)</sup>,

$$P_{trans\_tower,u}(W_s = x_u) = \min\{2 \times 10^{-7} e^{0.0834x_u}, 1\} \quad (18)$$

For the gas system subject to a hurricane, underground pipelines are mostly invulnerable to wind hazards, and only the gas node failures are considered. The damage probabilities of compressor stations, pumping stations and meter stations are also calculated using Equation (18).

Underground cables and pipelines might be destroyed by the storm surge. The  $u$ th underground cable or pipeline damage probability can be approximated as functions of hurricane and flood severity <sup>(97)</sup>,

$$P_{under\_line,u} = [a + b(H - S)] \times I(H - S) \quad (19)$$

where  $P_{under\_line,u}$  is the  $u$ th underground facilities damage probability for given hurricane and storm surge categories.  $H$  is the hurricane category (1-5),  $S$  is the storm surge zone category (1-5), and  $a$  and  $b$  are tuning parameters,  $I(H-S)$  is an indicator function showing whether the area is affected by an incoming hurricane, and equals to 1 if  $H-S \geq 0$ , else equals to 0.

For the flood impacts on the power grid, transmission support structures are considered as safe, and only electric node failures are included in the model. For gas and oil networks, all kinds of components could be affected by flooding. HAZUS<sup>(95)</sup> provides the infrastructure failure probability under flood within specific areas. In accordance with the hurricane data, the relationship between infrastructure damage probability and flood depth are based on the data from US. Two damage levels are considered: low and high. The high damage probabilities with 10 feet flood depth are: 0.30 for power plants, 0.15 for transmission substations, 0.40 for compressor, pumping and meter stations of both, gas and oil transmission networks.

### 6.3 Sequential Hazard Impacts on Infrastructure

Damage probability functions discussed in the previous section are for separate hazards, hurricane or flood. Based on the temporal and spatial relationships of the two hazards, their impacts on infrastructure are not independent. Damage probabilities of infrastructure should be calculated according to their location and hazard occurrence time.

During  $t=1$  to  $t=12$ , hurricane affected the whole GTA, all infrastructure would be damaged with specific probability  $P'_u(H)$  that can be calculated by Equation (17) and (18) except the underground pipelines.

From  $t=13$  flooding begins to affect areas along rivers and streams of GTA. Only infrastructure located in these areas would be directly impacted by the flood. The damage probability of infrastructure only directly affected by the flood (submarine pipelines)  $P'_u(F)$  can be calculated using Equation (19). Other flooded infrastructure damage probability can be calculated by

$$P'_u(F | H) = P'_u(F) + \eta(1 - P'_u(F))P'_u(H) \quad (20)$$

where  $\eta$  is a restoration parameter, which could be 0 or 1. As gust wind speed occurs at  $t=1$ , there may be some time to restore hurricane damaged infrastructure. With limited resources, parts of the hurricane damaged infrastructure might be recovered. For this infrastructure,  $\eta = 0$ , and its damage probability under the flood would be  $P'_u(F)$ . For other infrastructure affected by hurricane and flood without restoration,  $\eta = 1$ . In addition, the infrastructure not located in the blue areas in Figure 12, would not be damaged by flooding due its location.

Based on the intra-network and inter-network failure interdependence models discussed in Section 5.2, infrastructure may also be non-operational due to interdependences. As the function of arcs are determined by their connecting nodes, there is no undirected arcs failure, only nodes would be non-operational when they lose the connection with the source nodes. Actual damage probability of each node can be calculated as Equation (15).

## 7 SEQUENTIAL HAZARD RESILIENCE SIMULATION

### 7.1 Joint Restoration Model of Interdependent Infrastructure System

Return to initial level of performance after the disturbance is the critical characteristic of system resilience, which is illustrated as the raising limb of the system performance curve shown in Figure 2-5. There is emerging literature studying the restoration processes of infrastructure systems. Most of the published research deals with the optimization of post-disaster individual infrastructure system restoration applying a variety of modelling approaches and focusing on different aspects of the restoration strategy. Examples include: minimization of the power systems restoration time under hurricane event <sup>(98,99)</sup>; maximization of power system resilience with different operations models; maximization of performance and minimization of a telecommunication system cost; maximization of resource efficiency in spatially distributed networks; and others. The joint restoration strategy work mostly considers a single layer infrastructure network resilience. Restoration strategies are always focused on the repair order of damaged system components or the addition of new components. The main questions are where and how to allocate limited repair resources.

In this study, the resilience of multi-layer infrastructure network is introduced as an objective that can be implemented in the assessment of various recovery strategies. So analytically, the objective of restoration is set to maximize the resilience of a multi-layer infrastructure network during a selected duration, which can be expressed as

$$\max r^{A_1, \dots, A_n}(t^*) \quad (21a)$$

$$\text{s.t.} \quad \begin{cases} \sum_u RN_u(t) \leq C_{RN}(t) \\ \sum_u TN_u(t) \leq C_{TN}(t) \end{cases} \quad (21b)$$

where  $r^{A_1, \dots, A_n}(t^*)$  is the multiple hazard  $A_1, \dots, A_n (n \geq 2)$  expected resilience value during  $[t_{A_1}^O, t^*]$ ;  $t$  is the specific time set for resilience assessment;  $t_{A_1}^O$  is the beginning time of the first hazard  $A_1$ ;  $RN_u$  denotes physical resources needed to repair the damage of  $u$ th individual infrastructure component at  $t$  ( $t < t^*$ );  $C_{RN}(t)$  denotes physical resources available at  $t$  ( $t < t^*$ );  $TN_u(t)$  is the time needed to repair the damaged  $u$ th individual infrastructure component at  $t$  ( $t < t^*$ ); and  $C_{TN}(t)$  is the total time available at  $t$  step, which can be measured as  $t^* - t$ .

The formulated restoration model (Equations 21a and 21b) is not easy to solve with standard optimization techniques, as the dynamic spatial impacts of hazards on infrastructures and failures propagation within and across networks are nonlinear and of high level of complexity. The evolutionary programming methods as for example, genetic algorithm proposed by Ouyang<sup>(18)</sup> can be used here, which has been successfully used in the literature to optimize failure components restoration sequences of infrastructure systems.

## 7.2 Sequential Hazard Resilience Simulation Process

System resilience analysis shows expected infrastructure system response to component fragilities and interaction of hazards and their intensities. Monte Carlo method is used for simulation of damage propagation due to its ability to include complex phenomena like cascading failures in the model<sup>(100)</sup>. As multiple hazards might occur at different times, simulation process could be divided into several phases to integrate components damage probabilities

calculation and their cascading failure effects. Every phase starts with a hazard occurrence, and includes direct hazards impact evolution, intra-network failure propagation analysis, and inter-network failure propagation analysis, as shown in Figure 13. In this case, the simulation progress is divided into two phases. The first phase is focused on the infrastructure network performance subject to hurricane. The second phase combines the flood impacts on the infrastructure system.

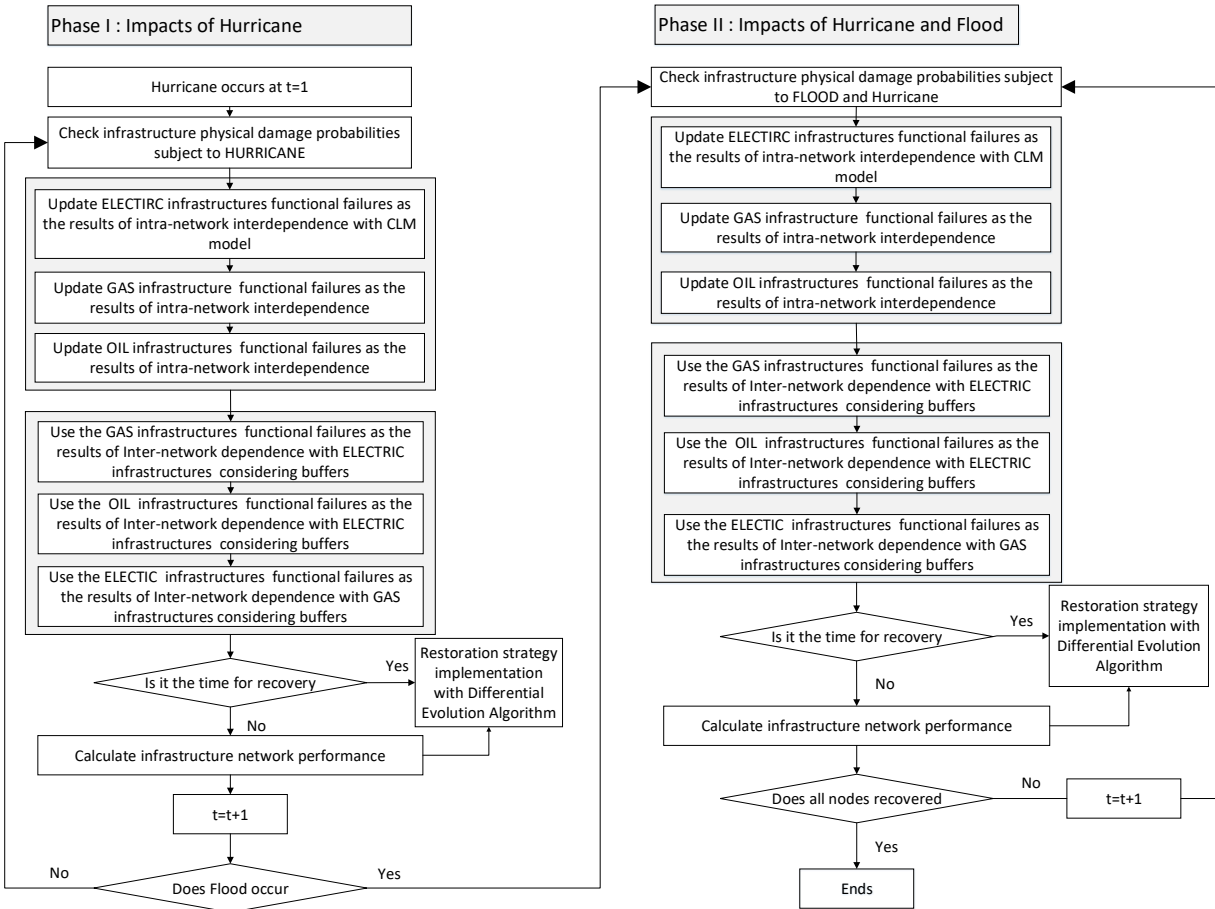


**Figure 13 Simulation procedure of GTA infrastructure system resilience under sequential hurricane and flood**

In this simulation, delivery time of electric, gas and oil is set to be equal to one-time step (two hours). Buffers usually have limited capacity in terms of the time, and are usually incorporated as a time delay between the node failure and its dependency loss. In this study, we set every node to have a backup of two hours.

To develop the restoration strategy at components level, i.e. determine the restoration sequence of damaged components at each time step, the following assumptions are added to the restoration model list: (i) restoration begins at the time step when component failures occur, or later; (ii) damaged component can recover to normal function in one-time step with restoration; and (iii) at most two damaged components can be restored in one-time step with the existing resource constraints. With gusting wind speeds occurring at  $t=1$ , there is 11 time steps before the flooding begins. After the wind speed weakens below a specific threshold, the restoration can begin. In our case this moment is at  $t=8$ . So, two restoration strategies with different starting times would be used in the simulation. One is a two-phase strategy, restoration from  $t=8$  to  $t=12$  and then starting at  $t=18$  after the flooding ends. The other is a one-phase strategy, starting at  $t=18$  after both hazards end. The final simulation results are averaged over 100 runs.

## **8 GTA ENERGY INFRASTRUCTURE SYSTEM PHYSICAL RESILIENCE**

### **8.1 Infrastructure Physical Performance Spatial Analysis**

GTA three-layer energy infrastructure network resilience is a measure of dynamic performance of all the components together. With the interdependence among infrastructure components, multi hazards would have significant diverse impacts on the multi-layer network. Electric transmission network, gas transmission network, and oil transmission network performance at six time points subject to different hazards are shown in Figure 9. The six time points are selected as the hazard occurrence time, one-time step after hazard occurrence time, the time when systems resilience returns to a new stable state after the first hazard, the second hazard occurrence time, the time when systems resilience returns to a new stable state after the second hazard, and the time when all nodes recover to normal state.

As shown in Figure 14, different hazards impact on the multi-layer infrastructure network have notable dynamic spatial features. Combining with disaster scenario in Figure 12, it is easy to find the directly damaged infrastructures by the hazards at different time, and easy to identify the indirectly failed infrastructures. For example, comparing the figures at  $t=1$  and figures at  $t=2$  in Figure 9, the number of infrastructures with damage probability larger than 0 are not only located in the area where hurricane occurs at  $t=2$ . These infrastructures are failed due to their interdependence on the damaged infrastructures. In Figure 14 (a), only a few infrastructures impacted by the flood directly are of darker color, and the failures don't spread through the whole multi-layer infrastructure network. In Figure 14 (b) (c) and (d), from  $t=1$  to  $t=8$ , damage probabilities of infrastructure components are the same, and the failures propagate with the hurricane path. From  $t=9$ , the infrastructure performances in the last three rows of Figure 14 begin to be different. In

the case of single hurricane, infrastructure component damage probabilities turn to be smaller and smaller with restoration beginning at  $t=8$ . But for the multi-layer infrastructure network subject to sequential hurricane and flood, their performances are worse at  $t=19$  than at  $t=13$  after the flood impact, whether there is in-between restoration or not.

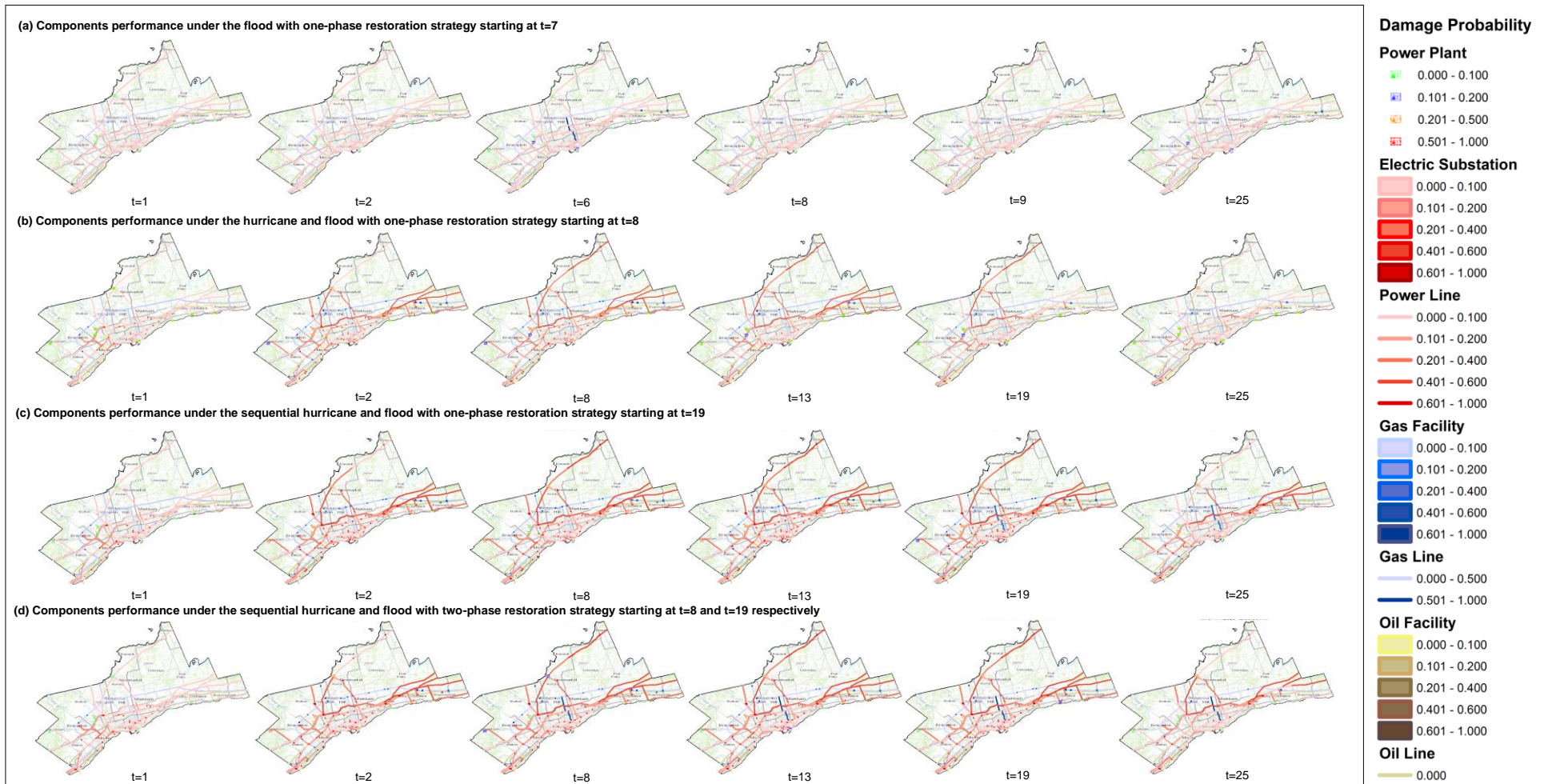


Figure 14 Spatial physical performance of GTA three-layer energy infrastructure network under different hazard scenarios

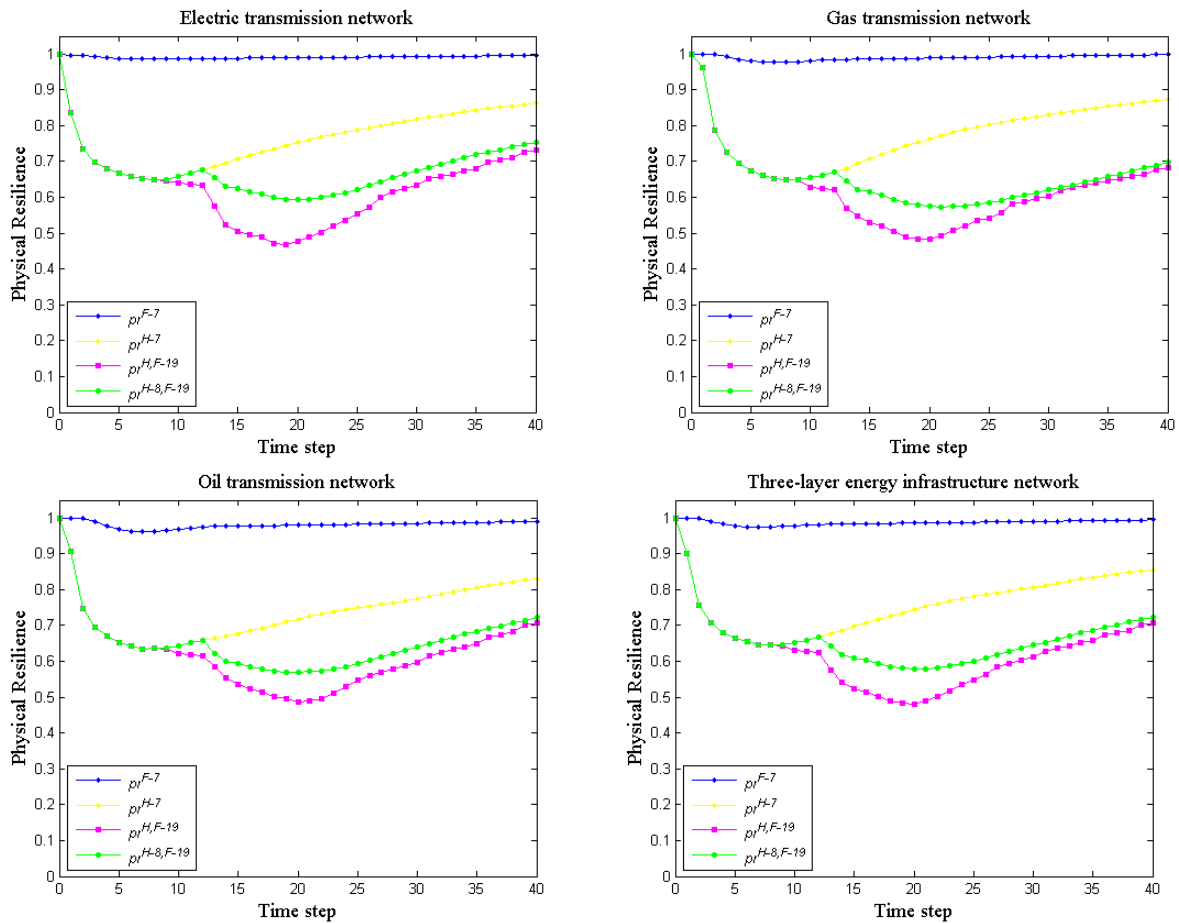
Damage probabilities of infrastructure components under sequential hurricane and flood hazards are not always smaller or bigger than the sum of single hurricane and flood impacts in Figure 14. After the end of both hazards at  $t=19$ , damage probability of almost all the infrastructures increases (nodes turn darker in Figure 14 (b) and (d)), not only the infrastructures directly affected by the flood. In the power grid, electric transmission substations (red nodes) near the power generation stations affected directly by the flood are always more sensitive to flooding, what can be observed from the comparison of Figures 14 (b) and (d) at  $t=19$ . The electric transmission substations far from the flood impacted areas, located in the southwestern and northeastern parts of GTA are always more robust to flooding. The results echo previous research in spatially localized impacts on interdependent networks<sup>(101)</sup>. Also, the hub electric substations with more connections, such as the 500 kv substations and 230 kv substations linking with 115 kv substations, are more susceptible to the undirected influence. In the gas transmission network, there are two notable features at  $t=19$ . One is that the number of dark blue nodes in Figure 14 (d) is larger than the number in Figure 14 (b), similar to the power grid. The other is that the 14 dark blue nodes in Figure 14 (d) are not localized but scattered throughout the network. The reason might be that the number of gas infrastructure elements is small and not clustered in space. The only gas infrastructure elements impacted by flooding indirectly are the underwater pipelines from a gas meter station to the Portlands Energy Center (which is a 550-megawatt natural gas electrical generating station on the Toronto waterfront). This would increase the damage probability of the power plant and related substations. In the oil transmission network at  $t=19$  in Figure 14 (d), all the nodes are darker when compared to Figure 14 (b), though no direct flood impacts are present. All impacts on gas and oil transmission networks are due to their dependence on the electric power.

The restoration strategy and its implementation starting time also play an important role in infrastructure components performance. It is worth noting that restoration strategies implemented with two scenarios (sequential hurricane and flood without in-between restoration, and sequential hurricane and flood with in-between restoration) have the same system resilience maximum objective, boundary conditions and use the same algorithm. The only difference is the strategy implementation starting time. In Figure 14(c), the restoration strategy implementation starts from  $t=19$  after all hazards end. In Figure 14(d), the implementation is in two-stages starting after the end of each hazard. The first stage lasts from  $t=8$  to  $t=12$ , and second from  $t=19$  until all infrastructure recovery. Comparison of Figures 14 (c) and (d) shows that, (i) at  $t=8$  (when the flood starts), only the directly affected Portlands Energy Center and connected

substations' damage probability increases; (ii) at  $t=13$ , more nodes in Figure 14 (c) turn lighter than that in Figure 14 (d); (iii) at  $t=19$  (when the flood ends) and  $t=25$ , the difference of the two figures is more obvious, damage probability of infrastructures with two-phase restoration strategy is much smaller than that with one-phase restoration strategy.

## 8.2 Dynamic Infrastructure System Physical Resilience

The infrastructure system dynamic physical resilience subject to different hazards is shown in Figure 15 for the multilayer infrastructure network, disaster scenario parameters, simulation procedures that maximize the whole infrastructure system physical resilience.



$pr$  is physical resilience of GTA three-layer energy infrastructure network.

Blue line  $pr^{F-7}$  is physical resilience of GTA multilayer energy infrastructure network under the flood with one-phase restoration strategy starting at  $t=7$ . Yellow line  $pr^{H-8}$  is physical resilience of GTA multilayer energy infrastructure network under the hurricane with one-phase restoration strategy starting at  $t=8$ . Pink line  $pr^{H,F-19}$  is physical resilience of GTA multilayer energy infrastructure network under sequential hurricane and flood with one-phase restoration strategy starting at  $t=19$ . Green line  $pr^{H-8,F-19}$  is physical resilience of GTA multilayer energy infrastructure network under sequential hurricane and flood with two-phase restoration strategy with starting time at  $t=8$  and  $t=19$  respectively.

**Figure 15** GTA three-layer infrastructure network dynamic physical resilience

According to Figure 15, different from static resilience, dynamic resilience fluctuates nonlinearly with the hazards occurrence, infrastructure interaction and infrastructure restoration. Single and multi-layer infrastructure network physical resilience subject to multiple hazards is not equal to the sum of the single hazard resilience, Infrastructure system physical resilience to sequential hurricane and flood hazards with in-between restoration (from  $t=8$  to  $t=12$ )  $pr^{H-8,F-19}$  (green line) is larger than the sum of single hurricane (blue line) and flood resilience (yellow line)  $pr^{H-8} + pr^{F-7} - 1$  before  $t=13$  for electric transmission network,  $t=13$  for gas transmission network,  $t=15$  for oil transmission network,  $t=14$  for multilayer network, and smaller after that time.

Though subject to the same sequential hurricane and flood, single and multi-layer infrastructure network physical resilience are different due to the different start of restoration time. Generally, the earlier start of restoration, the higher system resilience. According to Figure 15, the infrastructure system resilience with in-between restoration  $pr^{H-8,F-19}$  (green line) is always larger than the system resilience without in-between restoration  $pr^{H,F-19}$  (pink line). The in-between restoration not only influences the system resilience during corresponding repair time (from  $t=8$  to  $t=12$ ), but also impacts the follow-up system resilience (after  $t=12$ ). This is the positive effect of interdependence. Damage probabilities of repaired infrastructure decline and lead to the decline of damage probabilities of dependent infrastructure elements. The differences between the impacts of two restoration strategies are more obvious in electric transmission network.

## 9 GTA ENERGY INFRASTRUCTURE SYSTEM FUNCTIONAL RESILIENCE

### 9.1 Infrastructure Functional Performance Spatial Analysis

The impacted population of each electric transmission substation supported area is used for the analysis of spatial features of functional dynamic resilience (see Figure 16). For comparison, the six time points for presentation of spatial functional resilience analyses are the same as those used in the analyses of physical resilience.

As shown in Figure 16, the structural/physical importance of an infrastructure does not always agree with its social impact. Impacted population is larger in GTA periphery than that in the central areas. This might be because substations located at the edge usually serve larger area and population than those in the central areas.

In Figure 16(a), impacted population of all the areas is less than 100,000, as the flood only affects several electric infrastructure elements and has little impact on the whole infrastructure system. In Figure 16 (b) (c) and (d), from  $t=1$  to  $t=8$ , impacted population in each area is nearly the same, and failures propagate also by the hurricane path. From  $t=9$ , impacted population in each area is different, and the flood impacts on population are more obvious, which echo the functional resilience curve decrease after the flood in Figure 17. Comparing the difference between impacted population at  $t=13$  and  $t=19$  subjected to sequential hurricane and flood (Figure 16 (c) and (d)), the flood impacted areas (blue color in Figure 12) would not have a dramatic functional loss, but impacted population located at the edge areas increases sharply.

Time of implementation of restoration strategy also has a significant impact on the system resilience. There are only two restoration strategies considered in this work with the same system resilience maximization objective, boundary conditions and calculation algorithm - the only difference is in the strategy implementation starting time. In Figure 16 (c) the restoration strategy starts from  $t=19$  after all hazards end. In Figure 16(d), a two-stage strategy is implemented after the end of each hazard. The first stage lasts from  $t=8$  to  $t=12$ , and second from  $t=19$  until all infrastructure recovery. Comparison of the impacted population at  $t=25$  of Figure 16 (c) and (d) shows that the latter, with in-between restoration, is smaller than the former, without in-between restoration. The reason for the difference could be that the interdependence among diverse infrastructures aggravates the failures and restoration effects.

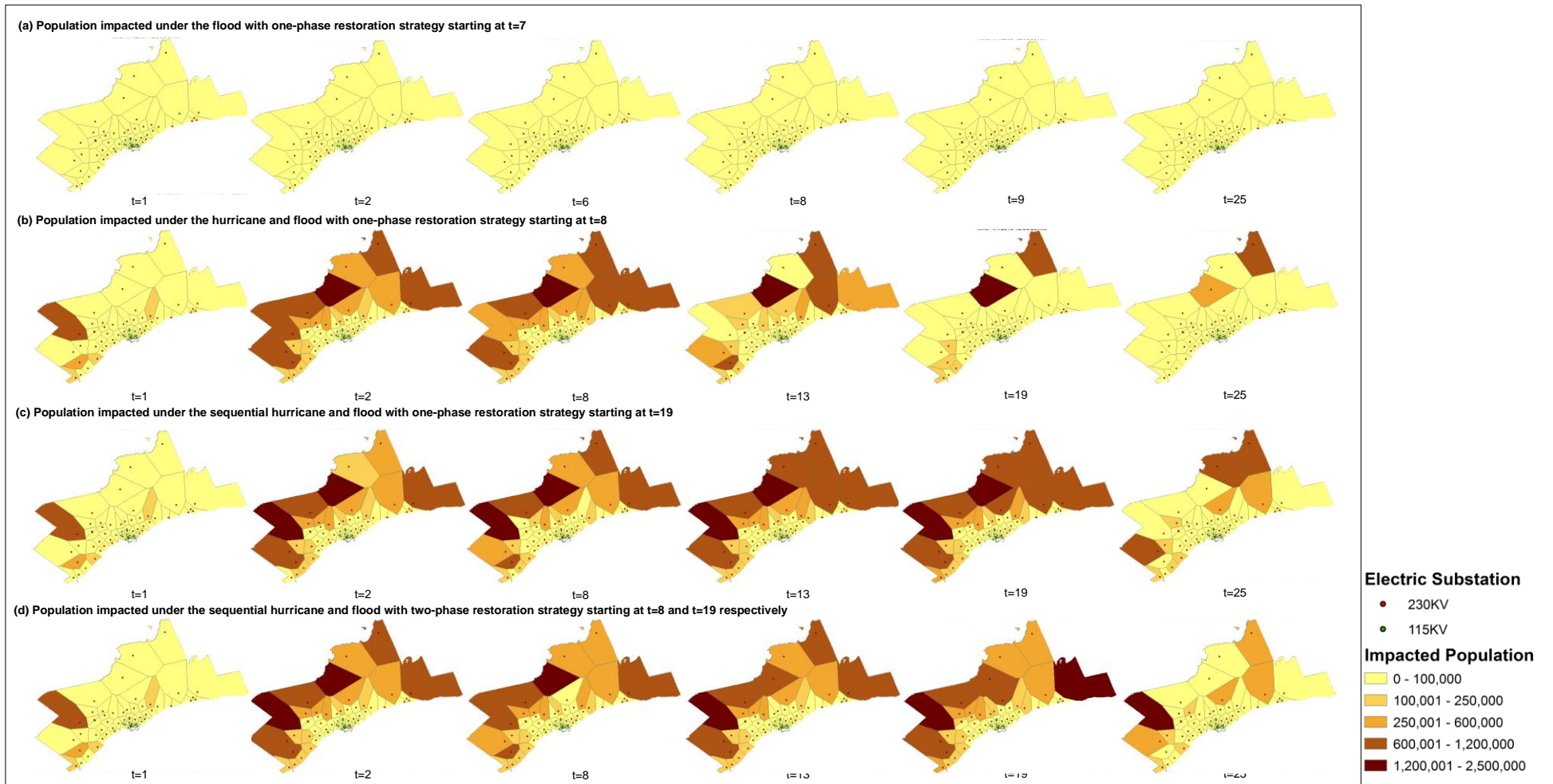
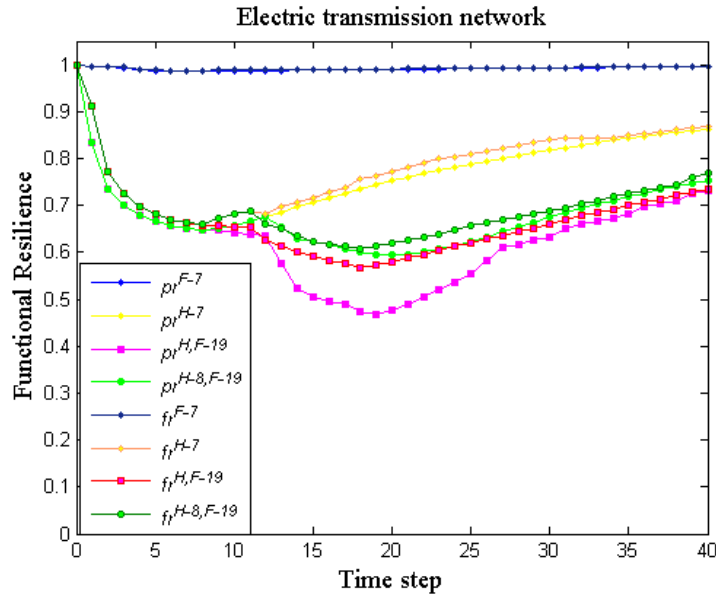


Figure 16 Spatial functional impacts of GTA three-layer energy infrastructure network under different hazards scenarios

## 9.2 Dynamic Infrastructure System Functional Resilience

GTA three-layer infrastructure network functional performance is measured by the ratio of population electric served by the transmission substation to the total population served. The system functional resilience shows the service recovery capacity of multi-layer infrastructure network. As the electric energy is the most important for people, GTA power grid dynamic functional resilience is chosen to represent the whole infrastructure system functional resilience. Based on the transmission substations damage probabilities and their supporting population, infrastructure system functional resilience is shown in Figure 17. In the figure, dark color lines denote functional resilience, and light color lines denote physical resilience.



$f_r$  is functional resilience of GTA electric transmission network.  $pr$  is physical resilience of GTA electric transmission network. Dark blue line  $f_r^{F-7}$  is functional resilience of GTA electric transmission network under the flood with one-phase restoration strategy starting at  $t=7$ . Light blue line  $pr^{F-7}$  is physical resilience of GTA electric transmission network under the flood with one-phase restoration strategy starting at  $t=7$ . Dark yellow line  $f_r^{H-8}$  is functional resilience of GTA electric transmission network under the hurricane with one-phase restoration strategy starting at  $t=8$ . Light yellow line  $pr^{H-8}$  is physical resilience of GTA electric transmission network under the hurricane with one-phase restoration strategy starting at  $t=8$ . Dark red line  $f_r^{H,F-19}$  is functional resilience of GTA electric transmission network under sequential hurricane and flood with one-phase restoration strategy starting at  $t=19$ . Light red line  $pr^{H,F-19}$  is physical resilience of GTA electric transmission network under sequential hurricane and flood with one-phase restoration strategy starting at  $t=19$ . Dark green line  $f_r^{H-8,F-19}$  is functional resilience of GTA electric transmission network under sequential hurricane and flood with two-phase restoration strategy with starting time at  $t=8$  and  $t=19$  respectively. Light green line  $pr^{H-8,F-19}$  is physical resilience of GTA electric transmission network under sequential hurricane and flood with two-phase restoration strategy with starting time at  $t=8$  and  $t=19$  respectively.

**Figure 17** GTA electric transmission network dynamic functional and physical resilience

According to Figure 17, functional resilience is always larger than the corresponding physical resilience, and shows more obvious decrease after the second hazard. There are possibly two explanations for that. First is that the multiple redundancy paths exist between electric transmission substations and power generating stations. Then some of the components experiencing physical failure would not experience the functional loss. Also, each component restoration might decrease damage probability of several infrastructure elements. The two effects could be strengthened by the interdependence among infrastructure elements. The second reason could be unequal population and substation distributions. Though substation capacities are used as the weight to calculate system resilience, population they serve is usually not proportional to their capacity.

Contrary to the physical resilience of power grid subject to multiple hazards, their functional resilience  $fr^{H,F}$  (dark green line in Figure 17) and  $fr^{H,(R),F}$  (dark red line in Figure 17) are always smaller than the sum of single hurricane and flood resilience ( $fr^H + fr^F - 1$ , dark blue line and dark orange line in Figure 17) before  $t=6$  subject to sequential hurricane and flood with in-between restoration, and before  $t=12$  subject to sequential hurricane and flood without in-between restoration.

The positive effects of restoration strategy are more obvious in change of functional resilience. Comparison of the functional resilience subject to sequential hurricane and flood without in-between restoration (light green line in Figure 17) and functional resilience subject to sequential hurricane and flood with in-between restoration (light red line in Figure 17) shows that the latter is always larger. Also, the difference between functional resilience of multiple hazards is also larger than the corresponding physical resilience (dark green line and dark red line in Figure 17).

GTA results show that the rapidity of all, single and three- layer, networks is less than 36 time steps (72 hours). But the physical and functional resilience of single layer and multi -layer infrastructure networks are not equal to, but approach the value of 1 at  $t=40$  according to Figures 12-15. This is because the resilience metric (Equation (6)) is a cumulative ratio of unaffected area to the expected area. It is not a measure of the system state, but a service capacity during a time period. Therefore, this ratio can be used to assess the system

service provision capacity during a period of time, which is the basic meaning of resilience. This might be another reason for the functional resilience being higher than the physical resilience in Figure 17.

## **10 DISCUSSION**

The multiple hazards spatiotemporal impacts on interdependent infrastructure system resilience is a complex process due to interactions of infrastructure interdependences, combined impacts of single hazards and diverse restoration strategies.

### **10.1 Single Hazard Marginal Impacts**

The single hazard impacts on physical and functional resilience do not only depend on their spatiotemporal characteristics or relationships with other hazards, but also on the intensity of the hazard. According to Figures 14 and 16, the flooding of lower magnitude (affecting 10 nodes and edges) only increases the damage probability of infrastructure located in, or near the floodplain areas, although infrastructure interdependence is considered in the model. Similarly, there is a small decrease in the resilience curves in Figures 15 and 17, especially in electric transmission network and multi-layer energy infrastructure network. The small size of gas and oil transmission networks is the reason for their more significant decrease in resilience after the flood.

The small marginal effects of the flood may be explained by the fact that: (i) the direct flood impacts on infrastructure components are small, damage probabilities of infrastructures subject to flooding are all smaller than 0.3 except two submarine transmission lines; (ii) there are redundant paths connecting every load node with multiple source nodes (Figure 10) - networks with more redundant topology structure would reduce the flood impacts, as the load nodes have a higher chance of connecting with a source nodes; and (iii) there is a slight increase in path efficiency.

The hurricane marginal effects are not as small as the flooding effects as shown in Figure 14 (b), Figure 16(b), and red line in Figures 15 and 17. Basically, the magnitude of the hazard is the determining factor. The high gust wind speed through the whole GTA causes large infrastructure damage probability, and indeed sharp

decrease of the resilience curves. Based on the Saffir-Simpson Hurricane Wind Scale, only hurricanes above category 3 (wind speed higher than 110 mph) cause flooding. Category 5 is the highest category for hurricane with wind speed 157 mph or higher. The hurricane list in Section 6.1 is with wind speed ( $w_s$ ) of 120mph, so the change in wind speed  $w_s$  from 110mph to 160mph with 10mph as the interval is considered in this study. According to the record and available Hurricane Hazus data, the flood list in Section 6.1 is with the highest flood depth (more than 10 ft), so the magnitude of flood does not change. GTA three-layer energy infrastructure network resilience is simulated with only the hurricane wind speed is changed and the other original value remains unchanged, which list in Figure 18.

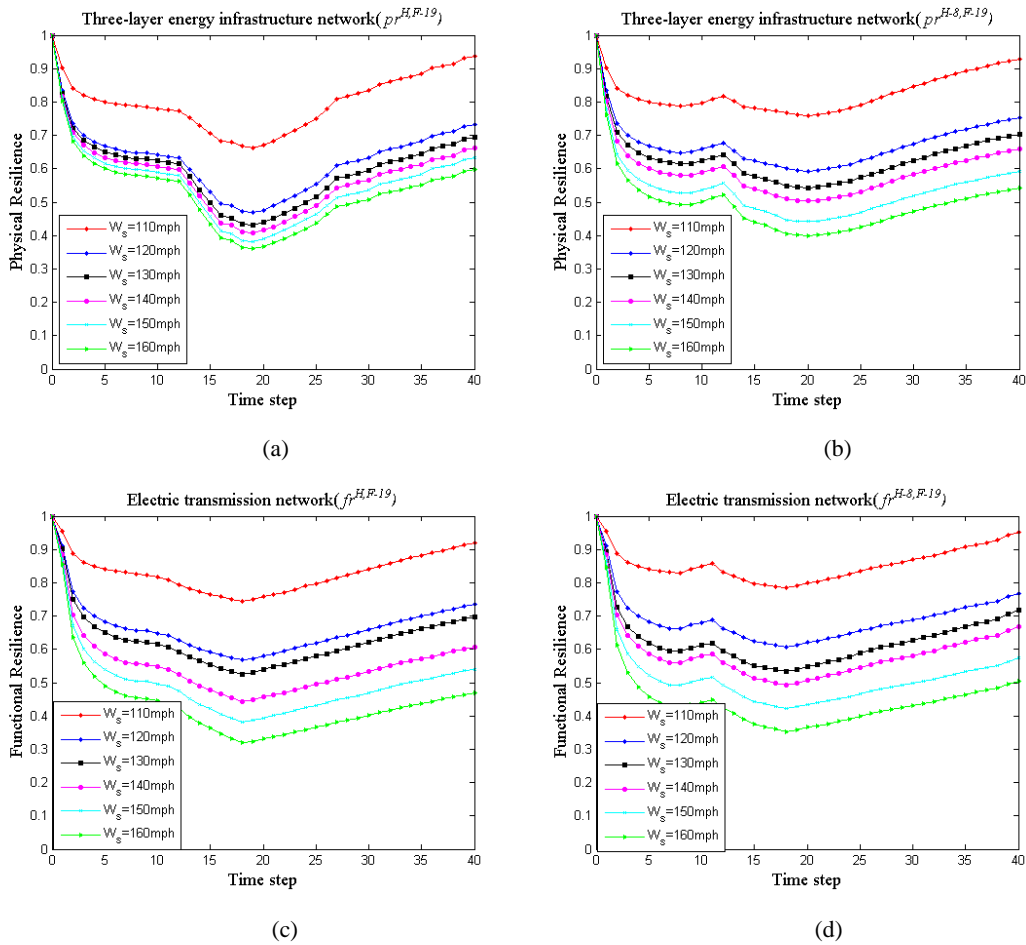


Figure 18 Resilience profiles for different magnitude of hazards

According to Figure 18, with the same spatiotemporal relationships of sequential hurricane and flood, GTA three-layer energy infrastructure network physical resilience and electric transmission network functional resilience change as the different magnitude of hurricane. The higher wind speed, the lower system resilience. Moreover, the higher the wind speed, the more significant is the resilience decrease. Meanwhile, the rule is more clear in the case of functional resilience than physical resilience, as the distances between two adjacent lines in Figures 18(c) and (d) are bigger than those in Figures 18(a) and (b). Comparing Figures 18 (a) and (b), two-phase restoration strategy is always better than one-phase restoration strategy, especially in the situation with lower wind speed, and so is the functional resilience. In addition, resilience with wind speed of 110 mph is significantly bigger than the resilience with higher wind speed.

## **10.2 Cascading Failure and Recovery Effects**

Infrastructure system restoration strategy is a complex problem, and is getting more and more attention among researchers. The main reason is the cascading recovery effect as consequence of infrastructure interdependence, which is obvious in simulation results.

The slopes of multi-layer infrastructure network resilience curves in Figure 15 (dark blue and red lines) are always larger than  $2/103$  (number of restoration nodes / number of all nodes). As demonstrated in Figure 15 all the single and multi-layer infrastructure networks resilience with two-phases restoration strategy are drastically higher than those with one-phase restoration strategy.

The cascading recovery effects in electric transmission network are particularly apparent. The electric transmission network resilience curve with two-phase restoration strategy (red line in Figure 15 and pink line in Figure 17) drops a bit after the flood, but clearly shows a rising tendency. Since the flood impacts are small, cascading recovery effects are the main reason for this behavior.

Cascading recovery effects can also be illustrated from the temporal and spatial sensitive analysis to time interval and overlap area of hurricane and flood.

(i) Sensitivity analysis to time interval of hazards

Temporal relationship of hazards is a traditional and significant topic of multi hazards resilience or risk analysis. Occurrence time is always used to describe the temporal relationship of multi hazards. However, the effects of time interval of hazards' occurrence time on system resilience has never been analyzed. For the sequential hazards scenario list in Section 6.1, a 24-hour interval (12 time steps in Figures 14-17) exists between hurricane and flood occurrence time. As the fragility curves of individual infrastructure components under simultaneous hurricane and flood is not available, we set the time interval between hurricane and flood from 4 to 24 with 4 time steps as interval. It means that the flood starts at  $t=13, 17, 21, 25, 29, 33,$  and  $37$  respectively. Then one-phase restoration strategy starts at the end of flood, two-phase restoration strategy starts at the end of hurricane. GTA energy infrastructure network resilience is simulated with only the time interval between hurricane and flood is changed, which list in Figure 19.

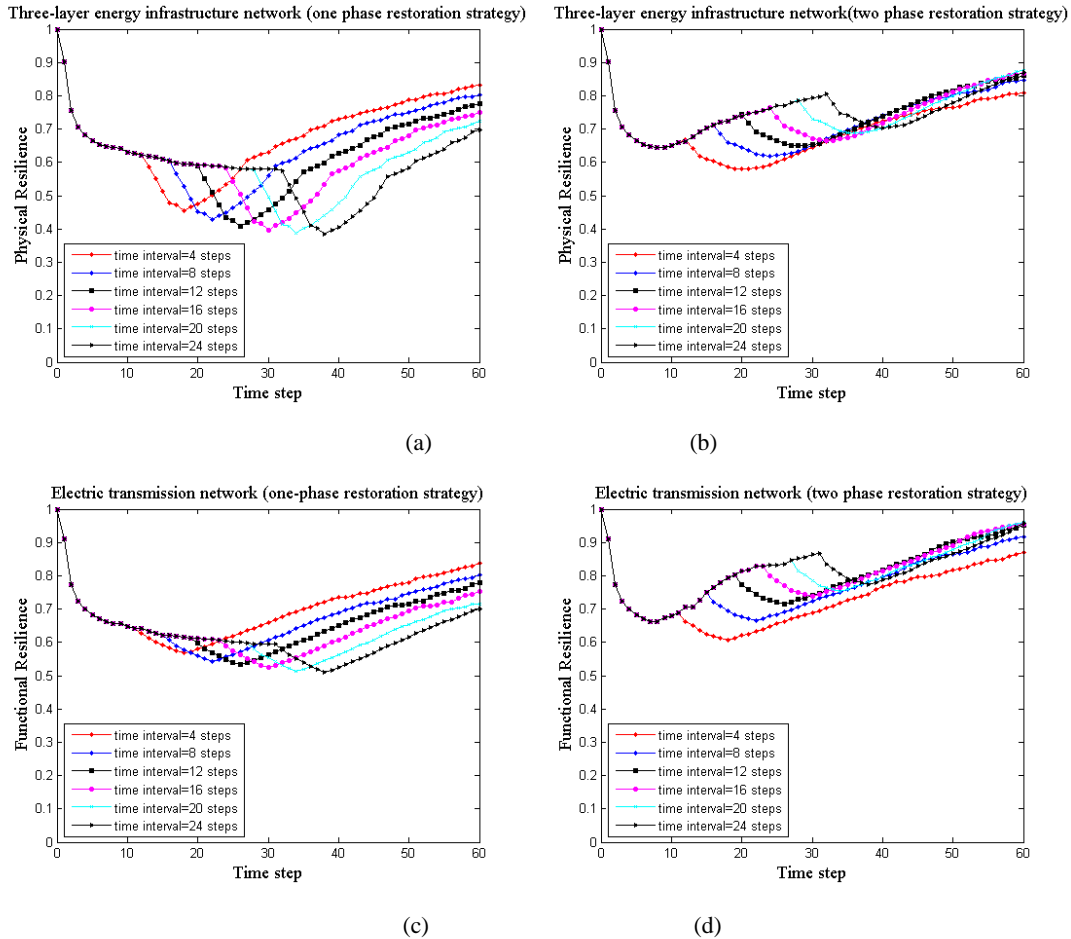


Figure 19 Resilience profiles for different time interval of hazards

According to Figure 19, though the magnitude and impact areas of hurricane and flood are constant, GTA three-layer energy infrastructure network physical resilience and electric transmission network functional resilience change as the different time intervals between the two hazards. Comparing Figures 19 (a) and (b), the advantage of two-phase restoration becomes more and more obvious as the time interval increasing. For one-phase restoration strategy, physical and functional resilience both decrease as the time interval increasing. This is because of the failure cascading within the network. For two-phase restoration strategy, physical and functional resilience both increase as the time interval increases. Though only 2 individual infrastructure components can be restored at each time step, the restoration cascading recovery effects of the first phase restoration leads to quick resilience increase.

(ii) Sensitivity analysis to spatial overlap of hazards

Spatial relationship of hazards does not obtain much attention and is mostly neglected in the current research. For the distributed infrastructure systems, hazards with different spatial relationships could impact different infrastructure components and cause very different impacts. Area of overlap can be used to measure the spatial relationships of hazards. Here we set the area of overlap of hurricane and flood in disaster scenario in Section 6.1 as 1 (the area of blue areas in Figure 17). Then enlarge the radius of the area by a factor of 1, 2, 3, 4 and 5 respectively. GTA three-layer energy infrastructure network resilience is simulated with only the spatial overlap between hurricane and flood is changed, which list in Figure 20.

According to Figure 20, though the magnitude and impact areas of hurricane and flood are constant, GTA three-layer energy infrastructure network resilience changes as the different spatial overlap of the two hazards. The bigger spatial overlap, the smaller system resilience. Moreover, comparing Figures 20 (a) and (b), the bigger spatial overlap, the smaller difference of the physical resilience with one-phase restoration strategy and two-phase restoration strategy. In addition, the physical resilience and functional resilience do not change much as the change of spatial overlap area. This is because that the damaged infrastructure components are always located concentrated. Even without the increase of overlap area, the damage probability of increased individual infrastructure components would be impacted by their near direct damaged individual infrastructure components. Also, they could be impacted by their near infrastructures recovery. The flood

impacted area takes a very small proportion of GTA area, even for the radius of the overlap area of hazards scaled up to 6 times. Therefore, the small damage of infrastructures within similar spatial areas would not decrease system resilience significantly.

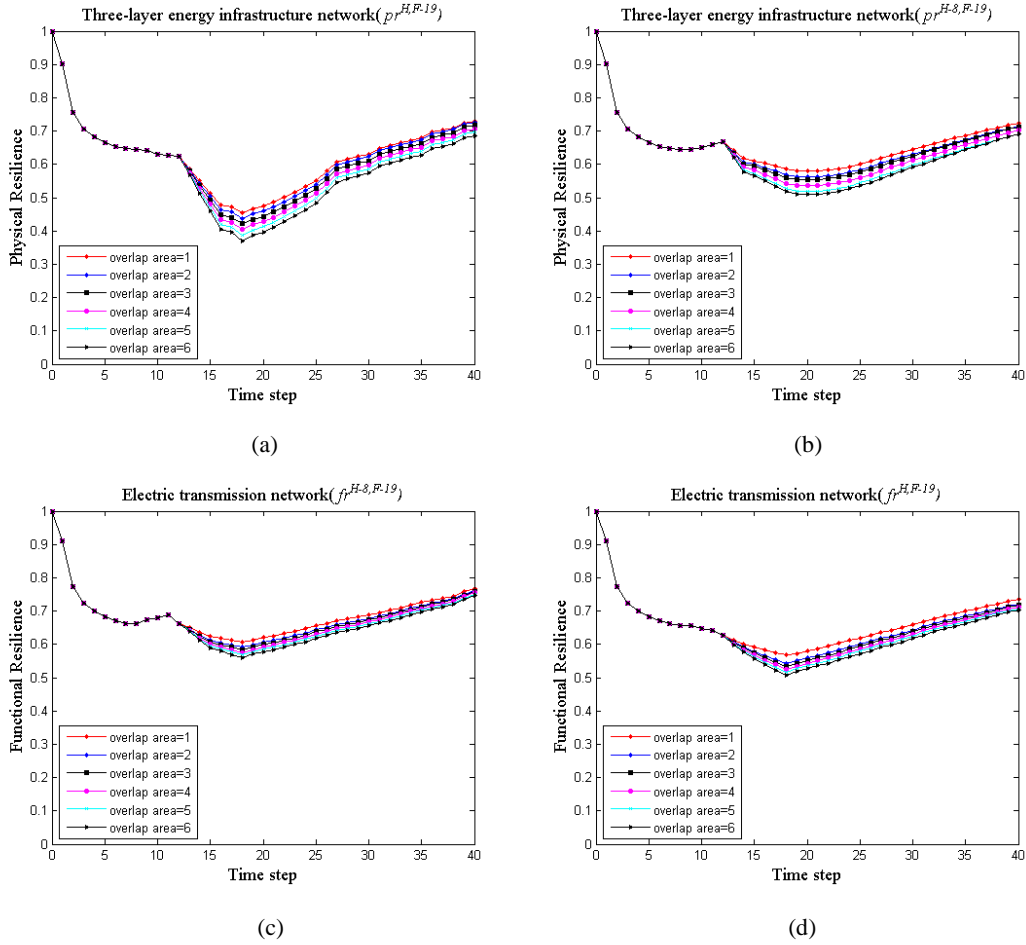


Figure 20 Resilience profiles for different spatial overlap area of hazards

It is worth noting that restoration strategy implementation is aiming at multi-layer network resilience maximization with limited two units of resources at one-step. All the single layer network resilience would be a bit smaller than the optimal ones.

### 10.3 Restoration Resource Limits

Disaster scenario, infrastructure system and restoration strategy together shape the system resilience curve. Disaster is always Force Majeure, and infrastructure system can not be changed during a short time. Restoration strategy is always determined by the available resource. As the constraint for restoration strategy in this research, 2 units is the original value. Here we simulate GTA three-layer energy infrastructure network resilience with only the number of available resource changed, which list in Figure 21.

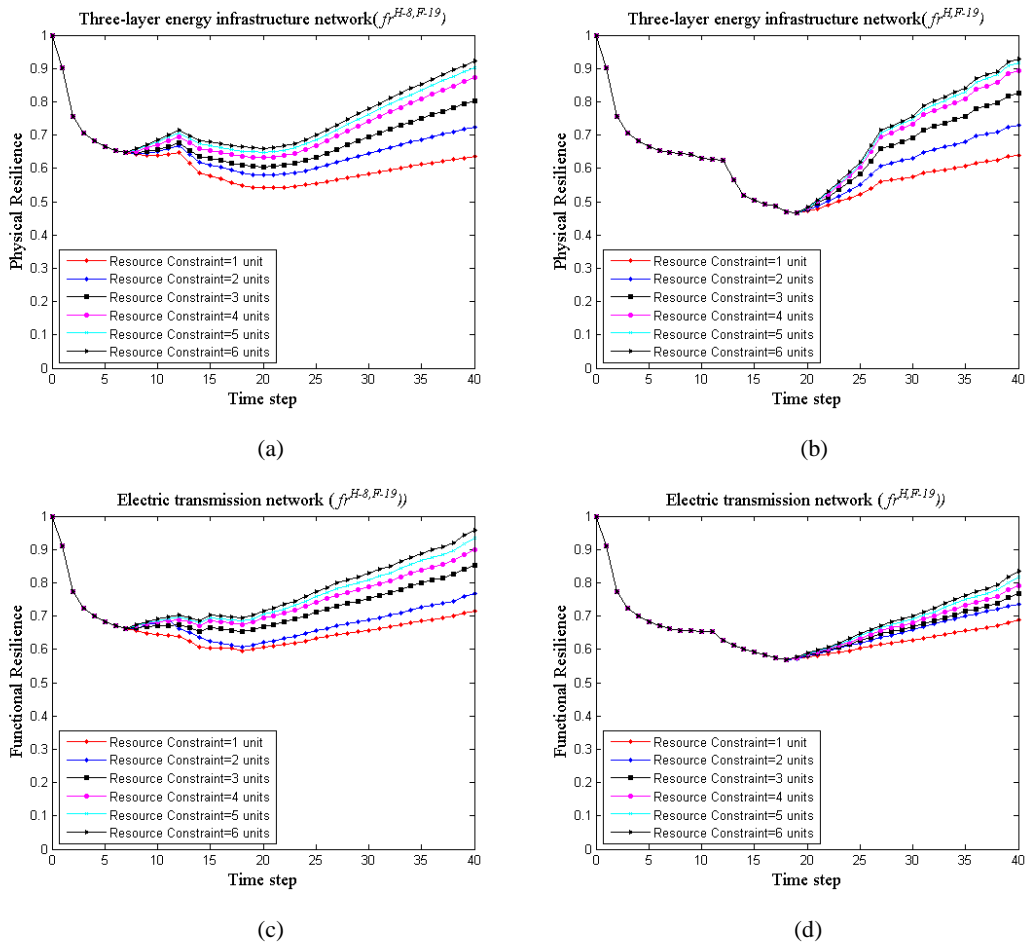


Figure 21 Resilience profiles for different resource constraints

According to Figure 21, GTA three-layer energy infrastructure network resilience changes with the different resource constraints. The more resources, the higher resilience. Moreover, the increase of resilience is slower with the resource increase. Based on the Figures 21 (a) and (b), the difference of resilience with larger than

4 units of resources is not so obvious. Comparing Figures 21 (c) and (d), resilience with two-phase restoration strategy is significantly larger than the resilience with one-phase restoration strategy. The difference is larger for more available resources. So, for GTA energy infrastructure system, the resources for recovery of 4 individual infrastructure components during 4 hours is essential for resilience improvement.

In addition, with the same resource limitations, dynamic resilience would be different as different recovery focus, such as maximising resilience during the specific time period, speeding the system recovery to an acceptable level, or minimizing system society losses, etc.

## **11 CONCLUSIONS**

While multi-hazard analyses are commonly restricted to qualitative and semi quantitative approaches, this article introduces a quantitative probabilistic multi hazard resilience analysis method of infrastructure system as an extension of resilience approaches to catastrophe risk management of infrastructure systems. This method integrates infrastructure interdependence, multi hazard relationships, dynamic resilience metric, and restoration strategy model through network theory and simulation. It can be used not only to study multi hazard resilience, but also multi hazard risk analysis of system-of-systems.

For the GTA energy infrastructure system case study, the simulation results show that the multi hazard resilience is always different from the sum of single hazard resilience. Infrastructure system resilience is sensitive to the hazard intensity and choice of restoration strategy. Though cascading failures could exacerbate impacts of single hazards, the cascading recovery effects could lower the impacts of hazards on system resilience. In this study, only the fixed amount of restoration resources is considered, and assumed to have the same effectiveness on restoration of different infrastructures. Though with sector-based operation and maintenance, a holistic method of optimal infrastructure system resilience provides for more systemic thinking and better choice of disaster recovery strategies at all levels (community, region or the country). So, the resilience model is highly recommended for planning and distribution of restoration resources.

Finally, actual infrastructure systems are of high complexity. The case study simplifies the real infrastructure system structure and its failure propagation mechanism. However, it is very clear that the framework can be easily extended to evaluate system resilience with more detailed infrastructure operation models. With the availability of more empirical data than what was available for this study, the method provided in this article can be more accurately verified in future research.

## REFERENCES

1. Zio E. Challenges in the vulnerability and risk analysis of critical infrastructures. *Reliability Engineering & System Safety*, 2016; 152: 137-150.
2. Shinozuka M, Chang SE, Cheng TC, Feng M, O'rourke TD, Saadeghvaziri MA, Shi P. Resilience of integrated power and water systems. *Research Progress and Accomplishments 2003-2004*: 65-86.
3. Labaka L, Hernantes J, Sarriegi JM. Resilience framework for critical infrastructures: An empirical study in a nuclear plant. *Reliability Engineering & System Safety*, 2015; 141: 92-105
4. Hosseini S, Barker K, Ramirez-Marquez JE. A review of definitions and measures of system resilience. *Reliability Engineering & System Safety*, 2016;145: 47-61.
5. Liu B, Siu YL, Mitchell G. Hazard interaction analysis for multi-hazard risk assessment: a systematic classification based on hazard-forming environment. *Natural Hazards and Earth System Sciences*, 2016; 16(2): 629-642.
6. Suleimani E, Hansen R, Haeussler PJ, editors. Numerical study of tsunami generated by multiple submarine slope failures in Resurrection Bay, Alaska, during the Mw 9.2 1964 earthquake. Berlin: Springer; 2009. (Cummins PR, Kong LSL, Satake K, editor. *Tsunami Science Four Years After the 2004 Indian Ocean Tsunami*)
7. Holling CS. Resilience and stability of ecological systems. *Annual Review of Ecology and Systematics*, 1973; 4: 1-23
8. Cutter SL, Ahearn JA, Amadei B. Disaster resilience: a national imperative. *Environment: Science and Policy for Sustainable Development*, 2013; 55(2): 25-29.
9. Zobel CW. Representing perceived tradeoffs in defining disaster resilience. *Decision Support Systems*, 2011; 50(2):394-403.
10. The infrastructure Security Partnership. *Regional disaster resilience: a guide for developing on action plan*. Reston,VA: American Society of Civil Engineers; 2006

11. National Infrastructure Advisory Council. Critical Infrastructure Resilience: Final Report and Recommendations,2009. Available at: <https://www.dhs.gov/sites/default/files/publications/niac-critical-infrastructure-resilience-final-report-09-08-09-508.pdf>, Accessed December 11, 2016.
12. Office of the Press Secretary of the White House. Presidential Policy Directive 21 -- Critical Infrastructure Security and Resilience,2013. Available at: <https://www.whitehouse.gov/the-press-office/2013/02/12/presidential-policy-directive-critical-infrastructure-security-and-resil>, Accessed December 11, 2016.
13. Ouyang M, Wang ZH. Resilience assessment of interdependent infrastructure systems: With a focus on joint restoration modeling and analysis. *Reliability Engineering & System Safety*, 2015; 141:74-82
14. Ayyub BM. Systems resilience for multihazard environments: definition, metrics, and valuation for decision making. *Risk Analysis*, 2014; 34(2): 340-355.
15. Aerts JC, Botzen WW, Emanuel K, Lin N, de Moel H, Michel-Kerjan EO. Evaluating flood resilience strategies for coastal megacities. *Science*, 2014; 344(6183): 473-475.
16. Bruneau M, Chang S, Eguchi R, Lee G, O'Rourke T, Reinhorn A, Shinozuka M, Tierney K, Wallace W, Von Winterfeldt D. A framework to quantitatively assess and enhance the seismic resilience of communities. *Earthquake Spectra*, 2003; 19:733-752.
17. Piratla, KR, Ariaratnam ST. Assessment of metrics for resilient design of water distribution networks. *Journal of Water Supply: Research and Technology-Aqua*, 2015; 64(6): 660-669.
18. Attoh-Okine NO, Cooper AT, Mensah SA. Formulation of resilience index of urban infrastructure using belief functions. *IEEE Systems Journal*, 2009; 3(2): 147-153.
19. Ouyang M, Dueñas-Osorio L. Multi-dimensional hurricane resilience assessment of electric power systems. *Structural Safety*, 2014; 48: 15-24.
20. Oddsdóttir F, Lucas B, Combaz É. Measuring disaster resilience. UK: GSDRC University of Birmingham. 2013
21. Simonovic SP. From flood risk management to quantitative flood disaster resilience: a paradigm shift. *International Journal of Safety and Security Engineering*, 2016; 6(2):85-95.
22. Kong JJ, Simonovic S P. A Generic Model of Interdependent Infrastructure Network Resilience *Journal of infrastructure systems*, under review.
23. Greiving S. Integrated risk assessment of multi-hazards: a new methodology. *Special Paper - Geological Survey of Finland*, 2006; 42(42):75-82.
24. Carpignano A, Golia E, Di Mauro C, Bouchon S, Nordvik J-R. A methodological approach for the definition of multi-risk maps at regional level: first application. *Journal of Risk Research*, 2009; 12: 513-534.

25. Clarke J, O'Brien EA. Multi-hazard risk assessment methodology, stress test framework and decision support tool for resilient critical infrastructure. *Transportation Research Procedia*, 2016; 14: 1355-1363.
26. Schmidt J, Matcham I, Reese S, King A, Bell R, Henderson R, Smart G, Cousins J, Smith W, Heron D. Quantitative multi-risk analysis for natural hazards: a framework for multi-risk modelling. *Natural Hazards*, 2011; 58:1169-1192.
27. Gallina V, Torresan S, Critto A, Sperotto A, Glade T, Marcomini A. A review of multi-risk methodologies for natural hazards: Consequences and challenges for a climate change impact assessment. *Journal of environmental management*, 2016;168: 123-132.
28. Eshrati L, Mahmoudzadeh A, Taghvaei M. Multi hazards risk assessment, a new methodology. *International Journal of Health System and Disaster Management*, 2015; 3(2): 79.
29. Wipulanusat W, Nakrod S, Prabnarong P. Multi-hazard risk assessment using GIS and RS applications: a case study of Pak Phanang Basin. *Walailak Journal of Science and Technology*, 2009; 6 (1): 109-125.
30. Ouyang M, Dueñas-Osorio L, Min X. A three-stage resilience analysis framework for urban infrastructure systems. *Structural Safety*, 2012; 36: 23-31.
31. Kappes M S, Keiler M, von Elverfeldt K, Glade T. Challenges of analyzing multi-hazard risk: a review. *Natural Hazards*, 2012; 64(2), 1925-1958.
32. Marzocchi W, Garcia-Aristizabal A, Gasparini P, Mastellone ML, Di Ruocco. A Basic principles of multi-risk assessment: a case study in Italy. *Natural Hazards*, 2012; 62: 551-573.
33. Kappes MS, Papathoma-Köhle M, Keiler M. Assessing physical vulnerability for multi-hazards using an indicator-based methodology. *Applied Geography*, 2012; 32(2): 577-590.
34. Aubrecht C, Fuchs S, Neuhold C. Spatiotemporal aspects and dimensions in integrated disaster risk management. *Natural Hazards*, 2013; 68(3):1205-1216.
35. Papathoma-Köhle M, Kappes M, Keiler M, Glade T. Physical vulnerability assessment for alpine hazards: state of the art and future needs. *Natural Hazards*, 2011; 58(2): 645-680
36. Satumtira G, Dueñas-Osorio L, editors. *Synthesis of Modeling and Simulation Methods on Critical Infrastructure Interdependencies Research*. Berlin: Springer Berlin Heidelberg; 2010. (Gopalakrishnan K, Peeta S, editors. *Sustainable and Resilient Critical Infrastructure Systems*)
37. Zhang J, Song B, Zhang Z, Liu H. An approach for modeling vulnerability of the network of networks. *Physica A: Statistical Mechanics and its Applications*, 2014; 412:127-136.
38. Kurant M, Thiran P. Layered Complex Networks. *Physical Review Letter*, 2006; 96:138701.
39. Johansson J, Hassel H. An approach for modelling interdependent infrastructures in the context of vulnerability analysis. *Reliability Engineering & System Safety*, 2010; 95(12):1335-1344.

40. Ouyang M, Dueñas-Osorio L. Time-dependent resilience assessment and improvement of urban infrastructure systems. *Chaos*, 2012; 22:033122.
41. Simonovic SP, Peck A. Dynamic resilience to climate change caused natural disasters in coastal megacities quantification framework. *British Journal of Environment and Climate Change*, 2013; 3(3): 378-401.
42. Liu Y, Singh C. A methodology for evaluation of hurricane impact on composite power system reliability. *IEEE Transactions on Power Systems*, 2011; 26(1): 145-152.
43. Winkler J, Duenas-Osorio L, Stein R, Subramanian D. Performance assessment of topologically diverse power systems subjected to hurricane events. *Reliability Engineering & System Safety*, 2010; 95(4): 323-336.
44. Poljanšek K, Bono F, Gutiérrez E. Seismic risk assessment of interdependent critical infrastructure systems: the case of European gas and electricity networks. *Earthquake Engineering & Structural Dynamics*, 2012; 41(1): 61-79.
45. Reed DA, Kapur KC, Christie R D. Methodology for assessing the resilience of networked infrastructure. *IEEE Systems Journal*, 2009; 3(2):174-180.
46. Baroud H, Ramirez-Marquez J E, Barker K, Rocco CM. Stochastic measures of network resilience: Applications to waterway commodity flows. *Risk Analysis*, 2014; 34(7): 1317-1335.
47. Baroud H, Barker K, Ramirez-Marquez J E, Rocco C M. Inherent costs and interdependent impacts of infrastructure network resilience. *Risk Analysis*, 2015; 35(4): 642-662.
48. Vugrin E D, Warren D E, Ehlen M A, Camphouse RC, editors. A framework for assessing the resilience of infrastructure and economic systems. Berlin: Springer Berlin Heidelberg; 2010. (Gopalakrishnan K, Peeta S, editors. Sustainable and Resilient Critical Infrastructure Systems).
49. National Infrastructure Advisory Council. Critical infrastructure resilience: final report and recommendations, 2009. Available at: <https://www.dhs.gov/sites/default/files/publications/niac-critical-infrastructure-resilience-final-report-09-08-09-508.pdf>, Accessed December 11, 2016.
50. Nan C, Sansavini G. A quantitative method for assessing resilience of interdependent infrastructures. *Reliability Engineering & System Safety*, 2017; 157: 35-53.
51. Gill JC, Malamud BD. Reviewing and visualizing the interactions of natural hazards. *Reviews of Geophysics*, 2014; 52(4): 680-722.
52. Reed D, Wang S, Kapur K, Zheng C. Systems-based approach to interdependent electric power delivery and telecommunications infrastructure resilience subject to weather-related hazards. *Journal of Structural Engineering*, 2015; 14(8): 1943-541X.0001395, C4015011.
53. LaRocca S, Johansson J, Hassel H, Guikema S. Topological performance measures as surrogates for physical flow models for risk and vulnerability analysis for electric power systems. *Risk Analysis*, 2015; 35(4), 608-623.

54. Bruneau M, Reinhorn AM. Exploring the concept of seismic resilience for acute care facilities. *Earthquake Spectra*, 2007; 23(1):41-62.
55. Delmonaco G, Margottini C, Spizzichino D. ARMONIA methodology for multi-risk assessment and the harmonisation of different natural risk maps. 2006. Available at: [http://forum.eionet.europa.eu/eionet-air-climate/library/public/2010\\_citiesproject/interchange/armonia\\_project/armonia\\_project\\_5/download/en/1/ARMONIA\\_PROJECT\\_Deliverable%203.1.1.pdf](http://forum.eionet.europa.eu/eionet-air-climate/library/public/2010_citiesproject/interchange/armonia_project/armonia_project_5/download/en/1/ARMONIA_PROJECT_Deliverable%203.1.1.pdf), Accessed December 11, 2016.
56. Federal Emergency Management Agency. Hazards U.S. Multi-Hazard (HAZUSMH) Assessment Tool v1.3, 2011. Available at: [www.fema.gov/plan/prevent/hazus/index.shtm](http://www.fema.gov/plan/prevent/hazus/index.shtm), Accessed December 11, 2016.
57. Hernandez-Fajardo I, Duenas-Osorio L. Probabilistic study of cascading failures in complex interdependent lifeline systems. *Reliability Engineering & System Safety*, 2013; 111: 260-272.
58. Sultana S, Chen Z. Modeling flood induced interdependencies among hydroelectricity generating infrastructures. *Journal of environmental management*, 2009; 90(11): 3272-3282.
59. Tanali IR, Harrald JR. Effects of water infrastructure failure on response capabilities after hurricane Katrina. Institute for Crisis, Disaster and Risk Management, The George Washington University, 2006.
60. Lee K, Rosowsky D. Fragility analysis of wood frame buildings considering combined snow and earthquake loading. *Structure Safety*, 2006; 28: 289-303.
61. Zuccaro G, Cacace F, Spence R, Baxter P. Impact of explosive eruption scenarios at Vesuvius. *Journal of Volcanology and Geothermal Research*, 2008; 178(3):416-453.
62. Liu Z, Nadim F, Garcia-Aristizabal A. A three-level framework for multi-risk assessment. *Georisk: Assessment and Management of Risk for Engineered Systems and Geohazards*, 2015; 9(2): 59-74.
63. Buldyrev SV, Parshani R, Paul G, Stanley H E, Havlin S. Catastrophic cascade of failures in interdependent networks. *Nature*, 2010; 464(7291): 1025-1028.
64. Motter AE, Lai Y-C. Cascade-based attacks on complex networks. *Physical Review E*, 2002; 66(6): 065102.
65. Crucitti P, Latora V, Marchiori M. Model for cascading failures in complex networks. *Physical Review E*, 2004; 69(4), 045104.
66. Dobson I, Carreras BA, Lynch VE, Newman DE. Complex systems analysis of series of blackouts: cascading failure, criticality, and self-organization. *Bulk Power System Dynamics and Control-VI*, 2004.
67. Carreras BA, Newman DE, Dobson I, Poole AB. Evidence for self-organized criticality in a time series of electric power system blackouts. *IEEE Transactions on Circuits and Systems I: Regular Papers*, 2004; 51(9): 1733-1740.
68. Fang Y, Pedroni N, Zio E. Optimization of cascade-resilient electrical infrastructures and its validation by power flow modeling. *Risk Analysis*, 2015; 35(4): 594-607.

69. Delamare D, Diallo A, Chaudet C. High-level modeling of critical infrastructure's interdependencies. *International Journal of Critical Infrastructures*, 2009; 5(1-2):100-119.
70. Ouyang M, Hong L, Mao ZJ, Yu M H, Qi F. A methodological approach to analyze vulnerability of interdependent infrastructures. *Simulation Modelling Practice and Theory*, 2009; 17(5): 817-828.
71. Rinaldi SM, Peerenboom JP, Kelly TK. Identifying, understanding, and analyzing critical infrastructure interdependencies. *Control Systems IEEE*, 2001; 21(6): 11-25.
72. Ouyang M. Review on modeling and simulation of interdependent critical infrastructure systems. *Reliability engineering & System safety*, 2014; 121: 43-60.
73. Liu H, Davidson R A, Apanasovich T V. Statistical forecasting of electric power restoration times in hurricanes and ice storms. *IEEE Transactions on Power Systems*, 2007; 22(4): 2270-2279.
74. Simonovic SP, Arunkumar R. Quantification of resilience to water scarcity, a dynamic measure in time and space. *Proceedings of the International Association of Hydrological Sciences*, 2016; 373: 13-17.
75. Simonovic SP, Arunkumar R. Comparison of static and dynamic resilience for a multi-purpose reservoir operation, *Water Resources Research*, 52, online first doi:10.1002/2016WR019551.
76. Government of Canada. Energy Infrastructure Map. Available at: <http://open.canada.ca/data/en/dataset/23387971-b6d3-4ded-a40b-c8e832b4ea08>. Accessed July 20, 2017.
77. The Independent Electricity System Operator. Ontario's Electricity System. Available at: <http://www.ieso.ca/ontarioenergymap/index.html>. Accessed July 20, 2017.
78. Hydro One Networks Inc. Transmission System: Southern Ontario. <http://www.hydroone.com/RegulatoryAffairs/Documents/EB-2012-0031/Exhibit%20A/A-07-01.pdf>. Accessed July 20, 2017.
79. Canadian Association of Petroleum Producers. Canadian Energy Pipeline Association (CEPA) liquids and natural gas pipelines maps. Available at: <http://www.capp.ca/canadian-oil-and-natural-gas/infrastructure-and-transportation/pipelines>. Accessed July 20, 2017.
80. Canadian Energy Pipeline Association. About Pipelines Map. Available at: <http://www.aboutpipelines.com>. Accessed July 20, 2017.
81. Buldyrev SV, Parshani R, Paul G, Stanley H E, Havlin S. Catastrophic cascade of failures in interdependent networks. *Nature*, 2010; 464(7291): 1025-1028.
82. Motter AE, Lai Y-C. Cascade-based attacks on complex networks. *Physical Review E*, 2002; 66(6): 065102.
83. Crucitti P, Latora V, Marchiori M. Model for cascading failures in complex networks. *Physical Review E*, 2004; 69(4), 045104.

84. Goh KI, Kahng B, Kim D. Universal behavior of load distribution in scale-free networks. *Physical Review Letters*, 2001; 87(27): 278701.
85. Canadian Census Analyser (CHASS). Canadian Census Data. Available at: <http://dc.chass.utoronto.ca/census/>, Accessed December 20, 2016.
86. Public Safety Canada. The Canadian Disaster Database. Available at: <http://www.publicsafety.gc.ca/cnt/rsrscs/cndn-dsstr-dtbs/index-eng.aspx>, Accessed December 20, 2016.
87. Environment and Climate Change Canada. Hurricane Hazel. Available at: <https://www.ec.gc.ca/ouragans-hurricanes/default.asp?lang=En&n=4343267B-1>, Accessed December 20, 2016.
88. National Oceanic and Atmospheric Administration. Types of Damage Due to Hurricane Winds. Available at: <http://www.nhc.noaa.gov/aboutsshws.php>. Accessed December 20, 2016.
89. Hurricane Hazel Path. Available at: <https://www.arcgis.com/home/item.html?id=871c5504798b4a62a45ab98348c72014>. Accessed December 20, 2016.
90. Willoughby H E. Forecasting hurricane intensity and impacts. *Science*, 2007; 315(5816): 1232-1233.
91. National Oceanic and Atmospheric Administration. Available at: <http://journals.ametsoc.org/doi/pdf/10.1175/BAMS-D-12-00089.1>, Accessed December 20, 2016.
92. Toronto and Region Conservation for The Living City. Flood Plain Mapping. Available at: <https://trca.ca/conservation/flood-risk-management/flood-plain-management/>, Accessed December 20, 2016.
93. Toronto and Region Conservation Authority Office of Emergency Management. City of Toronto Emergency Plan Risk Specific Plan: Flooding. October 2014. Available at:
94. [https://www1.toronto.ca/city\\_of\\_toronto/office\\_of\\_emergency\\_management/files/pdf/flood\\_rsp.pdf](https://www1.toronto.ca/city_of_toronto/office_of_emergency_management/files/pdf/flood_rsp.pdf), Accessed December 20, 2016.
95. Environment and Climate Change Canada. Hurricane Hazel – Impacts. Available at: <http://www.ec.gc.ca/ouragans-hurricanes/default.asp?lang=en&n=FE71002F-1> , Accessed December 20, 2016.
96. Federal Emergency Management Agency. Hazards U.S. multi-hazard (HAZUS-MH) assessment tool v1.3. Available at: <https://www.fema.gov/hazus-software>, Accessed December 20, 2016.
97. Quanta Technology. Undergrounding assessment phase 3 final report: ex ante cost and benefit modeling. Prepared for the Florida Electric Utilities and submitted to the Florida Public Service Commission per order PSC-06-0351-PAA-EI; May 2008.
98. Liu H, Davidson RA, Apanasovich T V. Statistical forecasting of electric power restoration times in hurricanes and ice storms. *IEEE Transactions on Power Systems*, 2007; 22(4): 2270-2279.

99. Nateghi R, Guikema SD, Quiring SM. Comparison and validation of statistical methods for predicting power outage durations in the event of hurricanes. *Risk analysis*, 2011; 31(12): 1897-1906.
100. Matisziw TC, Murray A T, Grubestic TH. Strategic network restoration. *Networks and Spatial Economics*, 2010; 10(3): 345-361.
101. Berezin Y, Bashan A, Danziger MM, Li D, Havlin S. Localized attacks on spatially embedded networks with dependencies. *Scientific reports*, 2015; 5.

## APPENDIX A: Data Resources

(1) GIS data of Greater Toronto Area (GTA) Boundary is available from Ontario Ministry of Natural Resources and published on Scholars Geo Portal ([http://geo1.scholarsportal.info/#r/search/\\_queries@=Greater%20Toronto%20Area%20%28GTA%29%20Boundary;&fields@=:&sort=relevance&limit=entitled](http://geo1.scholarsportal.info/#r/search/_queries@=Greater%20Toronto%20Area%20%28GTA%29%20Boundary;&fields@=:&sort=relevance&limit=entitled)).

(2) GIS data of electric infrastructures including location and attribution of electric generations, transmission stations and transmission lines is downloaded from CanVec database (canvec\_50K\_ON\_Res\_MGT) available from NRCan at Government of Canada website (<http://open.canada.ca/data/en/dataset/23387971-b6d3-4ded-a40b-c8e832b4ea08>). Ontario's Electric System map made by IESO is used to check the structure of GTA Bulk Power System and the generation data (<http://www.ieso.ca/ontarioenergymap/index.html>). Transmission system of Southern Ontario by Hydro One provides the data on transmission stations and transmission lines located in GTA especially the 115kv ones (<http://www.hydroone.com/RegulatoryAffairs/Documents/EB-2012-0031/Exhibit%20A/A-07-01.pdf>)

(3) GIS data of gas and oil infrastructure including location and attribution of pump stations, tank farm/terminal, meter/regulator stations and pipelines is also obtained from CanVec database (canvec\_50K\_ON\_Res\_MGT). The data is checked and updated with the pipelines maps obtained from CEPA (<http://www.aboutpipelines.com/>).

(4) GTA Population data (<http://dc.chass.utoronto.ca/census/>) and Dissemination Area boundaries (<http://www12.statcan.gc.ca/census-recensement/2011/geo/bound-limit/bound-limit-2011-eng.cfm>) are obtained from Canada Statistics website for 2011 Census.

(5) Disaster scenario is modelled based on the record of Hurricane Hazel, which was followed by a flood and struck Toronto on October 15, 1954. The path of Hurricane Hazel (Hurricane Hazel Storm Story Map) is obtained from NOAA GeoPlatform (<http://noaa.maps.arcgis.com/home/item.html?id=f8c2910c358e47d98ea2bdb03903462f>). The information of the hurricane, storm surge and flood impacts are from government websites: Hurricane Hazel: 60th Anniversary (<http://noaa.maps.arcgis.com/apps/StorytellingTextLegend/index.html?appid=f8c2910c358e47d98ea2bdb03903462f>) and Environment and Climate Change Canada (<http://www.ec.gc.ca/ouragans-hurricanes/default.asp?lang=en&n=FE71002F-1>).

## APPENDIX B: Model Code for MATLAB

### (1) Calculation of the performance of electric power system under hazard

```
function [fnode]=electric_performance(A,h,fnode,flink,C)
% A is the adjacent matrix;
% h is a 3*1 vector applied to denote the property of nodes,number<h(1) is generator, h(1)<number<=h(2)
is 500 substation, h(2)<number<=h(3) is 230 substation
% fnode(:,1) is the vector denoting the physical damaged nodes;fnode(:,2)denote the functional damaged
node
% flink is the n*2 vector denoting the damaged links
% C is threshold for the load of nodes
% fnode_update is a n*2 vector denoting the updated fnode
B=A;
D=plu(A);
cc=size(A);
%% change the adjacent matrix according to node damage
for i=1:cc(1)
    if fnode(i,1)==1 || fnode(i,2)==1 %% the links from the physical and functional damaged nodes are set
to fail
        B(fnode(i,1,:))=0;
    end
end
%% change the adjacent matrix according to link damage
u2=size(flink);
if u2(1)<1
    B=B;
elseif u2(1)>=1 && u2(2)>=1
for i=1:u2(1)
    if flink(i,1)>0
        B(flink(i,1),flink(i,2))=0;
    end
end
end
% calculate
f=[];
l=[]; %% denote the number of generators that each substation connected
% calculate the each substation's number of generators
for i=h(1)+1:cc(1)
    for j=1:h(1)
        f(i,j)=D(j,i); %% check the path from plants to substations
    end
    kkk=find(f(i,:)>0 & f(i,:)<Inf);
    ss=size(kkk);
    l(i)=ss(2); %% the substation i's number of generators
end
D1=plu(B);%% the shortest path for damaged system
f1=[];
ll=[]; %% denote the nodes fail due to lack of power input
for i=h(1)+1:cc(1)
    for j=1:h(1)
        f1(i,j)=D1(j,i); %% check
```

```
end
rrr=size(find(f1(i,.)>0 & f1(i,.)<Inf));
ll(i)=rrr(2);
if (ll(i)/l(i))<(1/C)
fnode(i,2)=1;
else
fnode(i,2)=0;
end
end
```

## (2) Calculation of the performance of gas supply system under hazard

```
function [gnode_update]=gas_performance(A,h,gnode,glink)
% A is the adjacent matrix;
% h is a number applied to denote the property of nodes,number<h(1) is generator, h(1)<number is
substation
% gnode(:,1) is the vector denoting the physical damaged nodes;gnode(:,2)denote the functional damaged
node
% glink is the n*2 vector denoting the damaged links
% gnode_update is a n*2 vector denoting the updated fnode
cc=size(A);
B=A;
for i=1:cc(1)
    if gnode(i,1)==1 || gnode(i,2)==1
        B(i,:)=0;
    end
end
u2=size(glink);
if u2(1)>=1
for i=1:u2(1)
    if glink(i,1)>0
        B(glink(i,1),glink(i,2))=0;
    end
end
end
D=plu(B);
f=[];
for i=h+1:cc(1)
    for j=1:h
        f(i,j)=1/D(j,i);
    end
end
if sum(f(i,:))==0 % denote the substation does not connect to any generator
    gnode(i,2)=1; % the node fail due to lack of gas injection
end
end
end
gnode_update=gnode;
```

### (3) Calculation of the performance of oil supply system under hazard

```
function [onode]=oil_performance(A,h,onode,olink)
%% calculate the performance of oil system under hazard
% A is the adjacent matrix;
% h is a number applied to denote the property of nodes,number<h(1) is generator, h(1)<number is
substation
% gnode(:,1) is the vector denoting the physical damaged nodes;gnode(:,2)denote the functional damaged
node
% glink is the n*2 vector denoting the damaged links
% gnode_update is a n*2 vector denoting the updated fnode
cc=size(A);
B=A;
for i=1:cc(1)
    if onode(i,1)==1 || onode(i,2)==1
        B(i,:)=0;
    end
end
u2=size(olink);
if u2(1)==0
    B=B;
elseif u2(1)>=1
    for i=1:u2(1)
        if olink(i,1)>0
            B(olink(i,1),olink(i,2))=0;
        end
    end
end
D=plu(B);
f=[];
for i=h+1:cc(1)
    for j=1:h
        f(i,j)=1/D(j,i);
    end
    if sum(f(i,:))==0 % denote the substation does not connect to any generator
        onode(i,2)=1; % the node fail due to lack of gas injection
    end
end
```

#### (4) Generation of the flood scenario

```
function [fnode,flink]=flood %% only occur on the electric power system
%the return is the damage on electric power system at each time step.
% [flood,lable1]=xlsread('FLOOD.xlsx');
% save Flood_data flood;
% save Flood_text lable1;
load Flood_data;
fnode=zeros(74,5); %% only denote the physical failure on nodes
flink=[];
JJ=rand(1,10);

if JJ(1,1)<0.3
    fnode(5,4:5)=1;
end
if JJ(1,2)<0.3
    fnode(8,5)=1;
end
if JJ(1,3)<0.15
    fnode(31,2:5)=1;
end
if JJ(1,4)<0.15
    fnode(32,2:5)=1;
end
if JJ(1,5)<0.15
    fnode(33,2:5)=1;
end
if JJ(1,6)<0.15
    fnode(52,5)=1;
end
if JJ(1,7)<0.15
    fnode(57,4:5)=1;
end
if JJ(1,8)<0.15
    fnode(59,4:5)=1;
end
if JJ(1,9)<0.15
    fnode(64,4:5)=1;
end
if JJ(1,10)<0.64 %%% occur on the 5th time step after flood
    flink(1,1)=64;
    flink(1,2)=57;
end
```

## (5) Generation of the hurricane scenario

```
function [hnode,hlink]=hurricane
%% honode is a x*4 vector, hlink is a x*4 vector about links
load FLN %% acquire fln, the number lable of links may be damaged
load hdb %% acquire h_a to calculate the damage probability of links
speed=120; %% the speed of wind
[ldp]=dp(h_a,speed); %% acquire the damage probability of links
hh=[]; %% 1,2 is link num_lable, 3 is damage_probility, 4 is damge time
hh(:,1:2)=fln;
hh(:,3)=ldp;
hh(:,4)=h_a(:,3);
ss=size(fl_n);
r=rand(ss(1),1);
for i=1:ss(1)
    if r(i)<hh(i,3)
        hh(i,3)=1;
    else
        hh(i,3)=0;
    end
end
b=find(hh(:,3)); %% find the damaged link due to hurricane
lc=[];
ss=size(b);
for i=1:ss(1)
    lc(i,1:2)=hh(b(i),1:2);
    lc(i,3)=hh(b(i),4);
end
ss=size(lc);
hlink=zeros(ss(1),4); %% the return of damaged links
d=find(lc(:,3)==1);
q=size(d);
for i=1:q
    hlink(i,1:2)=lc(d(i),1:2);
    hlink(i,3:4)=lc(d(i),1:2);
end
d1=find(lc(:,3)==2);
q1=size(d1);
for i=q+1:q+q1
    hlink(i,3:4)=lc(d1(i-q(1)),1:2);
end

%bout nodes
load IS_data; %% acquire matrix
load NT; %% acquire n_t
vv=size(matrix);
ww=rand(vv(1),1);
for i=1:8
    ww(i)=1;
end
ee=find(ww<0.2); %% find the number of failed nodes
cc=size(ee);
```

```

hhh=zeros(cc(1),2);
for i=1:cc(1)
    hhh(i,1)=ee(i);
    hhh(i,2)=n_t(ee(i)-8); %% the time of node fail
end
fnode=zeros(cc(1),4);
ddd1=find(hhh(:,2)==1);
ddd2=find(hhh(:,2)==2);
ddd3=find(hhh(:,2)==3);
ddd4=find(hhh(:,2)==4);
ss1=size(ddd1);
ss2=size(ddd2);
ss3=size(ddd3);
ss4=size(ddd4);
%% value the vector
for i=1:ss1(1)
    fnode(i,1)=hhh(ddd1(i,1));
    fnode(i,2)=hhh(ddd1(i,1));
    fnode(i,3)=hhh(ddd1(i,1));
    fnode(i,4)=hhh(ddd1(i,1));
end
for i=ss1(1)+1:ss1(1)+ss2(1)
    fnode(i,2)=hhh(ddd2(i-ss1(1)),1);
    fnode(i,3)=hhh(ddd2(i-ss1(1)),1);
    fnode(i,4)=hhh(ddd2(i-ss1(1)),1);
end
if ss3(1)>0
    for i=ss1(1)+ss2(1)+1:ss1(1)+ss2(1)+ss3(1)
        fnode(i,3)=hhh(ddd2(i-ss1(1)-ss2(1)),1);
        fnode(i,4)=hhh(ddd2(i-ss1(1)-ss2(1)),1);
    end
end
if ss4(1)>0
    for i=ss1(1)+ss2(1)+ss3(1)+1:ss1(1)+ss2(1)+ss3(1)+ss4(1)
        fnode(i,4)=hhh(ddd2(i-ss1(1)-ss2(1)-ss3(1)),1);
    end
end
hnode=fnode;

function [ldp]=dp(g,p) %% function to calculate the damage probability of links, g is the link related
parameter, p is the wind speed,ldp is the link damage probability
ldp=[];
ss=size(g);
tp=2*10^(-7)*exp(0.0834*p);
if tp>1;
    tp=1;
end
for i=1:ss(1)
    ldp(i,1)=(1-(1-tp)^g(i,2))/g(i,1);
end

```

## (6) Calculation of the performance of three systems under combined hurricane and flood scenario

```
function [power_pf,gas_pf,oil_pf,tt]=hmain(C) %% for hurrican senario
load IS_data;
A=matrix;
cc=size(A);
Power=A(1:74,1:74);
Gas=A(75:91,75:91);
Oil=A(92:96,92:96);
P_G=A(1:74,75:91);
P_O=A(1:74,92:96);
G_P=A(75:91,1:74);
h=[8,12,55]; % vector denote the characteristic of nodes in electric power
h1=1; % number denote the characteristic of nodes in gas
h2=1; % number denote the characteristic of nodes in oil
[hnode,hlink]=hurricane; %% generate the hurricane scenario
[h_pnode,h_gnode,h_onode,h_plink,h_pglink,h_polink]=Vtransfer(hnode,hlink);
tt=zeros(96,40);
for i=1:40
    %% denote the update state of nodes in three systems
    fnode=zeros(74,2);
    fgnode=zeros(17,2);
    fonode=zeros(5,2);
    glink=[];
    olink=[];
    if i==1
        %% determine the initial value
        fnode(:,1)=h_pnode(:,1);
        fgnode(:,1)=h_gnode(:,1);
        fonode(:,1)=h_onode(:,1);
        if sum(h_plink(:,1:2))~=0
            fplink=h_plink(:,1:2);
        else
            fplink=[];
        end
    end

    %%% state calculation
    % examine the state of power node
    [fnode]=electric_performance(Power,h,fnode,fplink,C);
    for j=1:74
        if sum(fnode(j,:))>0
            tt(j,i)=1;
        end
    end

    [fgnode]=gas_performance(Gas,h1,fgnode,glink);
    [fonode]=oil_performance(Oil,h2,fonode,olink);
    for j=1:17
        if sum(fgnode(j,i))>0
            tt(74+j,i)=1;
        end
    end
end
```

```

end
for j=1:5
    if sum(fonode(j,i))>0
        tt(91+j,i)=1;
    end
end
end
end
%%%%%%state 2, links determined, nodes change
if i==2 || i==3
    fnode=[h_pnode(:,i),fnode(:,2)];
    fgnode=[h_gnode(:,i),fgnode(:,2)];
    fonode=[h_onode(:,i),fonode(:,2)];
    if sum(h_plink(:,3:4))~=0
        fplink=h_plink(:,3:4);
    else
        fplink=[];
    end
    if sum(h_pglink)~=0
        fpglink=h_pglink(:,3:4);
    else
        fpglink=[];
    end
    if sum(h_polink)~=0
        fpolink=h_polink(:,3:4);
    else
        fpolink=[];
    end
    end
    [fnode]=electric_performance(Power,h,fnode,fplink,C);
    for j=1:74
        if sum(fnode(j,:))>0
            tt(j,i)=1;
        end
    end
    end
    [fgnode]=gas_performance(Gas,h1,fgnode,glink);
    [fonode]=oil_performance(Oil,h2,fonode,olink);
    %%% examine the state of gas and oil node due to interdependence,
    %%% stage 1
    for j=1:74
        if sum(fnode(j,:))>0
            for k=1:17 % examine the gas system
                if P_G(j,k)==1
                    fgnode(k,2)=1;
                    tt(74+k,i)=1; %% note in vector denoting if nodes fail
                end
            end
            for k=1:5 % examine the oil system
                if P_O(j,k)==1;
                    fonode(k,2)=1;
                    tt(91+k,i)=1;
                end
            end
        end
    end
end
end

```

```

end
%%stag2 the inter link
if sum(fpmlink)~=0
    ct=size(fpmlink);
    for j=1:ct(1)
        fgnode(fpmlink(j,2)-74,2)=1;
        tt(fpmlink(j,2),i)=1;
    end
end
if sum(fpmlink)~=0
    ct=size(fpmlink);
    for j=1:ct(1)
        fonode(fpmlink(j,2)-91,2)=1;
        tt(fpmlink(j,2),i)=1;
    end
end
% examine the electric power due to interdependence with gas
for j=1:17
    if sum(fgnode(j,:))>0
        for k=1:8
            if G_P(j,k)==1
                fnode(k,2)=1;
                tt(k,i)=1;
            end
        end
    end
end
end
%%%%%%%%%%
if i>=4
    fnode=[h_pnode(:,4),fnode(:,2)];
    fgnode=[h_gnode(:,4),fgnode(:,2)];
    fonode=[h_onode(:,4),fonode(:,2)];
    if sum(h_plink(:,3:4))~=0
        fplink=h_plink(:,3:4);
    else
        fplink=[];
    end
    if sum(h_pmlink)~=0
        fpmlink=h_pmlink(:,3:4);
    else
        fpmlink=[];
    end
    if sum(h_polink)~=0
        fpolink=h_polink(:,3:4);
    else
        fpolink=[];
    end
    [fnode]=electric_performance(Power,h,fnode,fplink,C);
    for j=1:74
        if sum(fnode(j,:))>0
            tt(j,i)=1;
        end
    end
end

```

```

end
[fgnode]=gas_performance(Gas,h1,fgnode,glink);
[fonode]=oil_performance(Oil,h2,fonode,olink);
%% examine the state of gas and oil node due to interdependence,
%% stage 1
for j=1:74
    if sum(fnode(j,:))>0
        for k=1:17 % examine the gas system
            if P_G(j,k)==1
                fgnode(k,2)=1;
                tt(74+k,i)=1; %% note in vector denoting if nodes fail
            end
        end
        for k=1:5 % examine the oil system
            if P_O(j,k)==1;
                fonode(k,2)=1;
                tt(91+k,i)=1;
            end
        end
    end
end
end
%% stag2 the inter link
if sum(fpmlink)~=0
    ct=size(fpmlink);
    for j=1:ct(1)
        fgnode(fpmlink(j,2)-74,2)=1;
        tt(fpmlink(j,2),i)=1;
    end
end
if sum(fpmlink)~=0
    ct=size(fpmlink);
    for j=1:ct(1)
        fonode(fpmlink(j,2)-91,2)=1;
        tt(fpmlink(j,2),i)=1;
    end
end
end
% examine the electric power due to interdependence with gas
for j=1:17
    if sum(fgnode(j,:))>0
        for k=1:8
            if G_P(j,k)==1
                fnode(k,2)=1;
                tt(k,i)=1;
            end
        end
    end
end
end
end
end
end
[power_pf]=measure_power(tt);
[gas_pf]=measure_gas(tt);

```

```

[oil_pf]=measure_oil(tt);
for i=3:7
    power_pf(i)=power_pf(i-1)-0.05*rand(1,1);
    gas_pf(i)=gas_pf(i-1)-0.02*rand(1,1);
    oil_pf(i)=oil_pf(i-1)-0.04*rand(1,1);
end
for i=8:40
    power_pf(i)=power_pf(i-1);
    gas_pf(i)=gas_pf(i-1);
    oil_pf(i)=oil_pf(i-1);
end
for i=1:40
    if power_pf(i)<0
        power_pf(i)=0;
    end
    if gas_pf(i)<0
        gas_pf(i)=0;
    end
    if oil_pf(i)<0
        oil_pf(i)=0;
    end
end
end

function [power_pf]=measure_power(tt) %% function for calculating the performance of power
uu=4*500+33*230+19*115;
power_pf=[];
for i=1:40
    power_pf(i)=(uu-(sum(tt(9:12,i))*500+sum(tt(13:55,i))*230+sum(tt(56:74,i))*115))/uu;
end

function [gas_pf]=measure_gas(tt)
gas_pf=[];
for i=1:40
    gas_pf(i)=(17-sum(tt(75:91,i)))/17;
end

function [oil_pf]=measure_oil(tt)
oil_pf=[];
for i=1:40
    oil_pf(i)=(5-sum(tt(92:96,i)))/5;
end
end

```

## (7) Calculation of the performance of three systems under flood scenario

```
function [power_pf,gas_pf,oil_pf,tt]=main(C)
load IS_data;
A=matrix;
cc=size(A);
Power=A(1:74,1:74);
Gas=A(75:91,75:91);
Oil=A(92:96,92:96);
P_G=A(1:74,75:91);
P_O=A(1:74,92:96);
G_P=A(75:91,1:74);
h=[8,12,55]; % vector denote the characteristic of nodes in electric power
h1=1; % number denote the characteristic of nodes in gas
h2=1; % number denote the characteristic of nodes in oil
% C=2 %% threshold for electric power system

%%% flood
[f_pnode,f_plink]=flood; %% return the physical failure nodes at each time step
tt=zeros(96,40); %% denote node state at each time step

%%% begin state update
for i=1:40
    %% denote the update state of nodes in three systems
    fnode=zeros(74,2);
    fgnode=zeros(17,2);
    fonode=zeros(5,2);
    enode=zeros(74,1); %% the node state of last step
    egnode=zeros(17,1); % the node state of last step
    %%% initial state
    if i==2 %% only need to examine the electric power
        fnode(:,1)=f_pnode(:,2);
        flink=[];
        [fnode]=electric_performance(Power,h,fnode,flink,C);
        for j=1:74
            if sum(fnode(j,:))>0
                tt(j,i)=1;
            end
        end
        enode=fnode(:,2);
    end
    %%% special state 1
    if i==3 || i==4
        fnode=[f_pnode(:,i),fnode(:,2)];
        flink=[];
        glink=[];
        olink=[];

        % examine the state of power node
        [fnode]=electric_performance(Power,h,fnode,flink,C);
```

```

for j=1:74
    if sum(fnode(j,:))>0
        tt(j,i)=1;
    end
end
% examine the state of power node
[fgnode]=gas_performance(Gas,h1,fgnode,glink);
[fonode]=oil_performance(Oil,h2,fonode,olink);
% examine the state of gas and oil node due to interdependence
for j=1:74
    if sum(fnode(j,:))>0
        for k=1:17 % examine the gas system
            if P_G(j,k)==1
                fgnode(k,2)=1;
                tt(74+k,i)=1; %% note in vector denoting if nodes fail
            end
        end
        for k=1:5 % examine the oil system
            if P_O(j,k)==1;
                fonode(k,2)=1;
                tt(91+k,i)=1;
            end
        end
    end
end
% examine the electric power due to interdependence with gas
for j=1:17
    if sum(fgnode(j,:))>0
        for k=1:8
            if G_P(j,k)==1
                fnode(k,2)=1;
                tt(k,i)=1;
            end
        end
    end
end
enode=fnode(:,2);
egnode=fgnode(:,2);
end
%% %% common procedure for state update
if i>4
    fnode=[f_pnode(:,5),fnode(:,2)];
    flink=f_plink;
    glink=[];
    olink=[];
    [fnode]=electric_performance(Power,h,fnode,flink,C);
    for j=1:74
        if sum(fnode(j,:))>0
            tt(j,i)=1;
        end
    end
    % examine the state of power node

```

```

[fgnode]=gas_performance(Gas,h1,fgnode,glink);
[gonode]=oil_performance(Oil,h2,fonode,olink);
% examine the state of gas and oil node due to interdependence
for j=1:74
    if sum(fnode(j,:))>0
        for k=1:17 % examine the gas system
            if P_G(j,k)==1
                fgnode(k,2)=1;
                tt(74+k,i)=1; %% note in vector denoting if nodes fail
            end
        end
        for k=1:5 % examine the oil system
            if P_O(j,k)==1;
                fonode(k,2)=1;
                tt(91+k,i)=1;
            end
        end
    end
end
end

% examine the electric power due to interdependence with gas
for j=1:17
    if sum(fgnode(j,:))>0
        for k=1:8
            if G_P(j,k)==1
                fnode(k,2)=1;
                tt(k,i)=1;
            end
        end
    end
end
enode=fnode(:,2);
egnode=fgnode(:,2);
end

end
[power_pf]=measure_power(tt);
[gas_pf]=measure_gas(tt);
[oil_pf]=measure_oil(tt);
[power_pf]=measure_power(tt);
[gas_pf]=measure_gas(tt);
[oil_pf]=measure_oil(tt);
for i=4:6
    power_pf(i)=power_pf(i-1)-0.05*rand(1,1);
    gas_pf(i)=gas_pf(i-1)-0.02*rand(1,1);
    oil_pf(i)=oil_pf(i-1)-0.04*rand(1,1);
end
for i=7:20
    power_pf(i)=power_pf(i-1);
    gas_pf(i)=gas_pf(i-1);
    oil_pf(i)=oil_pf(i-1);
end

```

```

end
for i=1:40
    if power_pf(i)<0
        power_pf(i)=0;
    end
    if gas_pf(i)<0
        gas_pf(i)=0;
    end
    if oil_pf(i)<0
        oil_pf(i)=0;
    end
end
end

```

```

function [power_pf]=measure_power(tt) %% function for calculating the performance of power
uu=4*500+33*230+19*115;
power_pf=[];
for i=1:40
    power_pf(i)=(uu-(sum(tt(9:12,i))*500+sum(tt(13:55,i))*230+sum(tt(56:74,i))*115))/uu;
end

```

```

function [gas_pf]=measure_gas(tt)
gas_pf=[];
for i=1:40
    gas_pf(i)=(17-sum(tt(75:91,i)))/17;
end

```

```

function [oil_pf]=measure_oil(tt)
oil_pf=[];
for i=1:40
    oil_pf(i)=(5-sum(tt(92:96,i)))/5;
end

```

## (8) Calculation of the performance of three systems under hurricane and flood scenario

```
function [power_pf,gas_pf,oil_pf,tt]=hfmain(C) %% for hurrican senario
load IS_data;
A=matrix;
cc=size(A);
Power=A(1:74,1:74);
Gas=A(75:91,75:91);
Oil=A(92:96,92:96);
P_G=A(1:74,75:91);
P_O=A(1:74,92:96);
G_P=A(75:91,1:74);
h=[8,12,55]; % vector denote the characteristic of nodes in electric power
h1=1; % number denote the characteristic of nodes in gas
h2=1; % number denote the characteristic of nodes in oil
[hnode,hlink]=hurricane; %% generate the hurricane scenario
[h_pnode,h_gnode,h_onode,h_plink,h_pglink,h_polink]=Vtransfer(hnode,hlink);
tt=zeros(96,40);
[n_node,n_link]=flood; %% return the physical failure nodes at each time step

for i=1:40
    %% denote the update state of nodes in three systems
    fnode=zeros(74,2);
    fgnode=zeros(17,2);
    fonode=zeros(5,2);
    glink=[];
    olink=[];
    if i==1
        %% determine the initial value
        fnode(:,1)=h_pnode(:,1);
        fgnode(:,1)=h_gnode(:,1);
        fonode(:,1)=h_onode(:,1);
        if sum(h_plink(:,1:2))~=0
            fplink=h_plink(:,1:2);
        else
            fplink=[];
        end
    end

    %% state calculation
    % examine the state of power node
    [fnode]=electric_performance(Power,h,fnode,fplink,C);
    for j=1:74
        if sum(fnode(j,:))>0
            tt(j,i)=1;
        end
    end

    [fgnode]=gas_performance(Gas,h1,fgnode,glink);
    [fonode]=oil_performance(Oil,h2,fonode,olink);
    for j=1:17
        if sum(fgnode(j,i))>0
            tt(74+j,i)=1;
        end
    end
end
```

```

    end
end
for j=1:5
    if sum(fonode(j,i))>0
        tt(91+j,i)=1;
    end
end
end
end
%%%%%%state 2, links determined, nodes change
if i==2 || i==3
    fnode=[h_pnode(:,i),fnode(:,2)];
    fgnode=[h_gnode(:,i),fgnode(:,2)];
    fonode=[h_onode(:,i),fonode(:,2)];
    if sum(h_plink(:,3:4))~=0
        fplink=h_plink(:,3:4);
    else
        fplink=[];
    end
    if sum(h_pglink)~=0
        fpglink=h_pglink(:,3:4);
    else
        fpglink=[];
    end
    if sum(h_polink)~=0
        fpolink=h_polink(:,3:4);
    else
        fpolink=[];
    end
    [fnode]=electric_performance(Power,h,fnode,fplink,C);
    for j=1:74
        if sum(fnode(j,:))>0
            tt(j,i)=1;
        end
    end
    [fgnode]=gas_performance(Gas,h1,fgnode,glink);
    [fonode]=oil_performance(Oil,h2,fonode,olink);
    %%% examine the state of gas and oil node due to interdependence,
    %%% stage 1
    for j=1:74
        if sum(fnode(j,:))>0
            for k=1:17 % examine the gas system
                if P_G(j,k)==1
                    fgnode(k,2)=1;
                    tt(74+k,i)=1; %% note in vector denoting if nodes fail
                end
            end
            for k=1:5 % examine the oil system
                if P_O(j,k)==1;
                    fonode(k,2)=1;
                    tt(91+k,i)=1;
                end
            end
        end
    end
end
end

```

```

    end
end
%%stag2 the inter link
if sum(fpmlink)~=0
    ct=size(fpmlink);
    for j=1:ct(1)
        fgnode(fpmlink(j,2)-74,2)=1;
        tt(fpmlink(j,2),i)=1;
    end
end
if sum(fpmlink)~=0
    ct=size(fpmlink);
    for j=1:ct(1)
        fonode(fpmlink(j,2)-91,2)=1;
        tt(fpmlink(j,2),i)=1;
    end
end
% examine the electric power due to interdependence with gas
for j=1:17
    if sum(fgnode(j,:))>0
        for k=1:8
            if G_P(j,k)==1
                fnode(k,2)=1;
                tt(k,i)=1;
            end
        end
    end
end
end
end
end
%% % % % % % % % % % % % % % % %
if i>3 && i<=13
    fnode=[h_pnode(:,4),fnode(:,2)];
    fgnode=[h_gnode(:,4),fgnode(:,2)];
    fonode=[h_onode(:,4),fonode(:,2)];

    if sum(h_plink(:,3:4))~=0
        fplink=h_plink(:,3:4);
    else
        fplink=[];
    end
    if sum(h_pmlink)~=0
        fpmlink=h_pmlink(:,3:4);
    else
        fpmlink=[];
    end
    if sum(h_polink)~=0
        fpolink=h_polink(:,3:4);
    else
        fpolink=[];
    end
    [fnode]=electric_performance(Power,h,fnode,fplink,C);
    for j=1:74

```

```

    if sum(fnode(j,:))>0
        tt(j,i)=1;
    end
end
[fgnode]=gas_performance(Gas,h1,fgnode,glink);
[fonode]=oil_performance(Oil,h2,fonode,olink);
%% examine the state of gas and oil node due to interdependence,
%% stage 1
for j=1:74
    if sum(fnode(j,:))>0
        for k=1:17 % examine the gas system
            if P_G(j,k)==1
                fgnode(k,2)=1;
                tt(74+k,i)=1; %% note in vector denoting if nodes fail
            end
        end
        for k=1:5 % examine the oil system
            if P_O(j,k)==1;
                fonode(k,2)=1;
                tt(91+k,i)=1;
            end
        end
    end
end
%%stag2 the inter link
if sum(fpmlink)~=0
    ct=size(fpmlink);
    for j=1:ct(1)
        fgnode(fpmlink(j,2)-74,2)=1;
        tt(fpmlink(j,2),i)=1;
    end
end
if sum(fpmlink)~=0
    ct=size(fpmlink);
    for j=1:ct(1)
        fonode(fpmlink(j,2)-91,2)=1;
        tt(fpmlink(j,2),i)=1;
    end
end
% examine the electric power due to interdependence with gas
for j=1:17
    if sum(fgnode(j,:))>0
        for k=1:8
            if G_P(j,k)==1
                fnode(k,2)=1;
                tt(k,i)=1;
            end
        end
    end
end
end
end
end
end
end

```

```

%%%%%%
if i>13 && i<=17
    for j=1:74
        if h_pnode(j,4)+n_node(j,i-12)>0
            fnode(j,1)=1;
        end
    end
    fgnode=[h_gnode(:,4),fgnode(:,2)];
    fonode=[h_onode(:,4),fonode(:,2)];

if i>15
    if sum(n_link)~=0
        trr=size(h_plink(:,3:4));
        fplink(1:trr(1,:))=h_plink(:,3:4);
        fplink(trr(1)+1,:)=n_link;
    else
        fplink=h_plink(:,3:4);
    end
else
    fplink=h_plink(:,3:4);
end

if sum(h_pglink)~=0
    fpglink=h_pglink(:,3:4);
else
    fpglink=[];
end
if sum(h_polink)~=0
    fpolink=h_polink(:,3:4);
else
    fpolink=[];
end
[fnode]=electric_performance(Power,h,fnode,fplink,C);
for j=1:74
    if sum(fnode(j,:))>0
        tt(j,i)=1;
    end
end
[fgnode]=gas_performance(Gas,h1,fgnode,glink);
[fonode]=oil_performance(Oil,h2,fonode,olink);
%%% examine the state of gas and oil node due to interdependence,
%%% stage 1
for j=1:74
    if sum(fnode(j,:))>0
        for k=1:17 % examine the gas system
            if P_G(j,k)==1
                fgnode(k,2)=1;
                tt(74+k,i)=1; %% note in vector denoting if nodes fail
            end
        end
    end
    for k=1:5 % examine the oil system

```

```

        if P_O(j,k)==1;
            fonode(k,2)=1;
            tt(91+k,i)=1;
        end
    end
end
end
end
%%stag2 the inter link
if sum(fpmlink)~=0
    ct=size(fpmlink);
    for j=1:ct(1)
        fgnode(fpmlink(j,2)-74,2)=1;
        tt(fpmlink(j,2),i)=1;
    end
end
if sum(fpmlink)~=0
    ct=size(fpmlink);
    for j=1:ct(1)
        fonode(fpmlink(j,2)-91,2)=1;
        tt(fpmlink(j,2),i)=1;
    end
end
end
%% examine the electric power due to interdependence with gas
for j=1:17
    if sum(fgnode(j,:))>0
        for k=1:8
            if G_P(j,k)==1
                fnode(k,2)=1;
                tt(k,i)=1;
            end
        end
    end
end
end
end
end

%%%%%%%%%%
if i>17
    for j=1:74
        if h_pnode(j,4)+n_node(j,5)>0
            fnode(j,1)=1;
        end
    end
end

fgnode=[h_gnode(:,4),fgnode(:,2)];
fonode=[h_onode(:,4),fonode(:,2)];

if sum(n_link)~=0
    trr=size(h_plink(:,3:4));
    fplink(1:trr(1),:)=h_plink(:,3:4);
    fplink(trr(1)+1,:)=n_link;
else

```

```

    fplink=h_plink(:,3:4);
end
if sum(h_pglink)~=0
    fpglink=h_pglink(:,3:4);
else
    fpglink=[];
end
if sum(h_polink)~=0
    fpolink=h_polink(:,3:4);
else
    fpolink=[];
end
[fnode]=electric_performance(Power,h,fnode,fplink,C);
for j=1:74
    if sum(fnode(j,:))>0
        tt(j,i)=1;
    end
end
[fnode]=gas_performance(Gas,h1,fnode,glink);
[fonode]=oil_performance(Oil,h2,fonode,olink);
%%% examine the state of gas and oil node due to interdependence,
%%% stage 1
for j=1:74
    if sum(fnode(j,:))>0
        for k=1:17 % examine the gas system
            if P_G(j,k)==1
                fnode(k,2)=1;
                tt(74+k,i)=1; %% note in vector denoting if nodes fail
            end
        end
        for k=1:5 % examine the oil system
            if P_O(j,k)==1;
                fonode(k,2)=1;
                tt(91+k,i)=1;
            end
        end
    end
end
%%%stag2 the inter link
if sum(fpglink)~=0
    ct=size(fpglink);
    for j=1:ct(1)
        fnode(fpglink(j,2)-74,2)=1;
        tt(fpglink(j,2),i)=1;
    end
end
if sum(fpolink)~=0
    ct=size(fpolink);
    for j=1:ct(1)
        fonode(fpolink(j,2)-91,2)=1;
        tt(fpolink(j,2),i)=1;
    end
end

```

```

    end
    % examine the electric power due to interdependence with gas
    for j=1:17
    if sum(fgnode(j,:))>0
    for k=1:8
    if G_P(j,k)==1
    fnode(k,2)=1;
    tt(k,i)=1;
    end
    end
    end
    end
    end
end
[power_pf]=measure_power(tt);
[gas_pf]=measure_gas(tt);
[oil_pf]=measure_oil(tt);
for i=3:7
    power_pf(i)=power_pf(i-1)-0.05*rand(1,1);
    gas_pf(i)=gas_pf(i-1)-0.02*rand(1,1);
    oil_pf(i)=oil_pf(i-1)-0.04*rand(1,1);
end
for i=8:13
    power_pf(i)=power_pf(i-1);
    gas_pf(i)=gas_pf(i-1);
    oil_pf(i)=oil_pf(i-1);
end

for i=14:17
    power_pf(i)=power_pf(i)-(power_pf(2)-power_pf(8));
    gas_pf(i)=gas_pf(i)-(gas_pf(2)-gas_pf(8));
    oil_pf(i)=oil_pf(i)-(oil_pf(2)-oil_pf(8));
end

for i=17:19
    if power_pf(16)<power_pf(12) || power_pf(17)<power_pf(12)

    power_pf(i)=power_pf(i-1)-0.05*rand(1,1);
    gas_pf(i)=gas_pf(i-1)-0.03*rand(1,1);
    oil_pf(i)=oil_pf(i-1)-0.03*rand(1,1);
    else
    power_pf(i)=power_pf(i-1);
    gas_pf(i)=gas_pf(i-1);
    oil_pf(i)=oil_pf(i-1);
    end
end
for i=19:40
    power_pf(i)=power_pf(i-1);
    gas_pf(i)=gas_pf(i-1);
    oil_pf(i)=oil_pf(i-1);
end
end

```

```

for i=1:40
    if power_pf(i)<0
        power_pf(i)=0;
    end
    if gas_pf(i)<0
        gas_pf(i)=0;
    end
    if oil_pf(i)<0
        oil_pf(i)=0;
    end
end

```

```

function [power_pf]=measure_power(tt) %% function for calculating the performance of power
uu=4*500+33*230+19*115;
power_pf=[];
for i=1:40
    power_pf(i)=(uu-(sum(tt(9:12,i))*500+sum(tt(13:55,i))*230+sum(tt(56:74,i))*115))/uu;
end

```

```

function [gas_pf]=measure_gas(tt)
gas_pf=[];
for i=1:40
    gas_pf(i)=(17-sum(tt(75:91,i)))/17;
end

```

```

function [oil_pf]=measure_oil(tt)
oil_pf=[];
for i=1:40
    oil_pf(i)=(5-sum(tt(92:96,i)))/5;
end

```

## APPENDIX C: List of Previous Reports in the Series

ISSN: (Print) 1913-3200; (online) 1913-3219

[In addition to 78 previous reports \(No. 01 – No. 78\) prior to 2012](#)

Samiran Das and Slobodan P. Simonovic (2012). [Assessment of Uncertainty in Flood Flows under Climate Change](#). Water Resources Research Report no. 079, Facility for Intelligent Decision Support, Department of Civil and Environmental Engineering, London, Ontario, Canada, 67 pages. ISBN: (print) 978-0-7714-2960-6; (online) 978-0-7714-2961-3.

Rubaiya Sarwar, Sarah E. Irwin, Leanna King and Slobodan P. Simonovic (2012). [Assessment of Climatic Vulnerability in the Upper Thames River basin: Downscaling with SDSM](#). Water Resources Research Report no. 080, Facility for Intelligent Decision Support, Department of Civil and Environmental Engineering, London, Ontario, Canada, 65 pages. ISBN: (print) 978-0-7714-2962-0; (online) 978-0-7714-2963-7.

Sarah E. Irwin, Rubaiya Sarwar, Leanna King and Slobodan P. Simonovic (2012). [Assessment of Climatic Vulnerability in the Upper Thames River basin: Downscaling with LARS-WG](#). Water Resources Research Report no. 081, Facility for Intelligent Decision Support, Department of Civil and Environmental Engineering, London, Ontario, Canada, 80 pages. ISBN: (print) 978-0-7714-2964-4; (online) 978-0-7714-2965-1.

Samiran Das and Slobodan P. Simonovic (2012). [Guidelines for Flood Frequency Estimation under Climate Change](#). Water Resources Research Report no. 082, Facility for Intelligent Decision Support, Department of Civil and Environmental Engineering, London, Ontario, Canada, 44 pages. ISBN: (print) 978-0-7714-2973-6; (online) 978-0-7714-2974-3.

Angela Peck and Slobodan P. Simonovic (2013). [Coastal Cities at Risk \(CCaR\): Generic System Dynamics Simulation Models for Use with City Resilience Simulator](#). Water Resources Research Report no. 083, Facility for Intelligent Decision Support, Department of Civil and Environmental Engineering, London, Ontario, Canada, 55 pages. ISBN: (print) 978-0-7714-3024-4; (online) 978-0-7714-3025-1.

Roshan Srivastav and Slobodan P. Simonovic (2014). [Generic Framework for Computation of Spatial Dynamic Resilience](#). Water Resources Research Report no. 085, Facility for Intelligent Decision Support, Department of Civil and Environmental Engineering, London, Ontario, Canada, 81 pages. ISBN: (print) 978-0-7714-3067-1; (online) 978-0-7714-3068-8.

Angela Peck and Slobodan P. Simonovic (2014). [Coupling System Dynamics with Geographic Information Systems: CCaR Project Report](#). Water Resources Research Report no. 086, Facility for Intelligent Decision Support, Department of Civil and Environmental Engineering, London, Ontario, Canada, 60 pages. ISBN: (print) 978-0-7714-3069-5; (online) 978-0-7714-3070-1.

Sarah Irwin, Roshan Srivastav and Slobodan P. Simonovic (2014). [Instruction for Watershed Delineation in an ArcGIS Environment for Regionalization Studies](#). Water Resources Research Report no. 087, Facility for Intelligent Decision Support, Department of Civil and Environmental Engineering, London, Ontario, Canada, 45 pages. ISBN: (print) 978-0-7714-3071-8; (online) 978-0-7714-3072-5.

Andre Schardong, Roshan K. Srivastav and Slobodan P. Simonovic (2014). [Computerized Tool for the Development of Intensity-Duration-Frequency Curves under a Changing Climate: Users Manual v.1.](#) Water Resources Research Report no. 088, Facility for Intelligent Decision Support, Department of Civil and Environmental Engineering, London, Ontario, Canada, 68 pages. ISBN: (print) 978-0-7714-3085-5; (online) 978-0-7714-3086-2.

Roshan K. Srivastav, Andre Schardong and Slobodan P. Simonovic (2014). [Computerized Tool for the Development of Intensity-Duration-Frequency Curves under a Changing Climate: Technical Manual v.1.](#) Water Resources Research Report no. 089, Facility for Intelligent Decision Support, Department of Civil and Environmental Engineering, London, Ontario, Canada, 62 pages. ISBN: (print) 978-0-7714-3087-9; (online) 978-0-7714-3088-6.

Roshan K. Srivastav and Slobodan P. Simonovic (2014). [Simulation of Dynamic Resilience: A Railway Case Study](#). Water Resources Research Report no. 090, Facility for Intelligent Decision Support, Department of Civil and Environmental Engineering, London, Ontario, Canada, 91 pages. ISBN: (print) 978-0-7714-3089-3; (online) 978-0-7714-3090-9.

Nick Agam and Slobodan P. Simonovic (2015). [Development of Inundation Maps for the Vancouver Coastline Incorporating the Effects of Sea Level Rise and Extreme Events](#). Water Resources Research Report no. 091, Facility for Intelligent Decision Support, Department of Civil and Environmental Engineering, London, Ontario, Canada, 107 pages. ISBN: (print) 978-0-7714-3092-3; (online) 978-0-7714-3094-7.

Sarah Irwin, Roshan K. Srivastav and Slobodan P. Simonovic (2015). [Instructions for Operating the Proposed Regionalization Tool "Cluster-FCM" Using Fuzzy C-Means Clustering and L-Moment Statistics](#). Water Resources Research Report no. 092, Facility for Intelligent Decision Support, Department of Civil and Environmental Engineering, London, Ontario, Canada, 54 pages. ISBN: (print) 978-0-7714-3101-2; (online) 978-0-7714-3102-9.

Bogdan Pavlovic and Slobodan P. Simonovic (2016). [Automated Control Flaw Generation Procedure: Cheakamus Dam Case Study](#). Water Resources Research Report no. 093, Facility for Intelligent Decision Support, Department of Civil and Environmental Engineering, London, Ontario, Canada, 78 pages. ISBN: (print) 978-0-7714-3113-5; (online) 978-0-7714-3114-2.

Sarah Irwin, Slobodan P. Simonovic and Niru Nirupama (2016). [Introduction to ResilSIM: A Decision Support Tool for Estimating Disaster Resilience to Hydro-Meteorological Events](#). Water Resources Research Report no. 094, Facility for Intelligent Decision Support, Department of Civil

and Environmental Engineering, London, Ontario, Canada, 66 pages. ISBN: (print) 978-0-7714-3115-9; (online) 978-0-7714-3116-6.

Tommy Kokas, Slobodan P. Simonovic (2016). [Flood Risk Management in Canadian Urban Environments: A Comprehensive Framework for Water Resources Modeling and Decision-Making](#). Water Resources Research Report no. 095. Facility for Intelligent Decision Support, Department of Civil and Environmental Engineering, London, Ontario, Canada, 66 pages. ISBN: (print) 978-0-7714-3117-3; (online) 978-0-7714-3118-0.

Jingjing Kong and Slobodan P. Simonovic (2016). [Interdependent Infrastructure Network Resilience Model with Joint Restoration Strategy](#). Water Resources Research Report no. 096, Facility for Intelligent Decision Support, Department of Civil and Environmental Engineering, London, Ontario, Canada, 83 pages. ISBN: (print) 978-0-7714-3132-6; (online) 978-0-7714-3133-3.

Sohom Mandal, Patrick A. Breach and Slobodan P. Simonovic (2017). [Tools for Downscaling Climate Variables: A Technical Manual](#). Water Resources Research Report no. 097, Facility for Intelligent Decision Support, Department of Civil and Environmental Engineering, London, Ontario, Canada, 95 pages. ISBN: (print) 978-0-7714-3135-7; (online) 978-0-7714-3136-4.

R Arunkumar and Slobodan P. Simonovic (2017). [General Methodology for Developing a CFD Model for Studying Spillway Hydraulics using ANSYS Fluent](#). Water Resources Research Report no. 098, Facility for Intelligent Decision Support, Department of Civil and Environmental Engineering, London, Ontario, Canada, 39 pages. ISBN: (print) 978-0-7714-3148-7; (online) 978-0-7714-3149-4.

Andre Schardong, Slobodan P. Simonovic and Dan Sandink (2017). [Computerized Tool for the Development of Intensity-Duration-Frequency Curves Under a Changing Climate: Technical Manual v.2.1](#). Water Resources Research Report no. 099, Facility for Intelligent Decision Support, Department of Civil and Environmental Engineering, London, Ontario, Canada, 52 pages. ISBN: (print) 978-0-7714-3150-0; (online) 978-0-7714-3151-7.

Andre Schardong, Slobodan P. Simonovic and Dan Sandink (2017). [Computerized Tool for the Development of Intensity-Duration-Frequency Curves Under a Changing Climate: User's Manual v.2.1](#). Water Resources Research Report no. 100, Facility for Intelligent Decision Support, Department of Civil and Environmental Engineering, London, Ontario, Canada, 52 pages. ISBN: (print) 978-0-7714-3152-4; (online) 978-0-7714-3153-1.

Ayushi Gaur, Abhishek Gaur and Slobodan P. Simonovic (2017). [Modelling of High Resolution Flow from GCM Simulated Runoff using a Mesoscale Hydrodynamic Model: CAMA-FLOOD](#). Water Resources Research Report no. 101, Facility for Intelligent Decision Support, Department of Civil and Environmental Engineering, London, Ontario, Canada, 44 pages. ISBN: (print) 978-0-7714-3154-8; (online) 978-0-7714-3155-5.